CFD ANALYSES OF A FLOATING PVT SYSTEM

2024
MASTER THESIS
MECHANICAL ENGINEERING

Baseem Hasan HAMMADI

Thesis Advisor
Assist. Prof. Dr. Mutlu TEKİR

CFD ANALYSES OF A FLOATING PVT SYSTEM

Baseem Hasan HAMMADI

Thesis Advisor
Assist. Prof. Dr. Mutlu TEKIR

T.C.
Karabuk University
Institute of Graduate Programs
Department of Mechanical Engineering
Prepared as
Master Thesis

KARABUK
September 2024

I certify that, in my opinion, the thesis submitted by Baseem Hasan HAMMADI titled “CFD ANALYSES OF A FLOATING PVT SYSTEM” is fully adequate in scope and quality as a thesis for the degree of Master of Science.

Assist. Prof. Dr. Mutlu TEKİR .....
Thesis Advisor, Department of Mechanical Engineering

This thesis is accepted by the examining committee with a unanimous vote in the Department of Mechanical Engineering as a Master of Science thesis. 13/09/2024

Examining Committee Members (Institutions)	Signature
Chairman: Assoc. Prof. Dr. Mehmet GÜRDAL (KAU)	(Onlıne)
Member : Assist. Prof. Dr. Mutlucan BAYAT (KBU)	(Onlıne)
Member : Assist. Prof. Dr. Mutlu TEKİR (KBU)	.....

The degree of Master of Science by the thesis submitted is approved by the Administrative Board of the Institute of Graduate Programs, Karabuk University.

Assoc. Prof. Dr. Zeynep ÖZCAN .....
Director of the Institute of Graduate Programs

"I declare that all the information within this thesis has been gathered and presented under academic regulations and ethical principles, and I have, according to the requirements of these regulations and principles, cited all those which do not originate in this work as well."

Baseem Hasan HAMMADI

ABSTRACT

M. Sc. Thesis

CFD ANALYSES OF A FLOATING PVT SYSTEM

Baseem Hasan HAMMADI

Karabük University
Institute of Graduate Programs
Department of Mechanical Engineering

Thesis Advisor
Assist. Prof. Dr. Mutlu TEKİR
September 2024, 101 pages

The best technologies for capturing solar energy and converting it to heat or electricity are solar thermal and photovoltaic collectors. The floating photovoltaic thermal collector will be the main topic of this research, along with innovative development techniques for improving its performance. The aim of this research is to enhance the photovoltaic collector system by optimizing the electric energy generated from the photocell, thereby increasing the system's overall efficiency.

A three-dimensional model of a PV panel with dimensions of 0.99 m in width, 1.64 m in length, and 4.8 mm in thickness was created using ANSYS simulation. Regarding the pipes, 2 meters above lake level and 10 mm in diameter copper pipes were used. Where the FSI system was used and the CFD system was connected to the pipe. It is numerically simulated for various entrance velocities (0.1, 0.5, and 1 m/s) and inlet temperatures (lake temperatures of 6, 9, and 12°C), as well as for

various Reynolds numbers (1123.6, 5618, and 11236). The solar irradiation and panel temperature are the two most important elements in the MATLAB Simulink equations study.

The temperature distribution and solar panel cooling procedure using the simulation software are the two most crucial elements in this article. The maximum temperature was recorded at 12:00 in the afternoon, with a temperature of 32.42°C. It is seen that the value of the maximum temperature decreases with lowering the entrance temperature of the cooling tube. Achieving the highest efficiency achievable via simulations and calculations is the primary goal of the cooling process. The energy value difference between the various cooling systems at different times and at varied water inlet temperatures was 65.28 W, indicating that the cooling value contributes to an increase in electric power.

Through the use of a reenactment program, the temperature appropriation and cooling processes on the solar-powered chargers demonstrated that the maximum temperature worth of the reproduction cycle decreases as the cooling tube's section velocity increases. The temperature reached 28.1°C while moving at a velocity of 1 m/s into the water, which is the best scenario when compared to the excess instances. The long-term temperature transport at different delta velocities also shows that when water enters the cooling framework at a higher velocity, the temperature value on the outer layer of the solar-powered chargers decreases. The cooling system's main goal is to achieve the highest level of proficiency that can be attained using the product's calculations and reproductions. When the water passage velocity was 1 m/s, the electrical effectiveness was attained, and the electrical proficiency esteem was 7.66%. This proves that the cooling value contributes to the electrical energy expansion.

December's maximum temperature values are lower than those of previous months, according to the modeling software's calculations of the cooling process and

temperature distribution on solar panels. The simulation's highest temperature value for the solar panel's cooling pipe decreases in December, and the exit temperature in the month of July was 20.2°C. It has been noted that there is a seasonal change in temperature, with the lowest recorded surface temperature of solar panels occurring at noon in December. The electrical energy, which was measured at 65.15 W at 12:00 in winter and was entering the water at a velocity of 1 m/s, is enhanced by the cooling value. Maximizing efficiency is the main objective of the refrigeration process, and it may be done by using computer simulations and calculations.

The summertime effects of lake temperature and entrance velocity. The temperature upon entrance was 26°C, and the velocity changed as the weather changed. At an entrance velocity of 0.1 m/s, the pipe temperature gradient showed a maximum temperature of 58°C, while at 1 m/s, it reached 48°C. Because there was not enough time for heat to pass from the water to the solar panel, the temperature gradient of the panel decreased as the entrance velocity rose. The recorded temperatures were 0.1 m/s for 58°C, 0.5 m/s for 55°C, and 1 m/s for 49°C.

Keywords **:** Floating Solar Panel, PVT, CFD, Solar Energy.

Science Code **:**91411

ÖZET

Yüksek Lisans Tezi

YÜZEN PVT SİSTEMİNİN HAD ANALİZİ

Baseem Hasan HAMMADI

Karabük Üniversitesi
Lisansüstü Eğitim Enstitüsü
Makine Mühendisliği Anabilim Dalı

Tez Danışmanı
Dr. Öğr. Üyesi Mutlu TEKİR
Eylül 2024, 101 Sayfa

Güneş enerjisini yakalama ve ısı veya elektriğe dönüştürme konusunda en iyi teknolojiler, güneş termal ve fotovoltaik kolektörlerdir. Bu araştırmanın ana konusu, performansını iyileştirmek için yenilikçi geliştirme teknikleri ile birlikte yüzen fotovoltaik termal kolektör olacaktır. Bu araştırmanın amacı, fotopilden üretilen elektrik enerjisini optimize ederek fotovoltaik kolektör sistemini geliştirmek ve böylece sistemin genel verimliliğini artırmaktır.

Boyutları genişlik 0.99 m, uzunluk 1.64 m ve kalınlık 4.8 mm olan bir PV panelinin üç boyutlu modeli, ANSYS simülasyonu kullanılarak oluşturulmuştur. Borular için, göl seviyesinden 2 metre yükseklikte ve 10 mm çapında bakır borular kullanılmıştır. FSI sistemi kullanılan yerde, Hesaplamalı Akışkanlar Dinamiği (HAD) sistemi boruya bağlanmıştır. Giriş hızları (0.1, 0.5 ve 1 m/s) ve giriş sıcaklıkları (göl sıcaklıkları 6, 9 ve 12°C) için çeşitli Reynolds sayıları (1123.6, 5618 ve 11236) ile

sayısal olarak simüle edilmiştir. MATLAB Simulink denklemler çalışmasında en önemli iki unsur, güneş ışınımı ve panel sıcaklığıdır.

Bu makalede en kritik iki unsur, simülasyon yazılımı kullanılarak sıcaklık dağılımı ve güneş paneli soğutma işlemidir. En yüksek sıcaklık öğlen saat 12'de, 32.42℃ olarak kaydedilmiştir. Soğutma tüpünün giriş sıcaklığını düşürmek, maksimum sıcaklık değerinin azalmasını sağladığı görülmüştür. Soğutma işlemi için en yüksek verimliliğe ulaşmak, simülasyonlar ve hesaplamalar yoluyla elde edilen temel hedeftir. Farklı soğutma sistemleri arasında enerji değeri farkı, farklı zamanlarda ve çeşitli su giriş sıcaklıklarında 65.28 W olarak belirlenmiştir, bu da soğutma değerinin elektrik gücünü artırmaya katkı sağladığını göstermektedir.

Bir yeniden canlandırma programı kullanılarak yapılan güneş panellerindeki sıcaklık dağıtımı ve soğutma işlemi, soğutma tüpünün giriş hızı arttıkça yeniden canlandırma sürecinin maksimum sıcaklık değerinin azaldığını göstermiştir. Su, 1 m/s hızla hareket ederken ulaşılan sıcaklık 28.1°C'dir, bu da fazla durumlarla karşılaştırıldığında en iyi senaryodur. Uzun vadeli sıcaklık taşınımı, farklı delta hızlarında da göstermiştir ki, su soğutma çerçevesine daha yüksek bir hızla girdiğinde, güneş panellerinin dış yüzeyindeki sıcaklık değeri azalır. Soğutma sisteminin ana amacı, ürünün hesaplamaları ve yeniden canlandırmaları kullanılarak ulaşılabilecek en yüksek düzeyde ustalık elde etmektir. Su geçiş hızı 1 m/s iken, elektrik verimliliği sağlanmış ve elektrik verimliliği değeri %7.66 olarak gerçekleşmiştir. Bu, soğutma değerinin elektrik enerjisi genişlemesine katkıda bulunduğunu kanıtlar.

Aralık ayında maksimum sıcaklık değerleri önceki aylardan daha düşüktür, modelleme yazılımının soğutma işlemi ve güneş panelleri üzerindeki sıcaklık dağılımı hesaplamalarına göre. Simülasyonun güneş panelinin soğutma borusu için en yüksek sıcaklık değeri Aralık ayında azalır ve Temmuz ayındaki çıkış sıcaklığı 20.2°C'dir. Sıcaklıkta mevsimsel bir değişiklik olduğu, Aralık ayında öğlen saatlerinde güneş panellerinin kaydedilen en düşük yüzey sıcaklığının meydana geldiği belirtilmiştir. Kış aylarında saat 12'de 65.15 W olarak ölçülen elektrik enerjisi, 1 m/s hızla suya girerken soğutma değeri tarafından artırılmıştır. Verimliliği

en üst düzeye çıkarmak, buzdolabı işleminin ana amacıdır ve bilgisayar simülasyonları ve hesaplamaları kullanılarak yapılabilir.

Göl sıcaklığının ve giriş hızının yaz aylarındaki etkileri. Girişteki sıcaklık 26°C ve hava durumu değiştikçe hız değişti. 0.1 m/s'lik bir giriş hızında, boru sıcaklık gradyanı maksimum 58°C sıcaklığını gösterdi, 1 m/s hızında ise 48°C'ye ulaştı. Suya güneş paneline yeterince zaman için ısı geçmediği için, giriş hızı arttıkça panelin sıcaklık gradyanı azaldı. Kaydedilen sıcaklıklar 0.1 m/s için 58°C, 0.5 m/s için 55°C ve 1 m/s için 49°C idi.

Anahtar Kelimeler: Yüzen Güneş Paneli, PVT, HAD, Güneş Enerjisi.

Bilim Kodu :91411

ACKNOWLEDGMENT

I want to express my sincere gratitude to my thesis advisor, Dr. Mutlu TEKIR, for his unwavering support, guidance, and encouragement throughout my research.

I would also like to thank my thesis committee members for their insightful feedback and helpful suggestions. Their expertise and constructive criticism have been instrumental in shaping my research.

I want to thank my family, particularly my parents, for their unwavering love and support. Their encouragement and belief in me have been a constant source of strength and inspiration.

TABLE OF CONTENTS

Page

APPROVAL ii
ABSTRACT iv
ÖZET vii
ACKNOWLEDGMENT x
TABLE OF CONTENTS xi
LIST OF FIGURES xiv
LIST OF TABLES xvi

PART 1 1
INTRODUCTION 1
1.1. SOLAR ENERGY 2
1.2. SOLAR TECHNOLOGIES AND TECHNIQUES 3
1.3. SOLAR SYSTEM COMPONENTS 3
1.3.1. Solar PV Panels 4
1.3.2. Inverters 5
1.3.3. Monitoring 6
1.3.4. Racking 6
1.4. PHOTOVOLTAIC (PV) ENERGY OPTIMIZATION TECHNIQUES 7
1.4.1. PV Cooling Techniques 9
1.4.2. Floating PV Collector 10
1.4.3. Structural Balance of Collector (SBoC) 10
1.5. FLOATING PHOTOVOLTAIC THERMAL COLLECTOR 13
1.5.1. PVT Efficiency Enhancement 14

PART 2 15
LITERATURE REVIEW 15
2.1. OVERVIEW PV SOLAR 15
2.2. THEORETICAL WORK 17

Page

2.3. EXPERIMENTAL WORK 22
2.4. EXPERIMENTAL AND THEORETICAL WORK 27
2.5. AIM OF STUDY 34

PART 3 36
NUMERICAL ANALYSIS 36
3.1. COMPUTATIONAL ANALYSIS USING ANSYS PACKAGE 36
3.1.1. Governing Equations 37
3.1.2. Radiation Model Equations 39
3.1.2.1. Rossland 42
3.1.2.2. P1 (Non-Gray Model) 43
3.1.2.3. S2S (Surface to Surface Model) 43
3.1.2.4. DO (Discrete Model) 44
3.1.3. ANSYS Package 44
3.1.4. Problem Geometry 45
3.1.5. Mesh Generation 45
3.1.6. Boundary Conditions 46
3.1.7. Problem Solution 49
3.1.8. Solution Parameters 49
3.2. MATLAB SIMULINK EQUATIONS 51

PART 4 57
RESULTS AND DISCUSSION 57
4.1. VALIDATION 57
4.2. THE EFFECT OF INLET TEMPERATURES ON THE RESULTS 59
4.3. THE EFFECT OF INLET VELOCITY ON THE RESULTS 65
4.4. THE EFFECT OF SEASON ON THE RESULTS 72
4.5. THE EFFECT OF SUMMER SEASON 78
4.6. THE EFFECT OF RADIATION MODEL 83
4.7. THE EFFECT OF DIMPLED TUBE ON PV COOLING 86

PART 5 89

Page

CONCLUSIONS AND RECOMMENDATIONS 89
5.1. CONCLUSIONS 89
5.2. RECOMMENDATIONS 91
REFERENCES 92

APPENDIX A 97

CURRICULUM VITAE 101

LIST OF FIGURES

Page

Figure 1.1. Global electric energy production. 1
Figure 1.2. Heat process. 3
Figure 1.3. Solar panel. 4
Figure 1.4. Inverter device. 6
Figure 1.5. Improving techniques of PV. 7
Figure 1.6. PV cell schematic. 9
Figure 1.7. Three main cooling types. 10
Figure 1.8. Schematic of FPVT collector. 12
Figure 1.9. Cell materials. 13
Figure 2.1. Self-contained photovoltaic system. 16
Figure 2.2. Grid-connected solar power system. 17
Figure 3.1. Problem geometry. 36
Figure 3.2. Dimpled tube geometry. 37
Figure 3.3. Generated mesh. 45
Figure 3.4. Conditions of the boundary. 47
Figure 3.5. Solar radiation. 48
Figure 3.6. System coupling. 48
Figure 3.7. Flow chart of simulation in Ansys program. 50
Figure 3.8. Equivalent electrical-circuit for a PV module. 52
Figure 3.9. Representative current-voltage curve for photovoltaic cells. 52
Figure 3.10. Simulink programing of (a) PV block and (b) full system. 56
Figure 4.1. Temperature distribution in the photovoltaic cell structure with water cooling for Re = 2242 (a) present work, (b) Salim et. al. 58
Figure 4.2. Photovoltaic cell temperature as a function of Reynolds numbers. 59
Figure 4.3. Temperature contour of PV panel at velocity inlet 0.1 m/s in winter with different inlet temperature. (a) 6°C, (b) 9°C, (c) 12°C. 61
Figure 4.4. Temperature contour of cooling pipe at velocity inlet 0.1 m/s in winter with different inlet temperature. (a) 6°C, (b) 9°C, (c) 12°C. 62
Figure 4.5. Temperature distribution of PV panel with time at velocity inlet 0.1 m/s in winter with different inlet temperature. 63

Page

Figure 4.6. Electrical efficiency distribution of PV panel with time at velocity inlet 0.1 m/s in winter with different inlet temperature..... 65

Figure 4.7. Temperature contour of PV panel at inlet temperature 6°C in winter with different velocity inlet. (a) 0.1 m/s, (b) 0.5 m/s, (c) 1 m/s. 67

Figure 4.8. Temperature contour of cooling pipe at inlet temperature 6°C in winter with different velocity inlet. (a) 0.1 m/s, (b) 0.5 m/s, (c) 1 m/s. 68

Figure 4.9. Temperature distribution of PV panel with time at inlet temperature 6°C in winter with different velocity inlet..... 69

Figure 4.10. Power distribution of PV panel with time at inlet temperature 6°C in winter with different velocity inlet..... 70

Figure 4.11. Electrical efficiency distribution of PV panel with time at inlet temperature 6°C in winter with different velocity inlet. 71

Figure 4.12. Temperature contour of PV panel using inlet velocity of 1 m/s with different season. (a) July, (b) December. 73

Figure 4.13. Temperature contour of cooling pipe using inlet velocity of 1 m/s at different season. (a) July, (b) December. 74

Figure 4.14. Temperature distribution of PV panel with time using inlet velocity of 1 m/s at different seasons. 75

Figure 4.15. Power distribution of PV panel with time using inlet velocity of 1 m/s at different seasons..... 76

Figure 4.16. Electrical efficiency distribution of PV panel with time using inlet velocity of 1 m/s at different seasons. 77

Figure 4.17. The velocity contour of cooling pipe at inlet temperature of 26°C with inlet velocity of (a) 0.1 m/s, (b) 0.5 m/s, (c) 1 m/s..... 79

Figure 4.18. Temperature contour of cooling pipe at inlet temperature of 26°C with inlet velocity of (a) 0.1 m/s, (b) 0.5 m/s, (c) 1 m/s..... 81

Figure 4.19. Temperature contour of PV at inlet temperature of 26°C with inlet velocity of (a) 0.1 m/s, (b) 0.5 m/s, (c) 1 m/s..... 83

Figure 4.20. Outlet temperature with time for different radiation model. 84

Figure 4.21. Power with time for different radiation model. 85

Figure 4.22. Electrical efficiency with time for different radiation model. 86

Figure 4.23. Outlet temperature with time for different dimpled tube dimeter. 87

Figure 4.24. Power with time for different dimpled tube dimeter. 88

Figure 4.25. Electrical efficiency with time for different dimpled tube dimeter. 88

LIST OF TABLES

Page

Table 1.1. Different PV cooling solutions..... 11
Table 2.1. Through previous studies could summarize by the table below. 30
Table 3.1. Mesh independency..... 46

PART 1

INTRODUCTION

Renewable energy is a source of unlimited power that is constantly renewed, such as from the sun, water, wind, geothermal, hydropower, biomass energies, and many other applications used throughout life. Applications of renewable energy can be divided into: [1] domestic, such as water heating, cooking, medical, and charging, and industrial, such as chemical, heating and cooling, and electricity.

In this chapter, the focus will be on solar energy and how to use it in electric generation by using a using a new development method in the generation system. Because of the electric energy, 73.5% is non-renewable and 26.5% is renewable, as shown in Figure 1-1 [2].

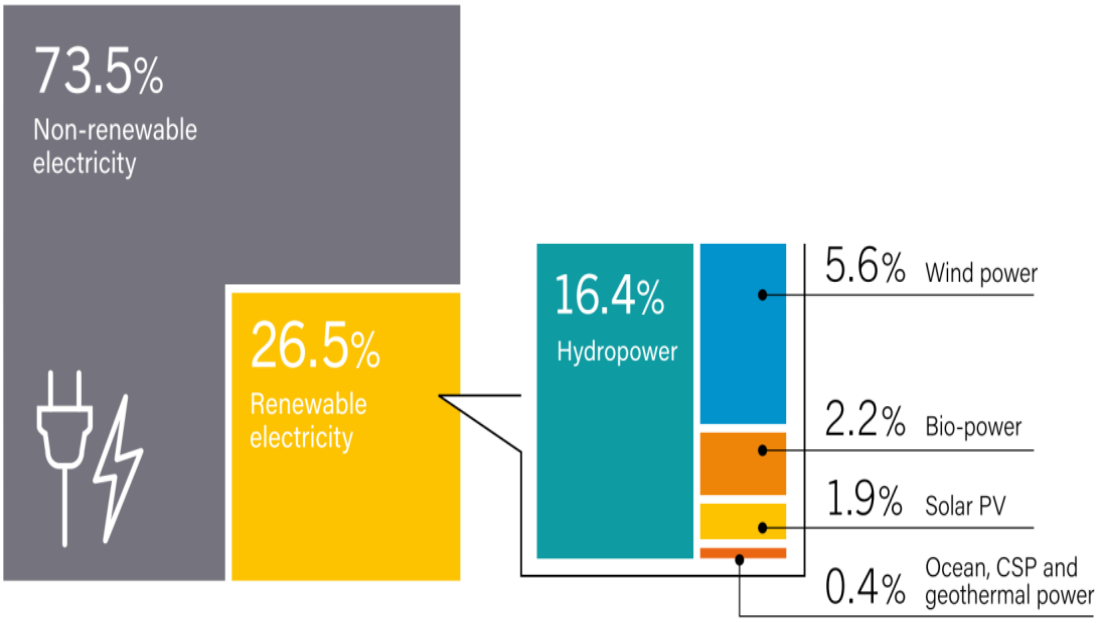

Figure 1.1. Global electric energy production [2].

1.1. SOLAR ENERGY

Every day, the sun radiates an unlimited amount of heat and light energy from helium and hydrogen atoms, which are made from them in plasma form. The nuclear fusion process [3] produces the solar energy. During it, a high temperature and pressure in the core of the sun cause separation of the nuclei from their electrons. The radiant heat energy reaches the earth surface at a speed of 186,000 miles per second. Click or tap here to enter text. About 30% of the fall radiant is reflected back, and the earth, clouds, and atmosphere absorb about 50% of it. In addition, the sun is considered a source for many energies, like the water cycle, wind formation, plant processes of photosynthesis, and even fossil fuels, which receive energy from the sun.

The largest source of heat in the world is the sun, as it produces an indefinite amount of heat daily and radiates that heat by means of light to travel in space and reach the surface of the earth through the atmosphere to be used in various fields. The transfer mechanism of thermal energy from the sun to the earth is through three processes: convection, conduction, and radiation. The main uses of solar energy are electricity, water heating, solar heating, ventilation, and lighting. The photovoltaic thermal (PVT) system converts the sun's light into electric power. The energy of heat through the PVT collector will be transported at different temperature degrees inside the collector layers until it reaches fluid, which flows in the pipe as shown in Figure 1.2 [4].

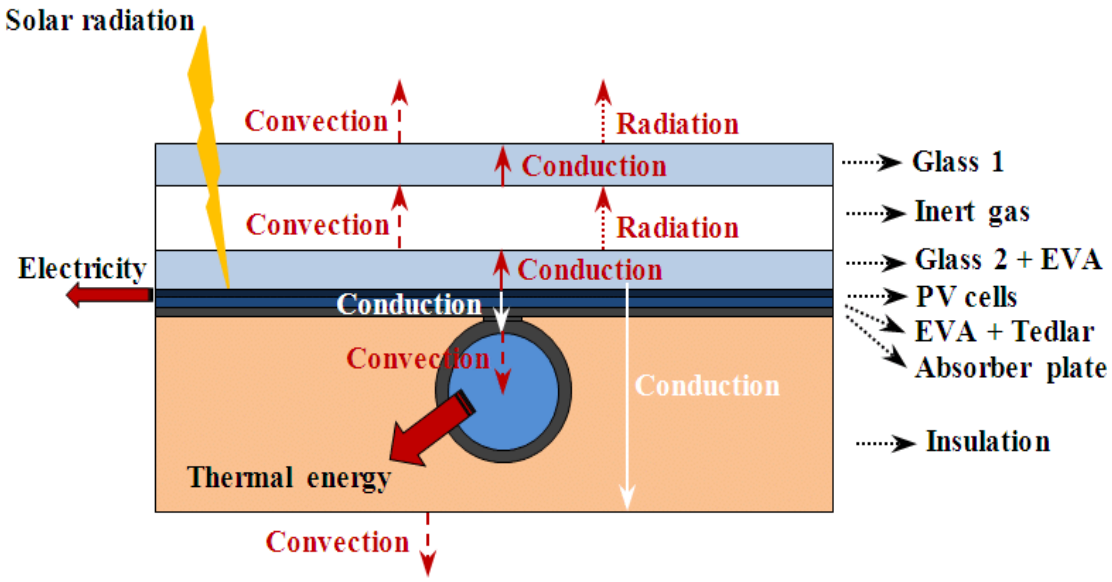

Figure 1.2. Heat process [4].

1.2. SOLAR TECHNOLOGIES AND TECHNIQUES

Solar radiation is largely used for practical purposes while discussing solar energy systems. Other than geothermal energy, all other renewable sources of energy rely on solar energy. Depending on how they capture, transform, and disperse sunlight, solar technologies can be roughly categorized as passive or active. In order to transform sunlight into useful outputs, active solar approaches employ photovoltaic modules (also known as photovoltaic panels) and solar thermal collectors (with electrical or mechanical equipment). A building's orientation toward the sun, the use of materials with advantageous thermal mass or light-diffusing qualities, and the creation of naturally ventilated rooms are all examples of passive solar approaches. Passive solar technologies lessen the need for alternative resources and are typically thought of as demand-side technologies, whereas active solar technologies enhance the energy supply and are classified as supply-side technologies [5].

1.3. SOLAR SYSTEM COMPONENTS

A solar energy system is a type of renewable energy generator that harnesses the sun's photovoltaic energy and transforms it into useful power. These systems, which

are frequently found as rooftop PV arrays, can be varied in size and be used to power diverse kinds of properties, including residential, commercial, and utility-scale zones. Numerous uses exist for photovoltaic systems: Other unconventional systems can be used to power other things or perform other functions, whereas conventional arrays like roof-top or ground-mounted systems serve to provide energy for a home or structure (such as space satellites, hand-held calculators, or vehicles). Solar panels, inverters, DC/AC disconnects, meters, wiring, racks, and mounting make up the heart of any standard home or commercial solar power system. These components are often grid-tied. Charge controllers, batteries, extra balance of system items, and other components are sometimes needed for some systems to work in order for them to be off-grid [6].

1.3.1. Solar PV Panels

The part of a photovoltaic array that is most widely recognized is a solar panel or a PV module. Solar panels function by gathering and utilizing photovoltaic energy from the sun and transferring that energy as "direct current" (DC) power to an inverter or converter component. Solar panels are primarily made of solar cells, frames, and glass (which may be a charge controller in some instances).

Figure 1.3. Solar panel [6].

A solar module produces DC power, which is an electric current that travels continuously in one direction. This form of power is typically not immediately usable

for ordinary electric demands; instead, it must be converted into "alternating current" (AC) power in order to be utilized for standard electric equipment within a structure or residence.

The two most popular forms of solar cells, polycrystalline and monocrystalline, make up solar panels. The difference lies in the methods used to collect, develop, and shape the silicon crystals in the ingots or wafers, each of which gives them a distinctive appearance and color. The capacity of both types of PV cells to generate solar power is recognized to be generally successful. The PVT system has a higher efficiency than other systems because it is built on water, which helps to decrease the temperature and increase the efficiency. In addition, the materials and structures used in PVT are not expensive, such as silicon material, electric cables, inverters, and transformers.

1.3.2. Inverters

An inverter (also known as a converter) takes the DC electricity produced by a solar panel and transforms it into AC power, which may then be routed to a breaker or other system component and used as usual. In some off-grid energy systems, inverters may be placed after a charge controller and battery bank. Inverters exist in a variety of shapes and sizes, and they employ a number of different technologies to create AC power efficiently. String inverters, central inverters, micro inverters, and battery-based inverters are the most popular types of inverters. Different mechanical and technological qualities will be present in each. Microinverters are typically installed to the back of each panel or (every other panel) to convert energy from each module into AC power, but string inverters can be wired for a row of solar panels to connect to one of multiple strings within the inverter to handle a succession of modules. Since each type of inverter has advantages, disadvantages, and unique technologies with application-specific uses, they are not always superior to one another [6].

Figure 1.4. Inverter device [7].

1.3.3. Monitoring

Typically attached to a competing inverter manufacturer, monitoring equipment components examine and transmit system energy information analyses to an internal console or a web-connected device using their own software. Components of the monitoring equipment may be incorporated within the inverter or, in certain cases, attached to another part of the solar array. Monitoring equipment may show data on everything from energy produced by solar panels to real-time data, energy yield data over a certain period, and rapid problem identification and troubleshooting. The system operator can benefit from a thorough monitoring system by having a better understanding of how the solar energy system is functioning (and actions that can be taken to improve yields, productivity, maintenance, and other factors) in real time or throughout the course of the system's lifecycle [6].

1.3.4. Racking

A PV array is linked to the ground or a roof via racking and mounting components, which are made up of several essential items that make up a whole racking system. For a comprehensive racking and mounting system, the majority of racking systems

will combine rails, flashings, lugs, mounting brackets, wire clips, splice kits, braces, end caps, attachments, tilt legs, and other parts. In order to install ground-mount systems on land, concrete, steel pipes, and a full racking kit are all necessary. Any solar energy system must have racks for mounting. To guarantee that the system can retain integrity and function for a lengthy period, both rooftop and ground-mount arrays need to be installed atop a strong and durable structure [6].

1.4. PHOTOVOLTAIC (PV) ENERGY OPTIMIZATION TECHNIQUES

Known as a method that generates electric energy from sun heat energy by converting it through solar panels, which consist of many photocells that contain photomaterials such as silicon. Even though the production cost of each watt has dropped dramatically, the manufacturing cost of PV remains higher than that of conventional electricity. Therefore, many studies have been conducted to develop the design and manufacturing methods of solar cells in order to enhance their efficiency. In the last few years, the idea of using PV has grown so fast because of its low operational cost, maintenance, and environmental friendliness. From a simple to a complicated system, it produces 46400 MW [8]. There are many techniques used to improve the PV system with different ways of installation, as shown in Figure 1.5.

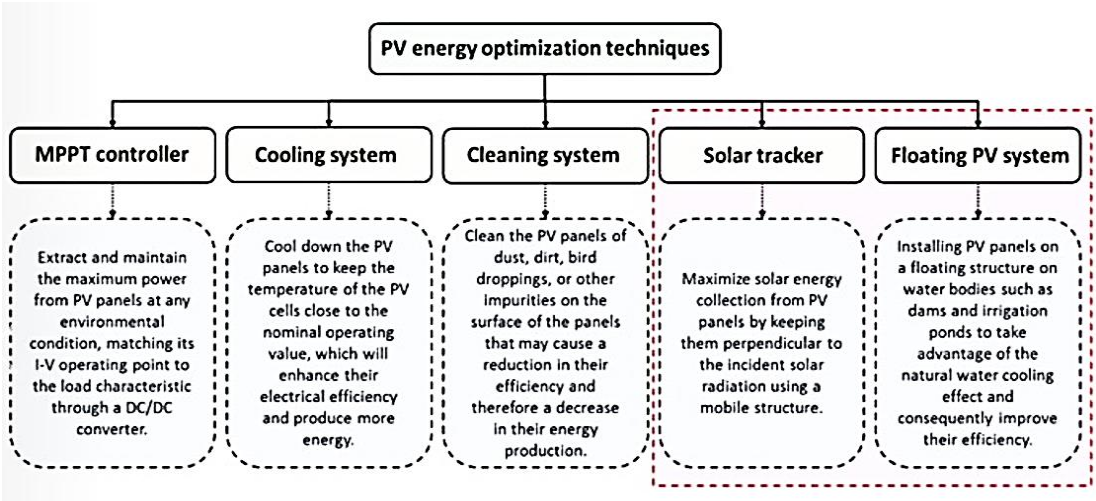

Figure 1.5. Improving techniques of PV [8].

In addition, the uses of photovoltaic electricity and its discovery are controversial. Some electrical materials, when they are highlighted and confirmed, generate a lot of electrical energy from electrodes placed in an electrically conductive solution (electrolyte) and electrical electrolyte placed in an electrolytic solution (electrolyte). The development of photovoltaic plains belongs to French scientist ADMOND because he noticed that some materials could produce energy when focusing light on them. One of those materials was selenium, where, in 1873, (Willoughby Smith (William Grylls) discovered the ability of selenium to conduct the PV [9], as shown in Figure 1.6. The first PV cell was made by Charles Fritts in 1883 from silicon and was able to operate an electric device for some hours. Its efficiency was also about 4%. In 1973, Delaware University built its first house working on PV energy, called a solar one, and this system was made of photovoltaic panels submitted to the roof of the house.

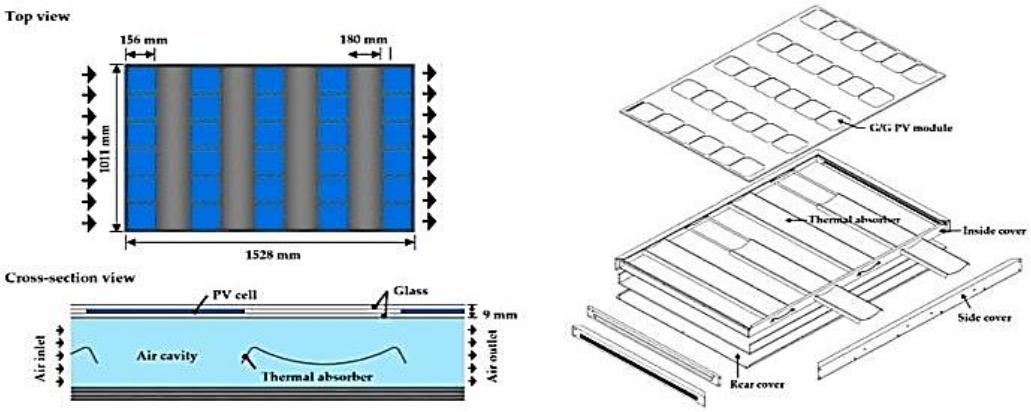

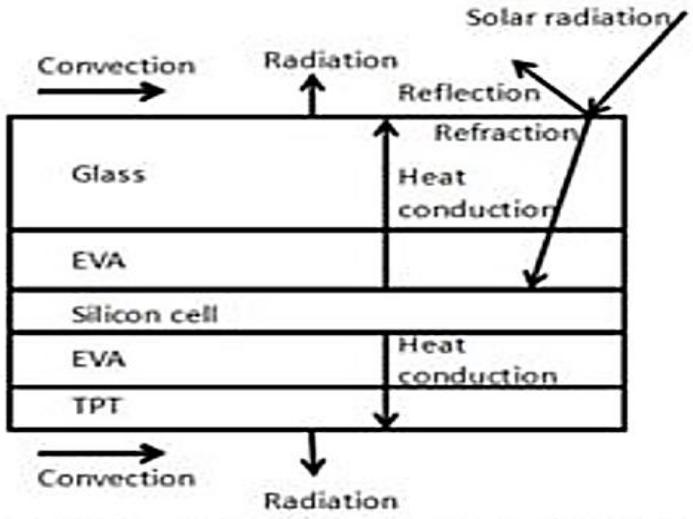

Figure 1.6. PV cell schematic.

1.4.1. PV Cooling Techniques

There are many technologies of PV cooling, each one used under the condition of work. These methods have advantages and disadvantages according to their design or working mechanism, as displayed in the table and figure below. The main purpose of using different methods of cooling is to achieve higher electrical efficiency by reducing the outside temperature to a minimum. In addition, the common methods that are used in cooling are air, liquid, and hybrid. Each way has been tested by previous researchers, and they had a lot of agreement about the liquid method because of its ability to reduce the collector temperature to a minimum quickly, as shown in Figure 1.7 [2].

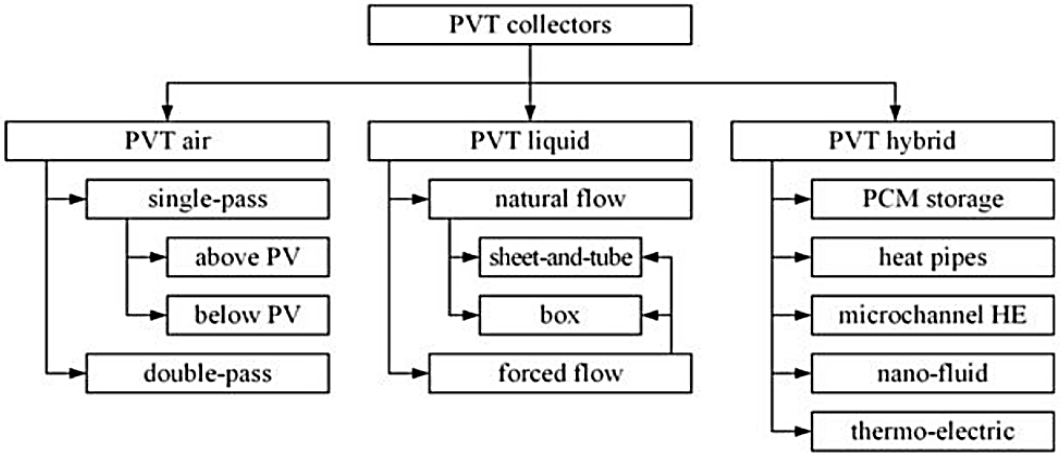

Figure 1.7. Three main cooling types [2].

1.4.2. Floating PV Collector

The floating photovoltaic (FPV) is one of the photovoltaic collector's most common types and is widely used in the present time because of its high work performance. In the United States, it is approximately estimated that 2.1 million FPVs FPV built on the water surface. The water-cooling method increases the energy yield and efficiency compared to ground-mounted PV. The FPV systems can be built in the ocean, hydropower reservoirs, industrial ponds, flood control reservoirs, and agricultural ponds, so they have the big benefit of reducing water evaporation. The type of anchoring solution and floating structure for the collector depend on site specifics. The instillation of FPV collectors needs detailed analysis of water depth, level, aspects of waves, and wave speed.

1.4.3. Structural Balance of Collector (SBoC)

Floats: the structure of floating support modules of PV, which are usually fixed tilt floats made of polyethylene material because it is cheaper and has fewer metal parts. Bolts fix the floats, and a large part of them is directly attached to modules. The instillation angle depends on the windy site. The system is established by the anchoring and mooring system, which minimizes the movement, rotation, and risk of floating objects. The elastic mooring is perfect because it extends the rig's longevity.

Electrical components: the electric cables and junction boxes connect the modules on a floating array. The central inverter and other electrical equipment were put on the shore. In the calculation of environmental loads, it is necessary to compute the equation of motion for the support structure because of the FPV movement.

Table 1.1. Different PV cooling solutions [9, 10].

Technology	Highlight	Advantages	Disadvantages
Air cooling	Forced air is more efficient than natural circulation. More effective in cold climatic conditions	Simplest, available, economical, less risk Increased efficiency is viable.	Lower efficiency than water Lower mass flow rates
Water cooling	Increases electrical efficiency, the bottom side is more efficient than the top. Temperature degree control by amount of mass flow rate	High efficiency of conversion to electric energy requires less space than for separate	Expensive initial costs may freeze in a cold climate. Electricity for pumping. leakage, corrosion
PCM cooling	The heat of PV is saved during PCM melting.	Store heat at a small temperature change. System could operate at off-sunshine phase-change happen at a constant temperature	Low thermal conductivity in solid matter. Fire safety issue. Disposal problem after the end-of-life cycle
Heat Pipes	Complex design pipe material choice influenced by improved thermal output corrosion issues	High heat fluxes Easy integration, passive heat exchange, Heat transfer over long distances	High-cost, difficult manufacturing Generate non-condensable gas.
MCHS cooling	Effective heat exchange Low contact thermal resistance between the heatsink and substrate	Low fluid inventorypower requirement, thermal resistance	Pressure drops, corrosion temperature distributions, and manufacturing prices
Nano-fluids	Enhance output, heat transfer, and heat removal. Sedimentation of nanoparticles is a problem.	Available Higher thermal efficiency	High-cost influences not determined (interaction with main fluids)
Water spraying (jet)	Higher efficiency and heat transfer characteristics. Water and heat absorbed were wasted.	High heat capacity, thermal conductivity, and energy conversion	The surface of the panel is partially cooled. Higher cost. Heat waste
Water immersion cooling	Efficiency increased when temperatures were reduced. Leak-proof design	Highly efficient heat transfer from front and back surfaces. friendly with environmentally	High-cost complex design, submersion depth influences efficiency

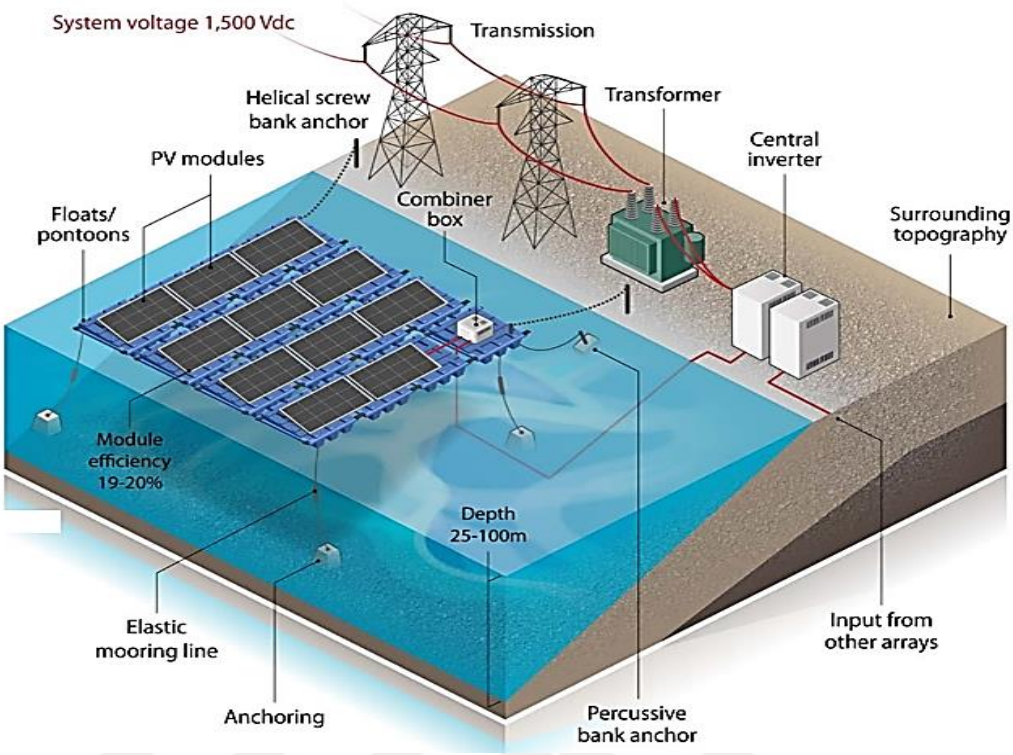

Figure 1.8. Schematic of FPVT collector [11].

The previous studies refer to the fact the fact that hybrid collectors are widely used because they have higher efficiency than other types, but they are also expensive. The important things in the systems of photovoltaic cells are the type of material used in the structure of the cell because the amount of power energy depends on it. Therefore, there are several materials, like Figure 1.9 [12].

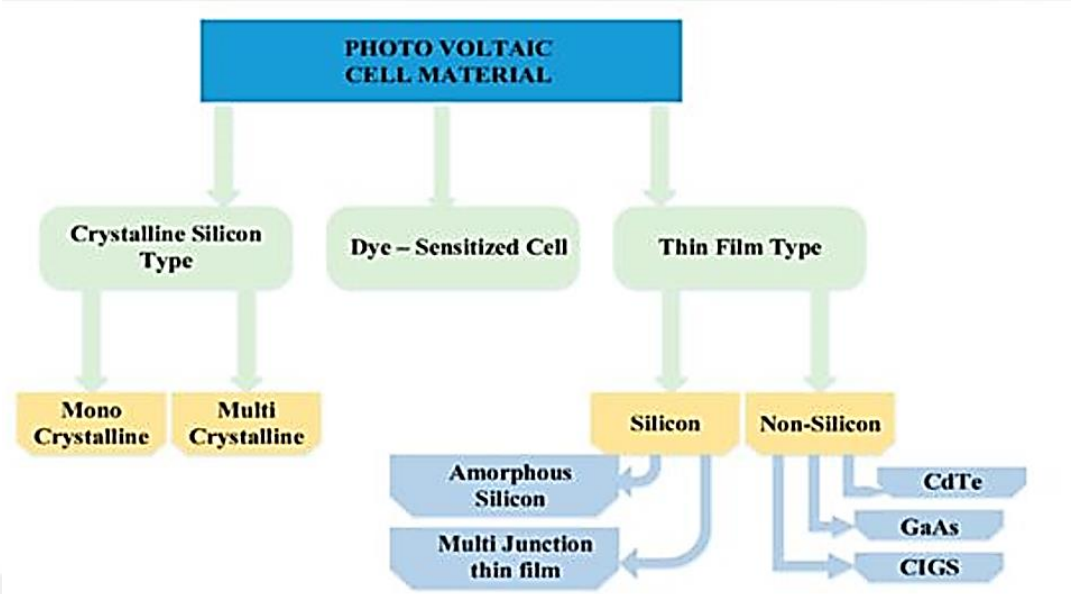

Figure 1.9. Cell materials [9].

From the figure above and the results of the previous test, it was found that the best type of material is crystalline silicon because of its high electrical conductivity, especially at high temperatures.

1.5. FLOATING PHOTOVOLTAIC THERMAL COLLECTOR

The solar thermal and floating Photovoltaics are a great technology to harness solar energy by converting it to heat or electric power. This study will focus on floating photovoltaic thermal (FPVT) and how to enhance its performance by using a new development method. Because it combines the advantages of solar thermal and photovoltaic cells into a single system. However, at first, we will look at the previous research that was associated with the enhancement and the results concluded by the researchers. [13] Previous studies indicated that the PVT efficiency could reach up to 81%, depending on the design of the system and the operating conditions. In addition, the average power capacity of FPVT is 11%, which is more than that of that of a panel on the ground, where 40% of water is lost by evaporation in open reservoirs, but when covered with just 30% of the water surface, it found that about 49% of the evaporation amount was reduced. In 2018, the total power capacity of the world was 512 GW, so there was an increase of about 27% in total capacity and 55%

in renewable resources. Therefore, it is predicted that in 2025, the FPVT system will increase by 7.38%, which is 485.4 GW.

1.5.1. PVT Efficiency Enhancement

The overall efficiency of the photovoltaic collector is a measurement of the system's work performance and a result of a combination of heat and electric efficiencies. Many studies were carried out to enhance the thermal efficiency of PVT systems until the presidential period. The efficiency is affected by various operation parameters, such as the flow rates of the working fluid, cell temperature, ambient temperature, intensity of solar radiation, location of the test rig, and many other factors. In the history of changing the efficiency of PV systems in 1957 and 1960, the PV efficiency was approximately 4%, but by the time and research developed to 14% by Hoffman Electronics Company, and then the University of South Wales reached 20% in 1985, the efficiency still increased until it reached 34.5%.

PART 2

LITERATURE REVIEW

The floating photovoltaic (FPV) collector is a new heat and electric generation system that has received wide attention at the present time due to its many operation advantages, high work performance in most life applications, and low cost of fabrication. Several studies and research studies have been conducted to develop the collector system and the work performance associated with the electric and mechanical parts of the system. The FPV is built on artificial water bodies such as ponds, lakes, or reservoirs to avoid the risk that occurs in natural water. The FPV solar panels are the same as in the land-based collector, where instead of fixing them on land, they are put on a plastic floating platform. These floats are sited together one by one to make a raft with cables of power that connect panels to power equipment's. The first online FPV collector was in 2007 in California, where the electric capacity was 2 MW and increased to 2,579 MW in 2021. The important element in FPV operation is the temperature of the cell, which affects mainly the increasing and decreasing of all the FPV efficiencies (thermal, electrical, and overall).

2.1. OVERVIEW PV SOLAR

By directly converting solar energy via the photovoltaic effect, a photovoltaic (PV) system is able to deliver electric energy to a specific demand. The system architecture is exceedingly adaptable. The primary construction pieces are PV modules, which may be assembled into arrays to boost electric energy generation. For energy to be converted into a usable form or to be stored for later use, extra equipment is often required. As a result, the final system will depend on the energy requirements (or loads) for a specific application. The two main categories into which PV systems may be generally divided are:

Self-Contained: These systems are cut off from the distribution network for electricity. The most typical system setup is shown in Figure 2.1. The system shown i/n Figure 2.1, which has all the components required to power AC appliances in a typical home or business application, is really one of the most complicated. To increase dependability, a second generator (such as one powered by wind or biodiesel) might be explored; however, it is not required. Depending on the kind of load being provided, the system's component count will vary. If solely DC loads are to be powered by the PV modules, the inverter might be removed or swapped out with a DC-to-DC converter. In situations where other storage options are employed or where operating schedules are not crucial, it is also possible to directly connect a PV array to a DC load. Water pumping applications are a nice example, where a PV module is directly connected to a DC pump and water is stored in a tank throughout the day as energy is available.

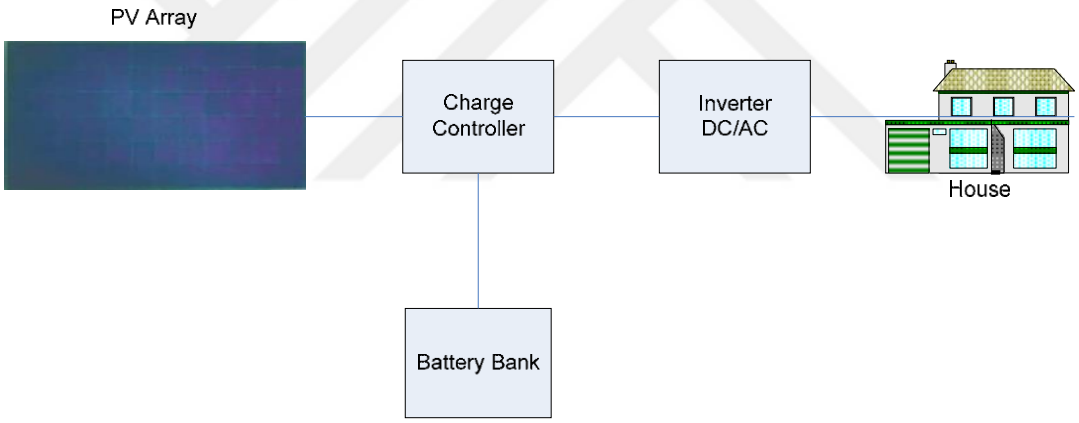

Figure 2.1. Self-contained photovoltaic system.

Grid-connected: These systems don't need battery storage because they are connected directly to the electric distribution network. The fundamental setup of the system is shown in Figure 2.2. Depending on the local energy usage patterns and the change in the solar resource during the day, electricity is either sold or purchased from the local electric utility; this mode of operation necessitates the use of an inverter to convert DC currents to AC currents. Grid-connected PV systems offer a number of advantages over conventional stand-alone solutions.

- The same load may be reliably supplied by smaller PV arrays.

- There is less requirement for system component balancing.
- Comparable potential for reducing emissions while utilizing current infrastructure.
- Reduces the expense of replacing and recycling batteries for individual clients and eliminates the necessity for energy storage. If required, storage can be added to increase client dependability.
- Use the current electrical infrastructure.
- Energy that is used effectively contributes to the necessary electrical grid generation when client demand is lower than PV output.

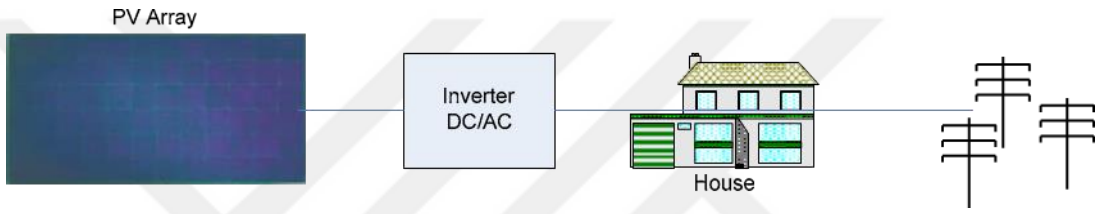

Figure 2.2. Grid-connected solar power system.

Hybrid systems: It may be feasible if grid connectivity and battery storage or a generator (or both) are coupled for increased dependability and scheduling flexibility (at additional cost). Pre-fabricated flat-plate solar modules are used in the majority of installed residential, commercial, and centralized systems since they are generally accessible. As a result, this type of technology is the subject of the majority of publications on PV system costs; thus, we will concentrate on it in this chapter. Other specialized technologies are available, although they are not as widely used commercially as the conventional PV module (for example, concentrating PV systems).

2.2. THEORETICAL WORK

Lupu et al. [2] reviewed the cooling technologies of photovoltaic systems. The need for energy has developed daily with the proliferation and evolution of humanity. The pollution increases and sharp decrease in sources of fossil fuels triggered research for sources of renewable energy. The energy from solar, which is sustainable and available, was converted into thermal and electricity energy. The paradox of a

photovoltaic collector (which needs solar power to function while the electric output power decreases when the temperature of the cell rises under the rising sun's heat) is controlled through different cooling methods for panels. Many papers have been classified, reviewed, and published to date in the literature on energy conversion in collector applications. The focus was placed on methods that were used to enhance solar efficiency for converting electricity into energy.

Parthiban and Ponnambalam [9] reviewed the efficiency enhancement of solar panels. Recently, solar panels have gained popularity in the non-conventional energy sources field for clean electric power and generating green energy. There is a deep relationship between the ambient temperature degree and the thermal and electrical performance of the system. This excessive heat was reduced by implementing cooling measures. So many cooling techniques were implemented, referred to as passive and active methods. Therefore, it was found that photovoltaic efficiency is reduced when the temperature increases and the energy produced drops by 0.33% for every degree. Therefore, many cooling systems have been used as passive and active methods to reduce this excessive heat and, finally, increase efficiency. Consequently, the generated electric power from the system panel is not sufficient to run the entire load. Therefore, it is necessary to know that in many applications, like standalone electric vehicles, the use of an additional panel to compensate for the decreased output energy could not be feasible.

Ebrahim [12] evaluated by ASHRAE Standard the photovoltaic/thermal (PVT) performance with numerical modeling at different fluid inlet and environment conditions, which happen when the system is connected to a GSHP. The PVT system produced both solar thermal and PV at the same time. There are many benefits to PVT collectors integrating with a ground-source heat pump (GSHP) system. It reduces the PVT temperatures operating, which leads to increased lifetime efficiency. They conclude that the electrical and thermal efficiencies were approximately 19.0–19.2% and 48.0-53.4%, respectively, at an irradiance of 800-1000 W/m^2, a temperature reduction to zero, and a mass flow rate of 0.026 kg/s·m^2. Which was determined to enhance the performance, as well as the total heat loss coefficient (U_L) and heat removal factor (F_R) of 53.4-53.5 and 0.56-0.62 W/m^{2}K,

respectively. In addition, the different conditions indicated that the inlet water temperature could affect the operation time and amount of thermal energy extracted throughout the year, especially in cold climate operations.

García and Balenzategui [15] estimated the yearly performance and temperature for different tilted angles of PVT by determining the parameter of nominal operation cell temperature (NOCT) in a reliable way. It is necessary to compute this parameter in a reliable way. It is also used to compare the performance of the performance of various module designs and could influence system predictions. The results obtained were compared with the international standards of NOCT, where different modules, glass-toddler and glass-glass structures, thin-film and crystalline technologies, and some special designs for building applications were compared. They conclude that instead of uncertainties in calculation, the inaccuracies about 3°C do not introduce errors (about 1.5%) on yearly performance calculations, and also that temperature has a second influence on output module energy.

Sawicka-Chudy et al. [16] tested the relationship between the operation of hybrid PVT and the generation of electric and thermal power from the collector under different insolation conditions to find the best tilt angles for the collector. The efficiency and characteristics of PV systems and the relation between efficiency, power, and solar-irradiance incidence angle were studied. Also ascertained the optimal conditions of work for commercial collectors. The system was investigated through working hours between 7.00 and 16.00 and determined under 1.5 air mass conditions by Polysun software, and they found that the PV efficiency varies slightly and increases with the range (40°, 65°) of the tilt angle. In addition, peaks occur at the lowest values of angles. In addition, they found that the max hybrid collector and solar thermal-collector efficiencies registered in the field conditions were higher than those measured under laboratory conditions.

Sanz [17] simulated the PVT tools of collectors and systems, where Polysun and TRNSYS were reported, and these environments might not prepare for the solutions of energy transient analysis but are interested in components (control strategies, collectors, etc.). There are about 24 different models, divided into 11 for system level

and 13 for modules. The features and performance of these tools indicated a difference between real experience and user expectations.
In addition, four main difficulties were identified for systems, which are:

- The parameter of the component is not an easy task.
- The components operation could lead to poor results when out of their conventional.
- Limited boundaries when determining meteorological data and load profiles.
- High sensitivity performance of economic key and environmental.

Finally, the parameterization PVT collector guideline includes a link between numerical tools and normative coefficients.

Boureima et al. [18] determined and compared theoretically the performances of hybrid PVT collectors through the establishment of thermal balances at various system levels. The Cholesky method of MATLAB software was adopted to simplify and solve the obtained equations, which were associated with the thermal, electrical, and overall efficiencies. In addition, the comparisons were made on different panels and obtained results. It was concluded that the rise in temperature showed heat up in PV cells, and the decrease in coolant temperature implies an increase in coolant flow. In addition, the power and global efficiency of hybrid panels are higher than those of simple panels, but the thermal power of them is lower than that of simple panels.

Abakam et al. [19] proposed the performance and modeling analysis of PVT with a new design of two semi-transparent panels that would replace the conventional glass cover. The semi-transparent photovoltaic (STPV) will replace conventional glass covers, which permit a percentage of radiation to pass inside them. The new configuration performance with single and double-glazing was investigated. The modern developments in PVT efficiencies yield thermal, electrical, and combined efficiencies of 54.6%, 13.8%, and 68.4%, while this design achieved 20.76%, 65.7%, and 86.5%, respectively. Moreover, it showed that glazing PVT is more effective at low ambient temperatures than at higher temperatures. Moreover, PVT collectors are not effective for locations with low ambient temperatures and solar radiation. Thus,

the improved energy harvested per unit area indicated a positive step in the application of multilayer semitransparent monocrystalline silicon.

Fudholi et al. [20] reviewed the energy and efficiency modeling for an air PVT collector with an extended area of heat transfer. In a PVT air collector, thermal and electrical energies are generated simultaneously. It has been shown that this type of PVT air collector produced the highest efficiency of any conventional air system. Also, the thermal efficiency with and without extended area was 21–83% and 12–70%, respectively, where the improvement was 15.7–42.8%. The efficiencies of energy and exergy for the PVT air system with an extended heat transfer area were 39%–94% and 12.66%–12.91%, respectively. The efficiencies vary depending on the differences in heat transfer area in the absorber (corrugated surfaces and finned absorbers) and the design and configuration of airflow (single and double pass; with or without glass cover). Generally, steady-state balance equations of energy were used in PVT mathematical modeling with heat transfer area extended. In addition, the first-order linear differential equations are presented for the solution of the mathematical model.

Zohora and Nasrin [21] numerically studied the efficiency improvement for three-dimensional systems of the PVT System by using FEM software to explain the effect of solar irradiance intensity on the total efficiency (electrical power and thermal energy). The testing ranges were 200–500 W/m^2 for solar irradiance, 30-180 L/h for water flow rate, 10-37°C for ambient temperature, and 0–30% partial shading. The results indicated that increasing the 100 W/m^2 irradiance led to an increase in outlet temperatures of 0.54°C, thermal energy of 113.3 W, electrical energy of 20.7 W, and cell energy of 2.17 W, and devalued the overall thermal and electrical energy by 0.83, 0.67, and 0.17, respectively. Also, when ambient temperature increases by 10°C, the water output temperature, cell, and thermal energy increase to 0.05°C, 1.7°C, and 9.89 W, but the electrical energy and efficiency reduce to 0.9 W and 0.1%.

Liu et al. [22] investigated the efficiency of power generation and the prospects of floating collector systems. Where the FPV technology for power generation is still the modern type of power generation in reality, the solar system is restricted by

different factors, like the supply of energy and environmental pollution, water, and land resources. The floating PV systems, compared with traditional terrestrial PV systems, save many water resources and land. Therefore, it first discusses PV development technology and then studies the efficiency of power generation.

Yao et al. [39] analyzed the efficiency of direct expansion PVT with roll bond panel for heat pump application, where the direct expansion-assisted PVT heat pump is a combination of heat pump and PVT technologies. Also, four types of evaporators were conducted and presented. The results referred to the roll bond evaporator with rectangle patterns and hexagons had a better a better temperature distribution than the linear and grid types, while the pressure losses were 0.109 and 0.230 for both and the difference in temperature was 0.038°C. Moreover, the efficiency factors were 0.564, 0.521, 0.342, and 0.549 for grid, hexagon, linear, and rectangle, respectively, when the width of the channel is 10 mm and the scaling ratio is 0.8 to 1.2.

2.3. EXPERIMENTAL WORK

Hammoumi et al. [5] investigated the optimization of power using floating solar panels (FPV) and solar trackers to meet increasing global power demand. These systems offer ease of implementation, environmental friendliness, and power source availability. However, they face challenges such as low conversion efficiency, high initial costs, and land use. Researchers have made improvements in materials, conversion efficiency, manufacturing costs, and optimizing power draw from PV panels. This work focuses on the use of floating collectors and solar tracking systems to maximize solar energy usage.

Herrando and Ramos [10] examined thermal photovoltaic systems for combined heating, power, and cooling in building applications, focusing on solar combined cooling, heating, and power (S-CCHP) provision. The renewable energy share of H/C provision remains low at 22.0% in 2019. The study compares conventional solar H/C with S-CCHP systems, highlighting challenges and proposing improvements for cost-competitiveness. Air-based PV collectors are simpler and cheaper, with lower thermal performance compared to liquid-based collectors. These systems are suitable for high- and medium-latitude countries and are integrated with air sources for space

heating. Liquid-based designs are complex and higher in cost, but have larger thermal efficiency, making them suitable for water heating, solar cooling, and space heating. Advancements in PV liquid-based systems include PCMs or nanofluids. PV refrigerant-based systems have higher electric efficiency but a leakage risk. The best combination of H/C technology and PV collector depends on the application and location, such as ambient temperatures and solar irradiance.

Kim et al. [23] experimentally studied the electrical and thermal characteristics of PVT by using air as a heat transfer medium. A photovoltaic thermal system is a new technology that combines solar thermal collectors and photovoltaics to generate electrical and thermal energies together. The main advantage of PVT systems is that their output energy per unit area is higher than that of single-use systems. The air-based PVT type, which uses air as a heat transfer medium and flow patterns, is the more commonly used type because of these two important factors that affect its performance. In this study, the test rig was designed (under the test conditions of ISO 9806:2017) in round-shaped heat-absorbing plates to increase the path of air flow where the amount of inlet flow rate affects the thermal efficiency of the system. In addition, the electrical performance was analyzed under the same conditions. The results showed that the thermal efficiency of the collector increased from 29% to 42% when the airflow rate increased from 60 to 200 m^3/h, and the electrical efficiency was determined and developed according to the operating conditions.

Kim et al. [24] tested the PVT performance by using air medium, where the collector with monocrystalline was designed in order to confirm the thermal and electrical performance in an outdoor environment. From the obtained results, it was found that wormed air from an air-based collector was approximately 5°C higher than outdoor air. In addition, the results indicated that the electrical and thermal efficiencies of the system were 15% and 22%, respectively. For the electrical power efficiency, the air collector operated at maximum output through temperature rise prevention by forced exhaust, so the air PVT collector performance was similar to the standard test condition (STC) without efficiency decreasing due to PV temperature rising. In addition, they concluded that the heated air produced by PVT could be supplied into the ventilation system as pre-heated fresh air and contribute to high electrical

performance. To design the experimental model of PVT, it is necessary to verify its performance under standard test conditions in order to assess the collector's contribution to the energy performance of the building.

Ghadiri et al. [25] investigated the performance of a photovoltaic system by using nanofluids. The fluids that were used were distilled water and Fe_3O_4-water, with concentrations of 1% and 3% by weight (wt%). The radiation amount taken was 1100 and 600 W/m^2. The ferrofluids were placed at alternating magnetic and constant fields to check the effect of magnetic fields on efficiency. The results indicated that using 3 wt% ferrofluid, the efficiency increased by 45% and the overall efficiency was 50% at the 50 Hz alternating field frequency. In addition, when using 3 wt% of ferrofluid in an alternating magnetic field, the total energy increased to 48 W.

Özakın et al. [26] investigated the thermal performance of PVT. The PV collector works on semiconductor physics principles, where it operates on semiconductor elements like silicon. PV cells generate electric power when they receive a certain quantity of photon energy by converting a fraction of the sun's irradiance in the electromagnetic spectrum to electrical energy. Moreover, the remaining is stored in the form of heat energy in the systems, so that caused irreversibility's. They aimed to remove the accumulated heat from the collector and convert it to useful energy because it reduces the total efficiency of systems. The results showed that the optimal running range of the temperature of the PV cell was between 40 and 60°C, and in that range, the ratio of improvement in electrical efficiency was 20%. The cylindrical fins that were used in the enhancement were made of copper and aluminum materials. They also conclude that at an air velocity of 5 m/s, the ambient air and fin bodies cooled down by about 50%, and efficiency decreased from 12% to 9.5%.

Fu et al. [27] investigated the thermal and electrical efficiency enhancement of PVT by using a low concentration of working fluid in the outdoor (MPCM) Microencapsulated-Phase Change Material type as a cooling medium, where the PVT converts a small percentage of solar radiation into electric power and the

remaining heat. The heat might be collected by different working mediums. The measured thermal and electrical efficiency of the PVT collector by MPCM slurry or tap water under different operation conditions were compared. Moreover, the practical performance was investigated with this similar collector with a PCM layer and a traditional cooled water PVT system. They conclude that increasing the MPCM flow rate reduces the cell temperature, which leads to an increase in the total efficiency of PV. In addition, the use of MPCM produced better results than fluid with a PCM layer or pure tap, where the maximum average thermal and electric efficiency was 13.5% and 0.8%, respectively.

Saadoon et al. [28] prepared nanofluid (Al_2O_3) material to improve the efficiency of photovoltaic solar. The PV panels generate electrical power comparable to the cumulative amount of solar radiation on the surface. Where solar modules are affected by panel temperature, to work under the standard specifications in the Iraqi environment, it used new nanofluid technology, in which the direct flow technique at the rear sides of the panel helps to reduce the temperature, which leads to enhanced thermal and electrical performance of FPV for cooling and performance improvement. The overall efficiency enhancement at 1 g quantity of nanofluid showed 15%, but at 1.5 g nanofluid, it was 18%, and the thermal efficiency at 1 g and 1.5 g of nanofluid was 19% and 27%, respectively. In addition, the electrical efficiency in 1 g of nanofluid was 11% and in 1.5 g of nanofluid was 14%, and the coefficient of Nusselt number and heat transfer rose with the concentration of nanofluid.

Gundala et al. [29] studied the experimental performance of SPVTC by using nanofluids for sustainable improvement. The collector was designed by nanoparticles as a working fluid to check the effect of graphene nanoplatelets on water at 0.05 wt% of the structure's performance. The assessments computed at float prices (0.5 and 1.0 L/min) for the nanofluids and the results that were analyzed from the active angle were confirmed. And computed that water graphene nanofluid is higher in terms of system conversion than water, which could generate perfect thermal performance sooner or later of sun radiation low period and high temperature of mobile, where the

inclusion of water increases average electric efficiency (7.8% and 8.5%) and thermal efficiency (24.9% and 26.3%) at 0.5 and 1.0 LPM flow rates, respectively.

Jaffar et al. [30] enhanced the photovoltaic system performance through forced air, where it was affected by ambient conditions like air temperature and solar irradiance. The increase in ambient temperature led to an increase in collector temperature, which reduced the performance of the system. The PVT is integrated with an air duct and connected to a centrifugal fan to supply air at different speeds [1.5, 2.5, and 3.5 m/s]. The results show that using forced air reduces PV temperature from 16 to 5°C when the air volume rate changes from 335 to 760 m3/h, and the highest enhancements in power and efficiency were 8.2% and 17.9%, respectively, at 760 m3/h. In addition, the maximum voltage power of the PV module dropped to 14.2 V at a maximum temperature of 69°C, and the voltage recorded was higher than 15.1 V when compared with the reference system.

Hasan et al. [31] evaluated the thermoelectrical performance of PVTS by heat sink water-cooled in the south of Iraq during the summer season. The heat sink is applied to thermally manage the collector cells, and that leads to a boost the electrical output of the system. The parameters (water intake, exit, cell temperatures, atmospheric pressure, solar irradiation, and wind velocity) were monitored, as was the effect of solar irradiation on thermal-electrical efficiency, electrical power, and average temperature. They concluded that the irradiation increased from 500 to 960 W/m^2 and the output power from 35 to 55 W when the temperature of PV increased from 65 to 73°C. In addition, the increased mass flow rate through a range of 4 to 16 L/min led to a decrease in cell temperature through the daytime.

Sheikh et al. [32] improved the design of the cooling system to increase the efficiency of floating-photovoltaic systems. A minimally invasive and lightweight cooling system was designed with forced water-cooling to improve the performance of the FPV by reducing the temperature of the temperature of the solar cells. The fluid flow and thermal analyses were presented to assess the improvement of output efficiency numerically with a commercial system panel. The result indicated that a 395 W commercial panel improved the output power up to 49.4 W (14.29%) at 1000

W/m^2 of irradiance intensity and 35°C ambient temperature. In addition, the losses of water pump operation are limited to (8.5 W) as the maximum.

2.4. EXPERIMENTAL AND THEORETICAL WORK

Lee et al. [14] studied the effect of using nanofluids on the flat-plate photovoltaic efficiency. Highest thermal conductivity nanofluids were selected and added to the surfactant CTAB (Cetyltrimethylammonium Bromide) or AG (Arabic Gum) in different concentrations. All nanofluids thermal conductivities were higher than those of water, and there was a difference in the conductivity between the water and nanofluids. The selected nanofluids with the highest thermal conductivity were AG+CuO (1/2 times the nanoparticle number) and CTAB+Al_2O_3 (1/10 times the CMC concentration). Where the thermal conductivities of Al_2O_3 /water and CuO/water are 0.829 W/m·°C and 0.901 W/m·°C, respectively. The analysis was taken under various water flow rates, where the efficiency of the system was highest at 3 L/min than with 1, 2, and 4 L/min; therefore, the electrical, thermal, energy-saving, and overall efficiencies were 12.80%, 23.59%, 57.28%, and 36.39%, respectively. In addition, the use of nanofluids (Al_2O_3/water and CuO/water) at a 0.05 wt% water concentration increased the electrical and thermal efficiencies by 0.07% and 21.30%, respectively, compared to only the water system. Moreover, that increase was not significant, especially in electrical efficiency, because of the errors in measurement. The thermal efficiency of the PVT system with Al_2O_3/water as nanofluid increased by 15.14%, but there was no difference in the electrical efficiency between Al_2O_3/water and natural water.

Hasan [33] improved the PV performance by using fins as heat sink fins in panels, which reduced cell temperature and enhanced electrical yield and efficiency. The fins have a rectangular cross section attached to the panel, providing satisfactory cooling. Analytical models were designed to predict panel temperature, and the fin technique increased output power by 15.3% and solar temperature by 5.7°C. The fin system reduced panel temperature by 9.4%, attributed to surface area extension and heat transfer at the backside. The thermally proposed system for temperature prediction was accurate, with a 3% discrepancy in measured values.

Abdullah et al. [34] critically reviewed the parameters of design, operational factors, and climate that affect the electrical, thermal, and total efficiency of the PVT collector to improve the electrical performance of the cooling system by reducing cell temperature with an absorber under the collector, which takes the heat underneath PV and transfers it to water. The harvested heat is used for domestic water preheating, space heating, and hot water supply applications at low-temperatures. It was concluded that thermal efficiency decreases by increasing the following parameters: packing factor, channel depth, inlet mass flow rate velocity, thermal resistance, inlet temperature, wind speed, mass flow rate, heat loss coefficient, ambient temperature, tilt angle far from latitude angle, duct length, and insulation thermal conductivity. Also, the efficiency increases with the following parameters increasing: tilt angle near the latitude angle, tracking system, solar irradiance, and absorber absorption, number of air inlets, using a booster diffuser reflector, and supporting metal bars.

Ramos et al. [35] experimentally and theoretically reviewed and studied cases of enhancement and global panorama on photovoltaic thermal technology, where a system of flat-plate collectors with a working fluid of water was used. The main objective of solar conversion technology optimization was to cool the cells to increase electricity generation. Therefore, the main obstacle in electric generation is the fact that PV cells give low energy as ambient temperature increases, so the results indicated good agreement between theoretical and experimental datasets, and the electrical power increased with solar cell cooling, so that PVT systems are considered more useful to generate electric and thermal energy simultaneously.

Gomaa et al. [36] improved the performance of a grid-tied PV collector by proposing two different cooling techniques: the first is directly active cooling by water, while the second is passive cooling, which uses fins mounted on the PV backside. Moreover, on the other hand, a second PV module without any cooling technology was employed as a reference for comparison. The results of these three individuals' systems showed that the PV surface temperature was reduced in the two cooling techniques by comparison with the non-cooling module, and the maximum

temperature values were 58, 55, and 38°C for the non-cooling module, fins cooling, and water-cooling, respectively. These low temperatures of cooling systems help to increase the PV performance, and it was found that energy increased by 10.2% and 7% compared with non-cooling collectors, and the performance ratio improved up to 84% and 81%, respectively, compared with 77% for non-cooling.

Majumder et al. [37] analyzed and estimated the thermal performance of two PV panels (one as a reference and the other for tests). Moreover, evaporation losses by shading effect reduction of floating PV System to achieve dual-positive effects, where the efficiency of panel was evaluated by raising the panels over water surface while the operation temperature was reduced by the effects of passive convection cooling. The efficiency and actual temperature reduction were computed by panel P1 through achieved water-cooling via panel P2 measurement of efficiencies and temperatures at environmental conditions. The height of water was maintained at 7.5 cm in the basin underneath P1, which covered 17% of the water surface area. Moreover, that leads to an increment average efficiency of 17.22% relative and 2.7% absolute, while the P1 temperature dropped by 2.7°C. It also showed a 30% reduction in water evaporation by comparing the water with and without the panel.

Yazdanpanahi et al. [38] tested numerically and experimentally the exergy efficiency of a photovoltaic water system based on exergy losses. The experimental work measured the intensity of solar radiation, (solar cells, ambient, fluid inlet and outlet) temperatures, wind speed, (open circuit maximum power point) voltages, and (short circuit maximum power point) currents. The numerical work is carried out on the models (four parameters: current-voltage and one-dimensional steady thermal). The results indicated good agreement between experimental measurements and numerical simulation, where the modified efficiency of exercise has no deficiencies when compared with previous work and shows directly the exercise loss terms in the PVT collector.

Table 2.1. Through previous studies could summarize by the table below.

Reference	Type, geometry and novelty	Conclusions
[2]	PVT	When a cell's temperature increases due to the sun's increasing heat, its electrical output power drops.
[5]	floating solar panels (FPV) and solar trackers	Improvements at the material level, as conversion rates at PV panels rise while production costs fall.
[9]	PVT solar panel	When temperatures rise, photovoltaic efficiency decreases, and energy output drops by 0.33% for every degree.
[10]	thermal photovoltaic systems for combined heating	The optimal H/C technology and PV collector combination depends on the application and the area (ambient temperatures, solar irradiance).
[12]	Standard (PVT)	At an irradiation of 800-1000 W/m^2, a temperature reduction to zero, and a mass flow rate of 0.026 kg/s·m^2, the electrical and thermal efficiencies were around 19.0–19.2% and 48.0–53.4%, respectively.
[14]	nanofluids flat-plate Photovoltaic	The electrical and thermal efficiencies were raised by 0.07% and 21.30%, respectively, compared to a system using only water when nanofluids (Al_2O_3/water and CuO/water), respectively, were used.
[15]	nominal operation cell temperature (NOCT) PVT	Inaccuracies of around 3°C do not create mistakes (about 1.5%) in calculations of yearly performance; moreover, temperature had a second impact on output module energy.
[16]	hybrid PVT 	Solar thermal collector efficiency max for hybrid collectors was greater under outdoor circumstances than in laboratory conditions.
[18]	hybrid PVT	The increase in temperature indicated that the PV cells had heated up, and the drop in coolant temperature suggests that the coolant flow had increased. Additionally, the power and global

		efficiency of hybrid panels are higher than those of simple panels, but their thermal output is lower than that of simple panels.
[19]	semi-transparent photovoltaic (STPV) 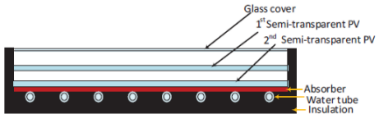	While this design achieved 20.76%, 65.7%, and 86.5%, respectively, recent advancements in PVT efficiencies offer thermal, electrical, and total efficiency of 54.6%, 13.8%, and 68.4%.
[20]	ea of heat transfer 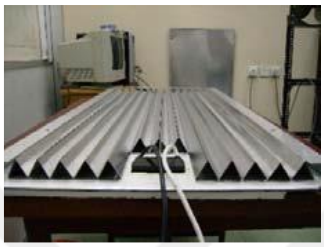	The improvement was 15.7–42.8% between the thermal efficiencies with and without the enlarged area, which were 21–83% and 12-70%, respectively. For PVT air systems with enlarged heat transfer areas, the energy and exergy efficiencies were 39%–94% and 12.66%–12.91%, respectively.
[21]	three-dimensional systems of PVT 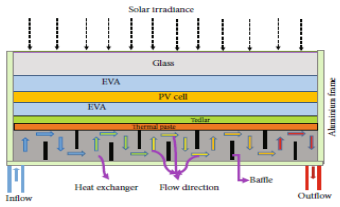	Input temperatures increased by 0.54°C, thermal energy increased by 113.3 W, electrical energy increased by 20.7 W, and cell values increased by 2.17 W/m^2 and were reduced by 0.83, 0.67, and 0.17%, respectively, as a result of the rise in 100 W/m^2 irradiance.
[22]	floating collector systems (FPV)	When FPV systems were compared to conventional terrestrial systems, efficiency rose by 1.58 to 2.00%.
[23]	PVT with air 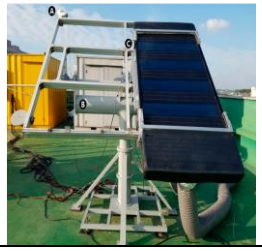	When airflow increases from 60 to 200 m^3/h, the thermal efficiency of the collector rises from 29 to 42%, and the electrical efficiency was also calculated and developed in accordance with operational circumstances.
[24]	PVT with air medium  air collector with mono-crystalline designed.	Wormed air from the collector's air base was around 5°C warmer than outside air. Additionally, the corresponding electrical and thermal efficiencies were 15% and 22%, respectively.
[25]	water and (Fe_3O_4-water) PVT	Therefore, when the alternating field frequency is 50 Hz, employing 3 wt% ferrofluid, the efficiency rises by 45%, and the overall efficiency is 50%.

	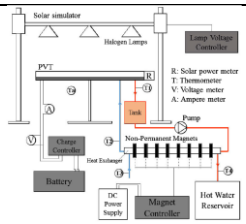 ferrofluid PVT system (consisting of a combined PV module and an absorber collector)	
[26]	semiconductor PVT 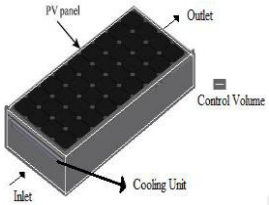	The PV cell's ideal operating range was between 40 and 60°C, where there was a 20% boost in electrical efficiency.
[27]	PVT with Microencapsulated-Phase Change Material (MPCM) 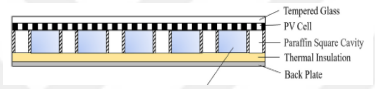	The outcome showed that a 395 W commercial panel could increase output power to 49.4 W (14.29%) at irradiance intensities of 1000 W/m^2 and ambient temperatures of 35°C.
[28]	PV (Al_2O_3) nanofluid 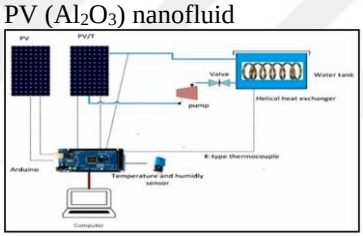	The total efficiency improvement was 15% at 1 g of nanofluid but increased to 18% at 1.5 g, and the thermal efficiency was 19% and 27% at 1 g and 1.5 g of nanofluid, respectively.
[29]	Nanofluids (PV) 	At 0.5 and 1.0 LPM flow rates, respectively, water improves average electric efficiency (7.8 and 8.5%) and thermal efficiency (24.9 and 26.3%).
[30]	Forced air PVT 	When air volume changed from 335 to 760 m^3/h, driven air reduced PV temperature from 16 to 5°C. At 760 m^3/h, the biggest increases in power and efficiency were 8.2% and 17.9%, respectively.
[31]	heat sink water-cooled PVTS	As the temperature of the PV grew from 65 to 73°C, the irradiation climbed from 500 to 960 W/m^2, and the output power increased from 35 to 55 W.

	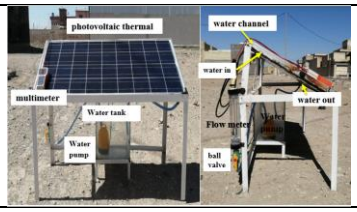	
[32]	floating-photovoltaic 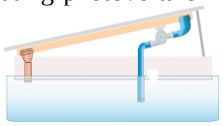  lightweight and minimally invasive cooling system	The outcome showed that a 395 W commercial panel could increase output power to 49.4 W (14.29%) at irradiance intensities of 1000 W/m^2 and ambient temperatures of 35°C.
[33]	Fins as Heat Sink FPV 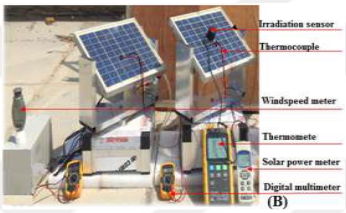	The cooling techniques used by solar panel fins (heat sinks) have an impact on the generation of current and voltage, increasing average output power by 15.3% and 19.3%, respectively.
[34]	PVT 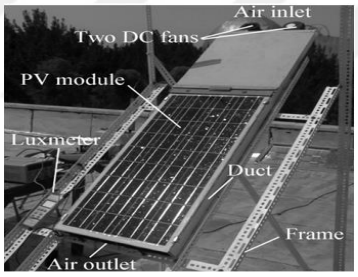	Raising the settings causes a drop in thermal efficiency. The following factors must be considered: packing factor, channel depth, inlet mass flow rate velocity, thermal resistance, inlet temperature, wind speed, mass flow rate, heat loss coefficient, ambient temperature, tilt angle far from latitude, duct length, and insulation. Temperature Conduction.
[35]	photovoltaic thermal	There is good agreement between theoretical and practical data, and electrical output rose as solar cells cooled, making PVT systems more useful for concurrently generating thermal and electric energy.
[36]	grid-tied PV 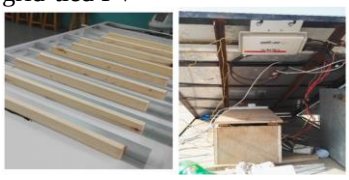	It was discovered that energy rose by 10.2% and 7% compared to non-cooling collectors, and that the performance ratio improved up to 84% and 81% because of the low temperatures of cooling systems. Nevertheless, 77% for non-cooling.
[37]	two PV panels	In the basin under P1, where 17% of the water surface area was covered, the water level was kept at 7.5 cm. Additionally, this results in an increase in average efficiency of 17.22% relative and 2.72%

	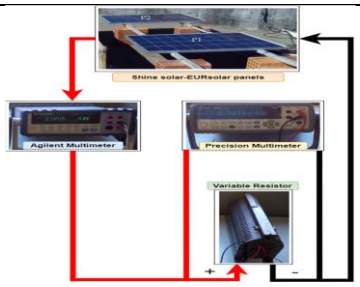	absolute, while the P1 temperature decreased by 2.7˚C. Additionally, it demonstrated a 30% decrease in water evaporation between the water with and without the panel.
[38]	photovoltaic water system based on exergy losses 	There is good agreement between experimental data and numerical simulations, and the updated exercise efficiency is shown to be without flaws by comparing it to earlier work and showing exercise loss terms in the PVT collector directly.
[39]	direct expansion assisted PVT heat pump 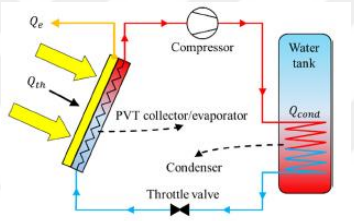	Temperature distribution was better on the roll bond evaporator with hexagon and rectangle patterns than on the linear and grid kinds.

2.5. AIM OF STUDY

The purpose of this study is to improve the photovoltaic collector system by improving the electric energy that it produces from the photocell, which leads to an improvement in the total efficiency of the system. There are many concepts that should be taken into account in the calculations and instructions of the collector, including the type of cell (silicon material), cooling material, position of the collector, angle of inclination, situation of the weather, and many other things to reach the optimum case of operation. The rise in sustainable living has led to the use of renewable energy sources for hot water consumption. A water collection system, an insulated pipe network, and storage tanks are used to harvest and distribute hot water throughout residential spaces. The lake is harvested through rooftop gutters and downspouts, and the collected water is directed into insulated storage tanks. An insulated pipe network connects these tanks to residential spaces, providing a

sustainable hot water source. Solar water heaters are integrated to reduce reliance on conventional energy sources. A well-designed pump system ensures consistent hot water flow, and the system aligns with sustainability goals and local regulations, contributing to a greener living environment. In addition, it will use dimpled tubes to increase the process of heat transfer and cooling of the solar panel to obtain the largest amount of heat exiting the tube and high electrical efficiency, three dimple diameters were used: 2, 4, and 6 mm to obtain the best thermal discharge process.

PART 3

NUMERICAL ANALYSIS

In this chapter, all the basic equations through which the results were obtained from within the numerical aspect, as well as the programs and settings required to obtain accurate and reliable results, will be reviewed.

3.1. COMPUTATIONAL ANALYSIS USING ANSYS PACKAGE

Solar radiation dynamics studies are being conducted to develop more in-depth knowledge of renewable energies. To explain the effect of the lake water in cooling the solar panels, the k-ε flow model is used. Accordingly, the mathematical ordering methods will process the Cartesian direction frames (x, y, and z). 3D geometry was created.

ANSYS 19.1 [40] will be used to generate and link the framework mathematics and then to reproduce a single case.

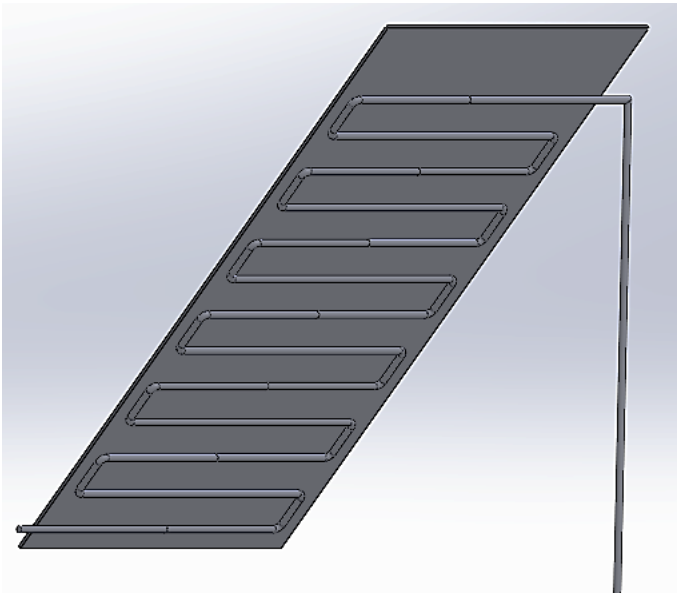

Figure 3.1. Problem geometry.

As shown in Figure 3.2, which shows the use of dimpled tubes to increase the process of heat transfer and cooling of the solar panel to obtain the largest amount of heat exiting the tube and high electrical efficiency, three dimple diameters were used: 2, 4, and 6 mm to obtain the best thermal discharge process. The model select for turbulence mode is k-e standard. Where a group of thermal radiation couplings were used, which were formed as a result of the options available in the ANSYS program, which represents system coupling, Ross land, P1, S2S, DO.

Figure 3.2. Dimpled tube geometry.

3.1.1. Governing Equations

Continuity equation [40]:

$$\nabla \cdot \vec{V} = 0$$

(3.1)

Momentum equation [40]:

$$\frac{\partial \vec{\mathrm{V}}}{\partial \mathrm{t}} + \vec{\mathrm{V}} \cdot \nabla \vec{\mathrm{V}} = \frac{1}{\rho}\left(-\nabla \mathrm{P} + \mu \nabla^2 \vec{\mathrm{V}} + \rho \vec{\mathrm{g}} \beta (\mathrm{T} - \mathrm{T}_{\mathrm{ref}})\right) + S_m$$

(3.2)

Energy equation [40]:

$$\frac{\partial h_{\mathrm{sens}}}{\partial t} + \frac{\partial h_{\mathrm{lat}}}{\partial t} + \nabla \cdot \left(\vec{V} h_{\mathrm{sens}}\right) = \nabla \cdot \left(\frac{k}{\rho c_p} \nabla h_{\mathrm{sens}}\right)$$

(3.3)

Both emitted and reflected energy contribute to the total energy flow exiting a surface. The incident energy flux from the environment is a necessary condition for the reflected energy flux, which may be written in terms of the energy flow departing from all other surfaces. Exiting energy from surface k is [40]:

$$q_{\text{out},k} = \varepsilon_k \sigma T_k^4 + \rho_k q_{in,k} \tag{3.4}$$

where $q_{in,k}$ is the energy flow incident on the surface from the surroundings and $q_{out,k}$ is the energy flux exiting the surface. The Stefan-Boltzmann constant is 5.6×10^{-8} kg. s^{-3}. K^{-4}.

The view factor F_{kj} between two surfaces is directly proportional to the quantity of incoming energy on the receiving surface. To calculate how much energy from surface j is incident on surface k, we use the view factor, F_{kj}. Mesh faces or (in 3D scenarios only) clusters of faces may be used to determine a view factor. The total energy exiting all surfaces may be represented as a function of the incident energy flux, $q_{in,k}$ [40].

$$A_k q_{in,k} = \sum_{j=1}^{N} A_j q_{\text{out},j} F_{jk} \tag{3.5}$$

where A_k is the area of surface k and F_{jk} is the view factor between surface k and surface j. For N surfaces, using the view factor reciprocity relationship gives [40]

$$A_j F_{jk} = A_k F_{kj} \text{ for } j = 1,2,3, \ldots N \tag{3.6}$$

so that [40]

$$q_{in,k} = \sum_{j=1}^{N} F_{kj} q_{\text{out},j} \tag{3.7}$$

Therefore [40],

$$q_{out,k} = \varepsilon_k \sigma T_k^4 + \rho_k \sum_{j=1}^{N} F_{kj} q_{out,j} \tag{3.8}$$

which can be written as [40]:

$$J_k = E_k + \rho_k \sum_{j=1}^{N} F_{kj} J_j \tag{3.9}$$

surface k's emitted energy, denoted by J_k., and its emissive power, denoted by E_k. This stands for N equations, which may be expressed as a matrix using the following notation [40]:

$$KJ = E \tag{3.10}$$

where K is a $N \times N$ matrix, J is the radiosity vector, and E is the emissive power vector. Referred to as the radiosity matrix equation, the view factor between two finite surfaces i and j is given by [40]:

$$F_{ij} = \frac{1}{A_i} \int_{A_i} \int_{A_j} \frac{\cos\theta_i \cos\theta_j}{\pi r^2} \delta_{ij} dA_i dA_j \tag{3.11}$$

where δ_{ij} is determined by the visibility of dA_j to dA_i. $\delta_{ij} = 1$ if dA_j is visible to dA_i and 0 otherwise [40].

3.1.2. Radiation Model Equations

The energy flux leaving a given surface is composed of directly emitted and reflected energy. The reflected energy flux is dependent on the incident energy flux from the surroundings, which can then be expressed in terms of the energy flux leaving all other surfaces. The energy leaving the surface *k* is [41]:

$$q_{\text{out } k} = \varepsilon_k \sigma T_k^4 + \rho_k q_{ink} \tag{3.12}$$

where $q_{\text{out } k}$ is the energy flux leaving the surface, ε_k is the emissivity, σ is the Stefan-Boltzmann constant, and q_{ink} is the energy flux incident on the surface from the surroundings.

The amount of incident energy upon a surface from another surface is a direct function of the surface-to-surface "view factor," F_{jk}. The view factor F_{jk} is the fraction of energy leaving surface j that is incident on the surface k. The surfaces used in the calculation of a view factor can be mesh faces or (for 3D cases only) clusters of faces. The incident energy flux q_{ink} can be expressed in terms of the energy flux leaving all other surfaces as [41]:

$$A_k q_{ink} = \sum_{j=1}^{N} A_j q_{\text{out},} F_{jk} \tag{3.13}$$

where A_k is the area of surface k and F_{jk} is the view factor between surface k and surface j. For N surfaces, using the view factor reciprocity relationship gives [41]:

$$A_j F_{jk} = A_k F_{kj} \text{ for } j = 1,2,3, \dots N \tag{3.14}$$

so that [41]:

$$q_{inkk} = \sum_{j=1}^{N} F_{kj} q_{\text{out},j} \tag{3.15}$$

Therefore [41],

$$q_{\text{out},k} = \varepsilon_k \sigma T_k^4 + \rho_k \sum_{j=1}^{N} F_{kj} q_{\text{out},j} \tag{3.16}$$

which can be written as [41]

$$J_k = E_k + \rho_k \sum_{j=1}^{N} F_{kj} J_j \tag{3.17}$$

where J_k represents the energy that is given off (or radiosity) by the surface k, and E_k represents the emissive power of the surface k. This represents N equations, which can be recast into matrix form as [42]:

$$KJ = E \tag{3.18}$$

where K is a $N \times N$ matrix, J is the radiosity vector, and E is the emissive power vector. The view factor between two finite surfaces i and j is given by [42]:

$$F_{ij} = \frac{1}{A_i} \iint_{A_i} \int_{A_j} \frac{\cos\theta_i \cos\theta_j}{\pi r^2} \delta_{ij} dA_i dA_j \tag{3.19}$$

where δ_{ij} is determined by the visibility of dA_j to dA_i. $\delta_{ij} = 1$ if dA_j is visible to dA_i and 0 otherwise.

The P1 model simplifies the radiative transfer equation (RTE) by making the assumption that the radiation field is isotropic in all directions within each control volume. The model under consideration exhibits a level of simplicity that renders it appropriate for certain technical applications, yet it may not adequately account for directional effects. The Discrete Ordinates Method (DOM) involves the discretization of the angular space into a finite number of discrete directions, known as ordinates. This method then proceeds to solve the radiative transfer equation (RTE) numerically for each of these directions. This method is well-suited for addressing challenges involving intricate geometries and scattering phenomena characterized by anisotropy. The Finite Volume Method (FVM) is a numerical technique that involves discretizing the domain into control volumes and employing a finite volume approach to solve the Radiative Transfer Equation (RTE). The utilization of this approach is frequently observed in commercial computational fluid dynamics (CFD) software owing to its resilience and precision. The Monte Carlo method is a computational technique that models the behavior of individual photons inside a given region, accurately tracing their interactions with matter. The method exhibits a high level of accuracy, albeit at a significant computing cost, rendering it mostly suitable for research and benchmarking endeavors. Spectral radiation models are employed when there is a substantial variation in the radiation properties of materials with respect to wavelength. These models incorporate the wavelength-dependent characteristics of radiation. Two often used spectrum models in the field of radiation are the discrete spectral radiation model and the statistical narrow-band model. View factor models are commonly employed in the calculation of radiative exchange across surfaces within a given region. The researchers ascertain the proportion of radiation emitted by a certain surface that is intercepted by another

surface. Participating media models encompass the consideration of radiative transfer within media that exhibit absorption, scattering, and emission of radiation. The category encompasses models pertaining to the radiation of soot in combustion processes as well as the radiation of gas in confined areas. Non-gray radiation models are utilized in situations where the radiation characteristics of a medium exhibit wavelength dependency. These models take into account a spectrum of wavelengths and their corresponding interactions. The selection of a radiation model is contingent upon the particular situation being simulated, encompassing factors such as geometric considerations, material properties, and temperature variations. When choosing a radiation model, it is imperative to take into account both processing resources and the accuracy of the simulation. Sophisticated models have the potential to yield improved accuracy, albeit at the expense of increased computing requirements.

3.1.2.1. Rossland

The average opacity over a wide range of frequencies and is given by [43]:

$$\frac{1}{\kappa_R} = \frac{1}{\kappa_e} + \frac{1}{\kappa_{ff}} + \frac{1}{\kappa_{bf}} \tag{3.20}$$

where:

- κ_e is the electron scattering opacity,
- κ_{ff} is the free-free (Bremsstrahlung) opacity,
- κ_{bf} is the bound-free (bound-free transitions) opacity.

Rosseland Mean Opacity Coefficient (K_R): This coefficient is related to the Rosseland mean opacity and is defined as [43]:

$$\frac{1}{K_R} = \int_0^\infty \frac{1}{\kappa_R(T,\nu)} \frac{\partial B_\nu(T)}{\partial T} d\nu \tag{3.21}$$

where:

- $B_\nu(T)$ is the Planck function,

- T is the temperature.

3.1.2.2. P1 (Non-Gray Model)

The P1 model simplifies the RTE to a single equation for the radiation intensity [43]:

$$\frac{1}{c}\frac{\partial I}{\partial t} + \mathbf{\Omega} \cdot \nabla I = -\kappa I + \kappa \frac{B}{\pi} \tag{3.22}$$

where:

- c is the speed of light,
- I is the radiation intensity,
- Ω is the direction of propagation (unit vector),
- κ is the absorption coefficient,
- B is the Planck function.

The P1 model uses a closure relation to relate the radiation intensity I to the radiation flux [43]:

$$\mathbf{F} = -D\nabla B \tag{3.23}$$

where:

- $\mathbf{F}$ is the radiation flux,
- D is the diffusion coefficient.

3.1.2.3. S2S (Surface to Surface Model)

The $S2S$ model expands the radiation intensity I in terms of spherical harmonics $Y_{lm}(\theta, \phi)$ [44]:

$$\frac{1}{c}\frac{\partial I_{lm}}{\partial t} + \mathbf{\Omega} \cdot \nabla I_{lm} = -\kappa I_{lm} + \kappa \frac{B_{lm}}{4\pi} \tag{3.24}$$

where:

- c is the speed of light,

- I_{lm} is the radiation intensity in terms of spherical harmonics,
- Ω is the direction of propagation (unit vector),
- κ is the absorption coefficient,
- B_{lm} is the spherical harmonic expansion of the Planck function.

Spherical Harmonic Expansion: The radiation intensity I is expanded as [44]:

$$I(\mathbf{r}, \mathbf{\Omega}, t) = \sum_{l=0}^{\infty} \sum_{m=-l}^{l} I_{lm}(\mathbf{r}, t) Y_{lm}(\theta, \phi) \quad (3.25)$$

where $Y_{lm}(\theta, \phi)$ are the spherical harmonics.

3.1.2.4. DO (Discrete Model)

For each discrete direction $\mathbf{\Omega}_k$ (where k indexes the directions) [45]:

$$\frac{1}{c}\frac{\partial I_k}{\partial t} + \mathbf{\Omega}_k \cdot \nabla I_k = -\kappa I_k + \kappa \frac{B_k}{\pi} \quad (3.26)$$

where:

- c is the speed of light,
- I_k is the radiation intensity in direction Ω_k,
- κ is the absorption coefficient,
- B_k is the Planck function evaluated at temperature and frequency corresponding to direction Ω_k.

3.1.3. ANSYS Package

The stream conditions are addressed by utilizing two modules:

- The essential module is the preprocessor module; a program structure that makes the calculation and matrix as in the accompanying:
  a) Modeling of calculations.
  b) Mesh number.
  c) Boundary condition.

- The second module is the Solution module, for settling Navier-Stokes conditions (which incorporate progression, force, and energy conditions), as well as the violent stream model.

3.1.4. Problem Geometry

A three-dimensional model was designed as a PV panel with a width of 0.99 m, a length of 1.64 m, and a thickness 4.8 mm. As for the pipes, copper pipes with a diameter of 10 mm and a height of 2 m above lake level were used. The dimensions of the solar panels currently on the market are these dimensions.

3.1.5. Mesh Generation

Generally, because unstructured grids work well for complicated geometries, the unstructured tetrahedron grids were chosen in the current investigation. ANSYS supports solid geometry mesh generation and three-dimensional models with minimum input from a single phase from the user. The number of cells taken in this study was 482868; see Figure 3.3.

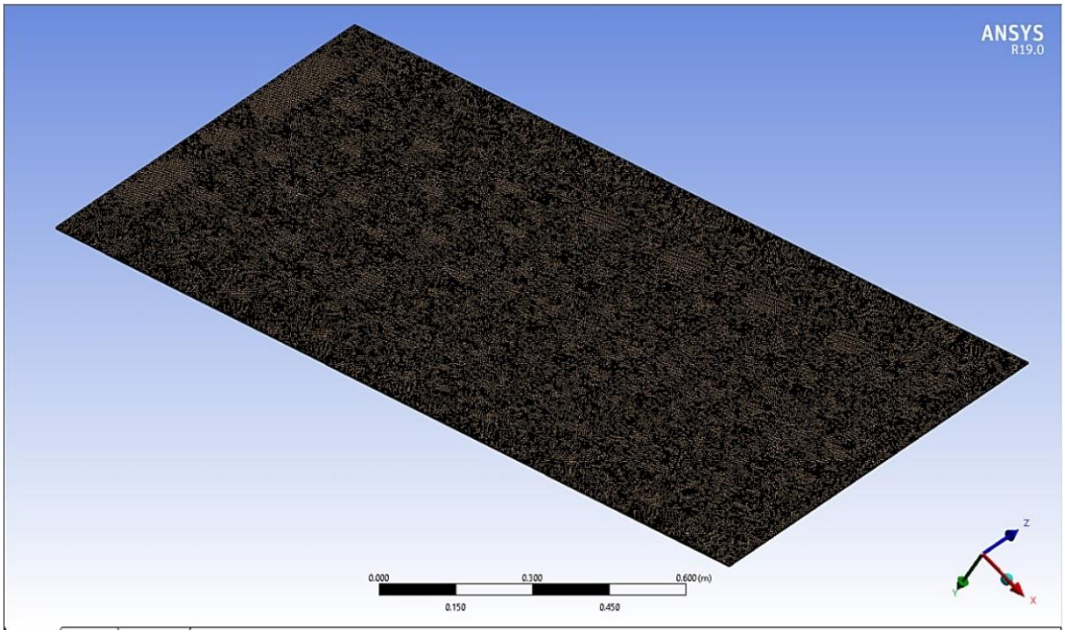

Figure 3.3. Generated mesh.

In order to obtain accurate and reliable results, a mesh independence must be made to see the clear change when changing the number of the element and the output results, as it stops when the stability of the output results is reached, where the element size is 0.005 m.

Table 3.1. Mesh independency.

Case	Element	Max. temperature (°C)	Change (%)
1	103633	33.75	
2	261431	33.18	-1.69
3	374433	33.13	-0.15
4	482868	33.12	-0.03

3.1.6. Boundary Conditions

Where the FSI system was used. Where the pipe enters the CFD system. Numerical simulation is done for it at different inlet velocities of 0.1, 0.5, and 1 m/s, the Reynolds numbers of 1123.6, 5618, 11236 [46], and at inlet temperatures, which are lake temperatures of 6, 9, and 12°C [47]. The selection of these velocities of 0.1, 0.5, and 1 m/s represents the range of pumps that are used in such cases. In addition, the selection of these temperatures of 6, 9, and 12°C represents the temperatures of lakes in the months of the study. The summer season was studied as a variable for lake temperature, where an inlet temperature of 26°C was used, representing the lake temperature and a variable inlet velocity.

Lakes in northern Iraq or those with groundwater feeds approach these lower temperatures during colder months or due to specific environmental conditions. Lake Sawa in southern Iraq is a unique water body. The lake is facing significant environmental challenges, including drying up in recent years due to climate change and mismanagement, which affects its ability to support consistent water levels and temperatures. For sustained lake temperatures in the range of 6°C to 12°C, northern

Iraq, specifically in the Kurdistan Region, offer colder bodies of water during winter months, particularly in elevated regions with mountainous terrain where groundwater lakes and reservoirs can exhibit these lower temperatures.

Lakes with water temperatures of 6°C, 9°C, or 12°C are likely to be found in cooler or higher-altitude regions of Turkey, particularly during specific seasons, such as:

- **Lake Van**: The largest lake in Turkey, located at a high altitude (about 1,640 meters above sea level), have cooler waters in spring, autumn, or at greater depths.
- **Lake Çıldır**: Located in the eastern part of Turkey, close to the Armenian border, this high-altitude lake (about 1,959 meters) often has cold water temperatures, particularly in late autumn, winter, and early spring.
- **Lake Abant**: Situated in Bolu Province in northwestern Turkey, this lake is in a mountainous region and is known for having cooler temperatures.
- **Lake Beyşehir**: The largest freshwater lake in Turkey, located in Central Anatolia, have such temperatures depending on the depth and the season.

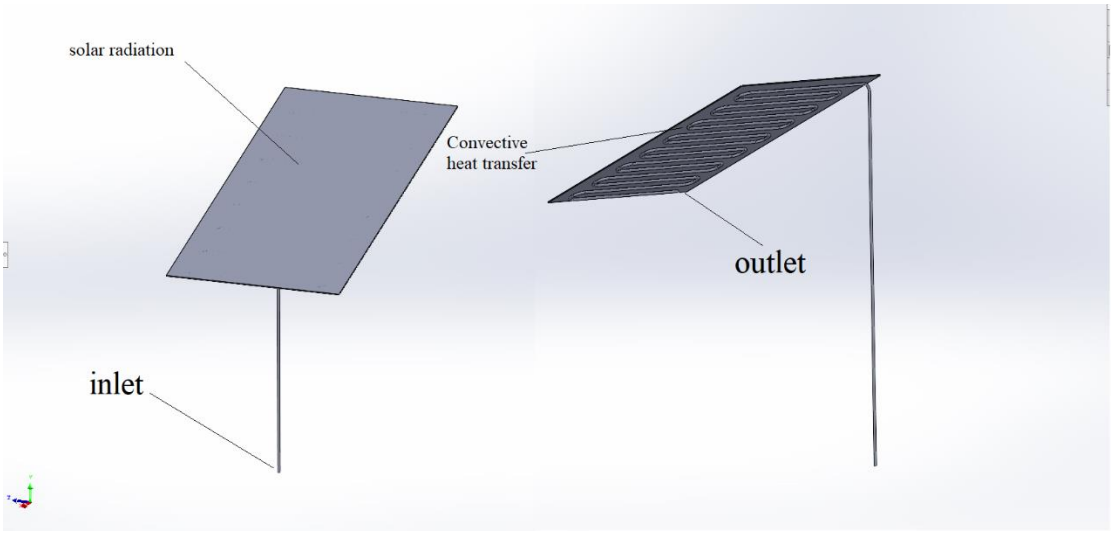

Figure 3.4. Conditions of the boundary.

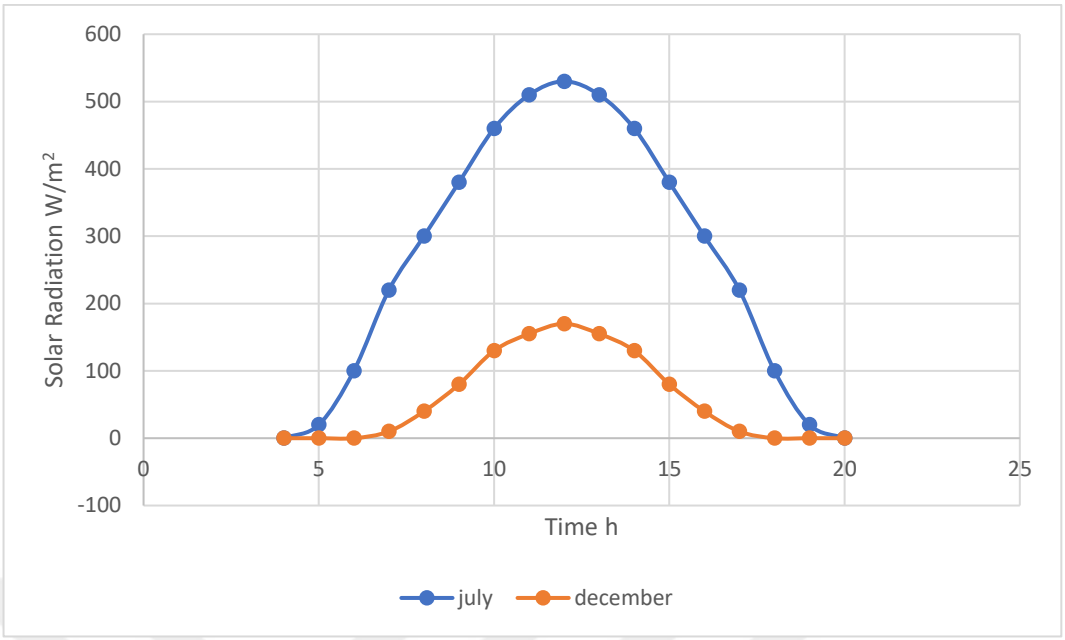

Figure 3.5. Solar radiation.

These two months were taken because they contain the worst climatic conditions in the winter and summer seasons.

Then moving to the solar panel, which is simulated by the transient thermal model to simulate the temperatures of the incident solar radiation, which are in two months, July and December, as in Figure 3.5.

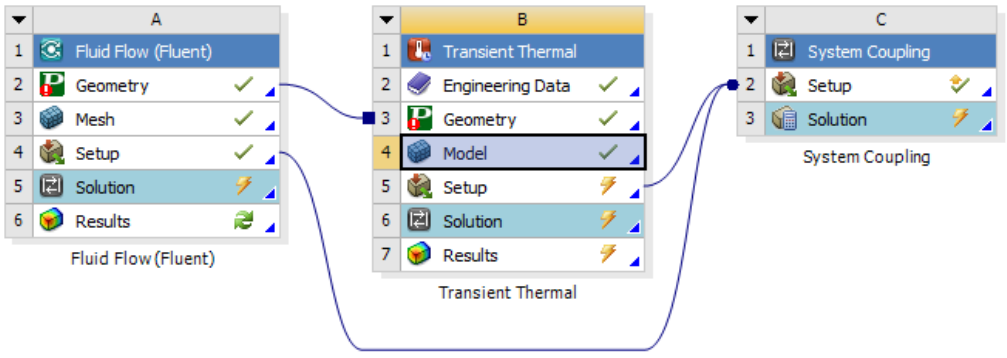

Figure 3.6. System coupling.

3.1.7. Problem Solution

A volume of the control-dependent technique that comprises the accompanying advances, which can be utilized for arrangement:

- A network is created on the field.
- Sets of conditions like speed, pressure, and preserved scalars are mathematically built by the combination of each control volume of the administering conditions.
- The discretized equations are linearized and tackled iteratively.

3.1.8. Solution Parameters

The solution parameters include the following

3.1.8.1. Precision Solver Type

Ordinarily, accuracy solvers are found by single and twofold as it were. On a PC with limitless accuracy, residuals would go to zero as the arrangement combined. In a genuine PC, the residuals rot to some little worth (“adjust”) and afterward end up changing (“level out”).

3.1.8.2. Iteration

This is the highest digit of iterations done before the solver terminates.

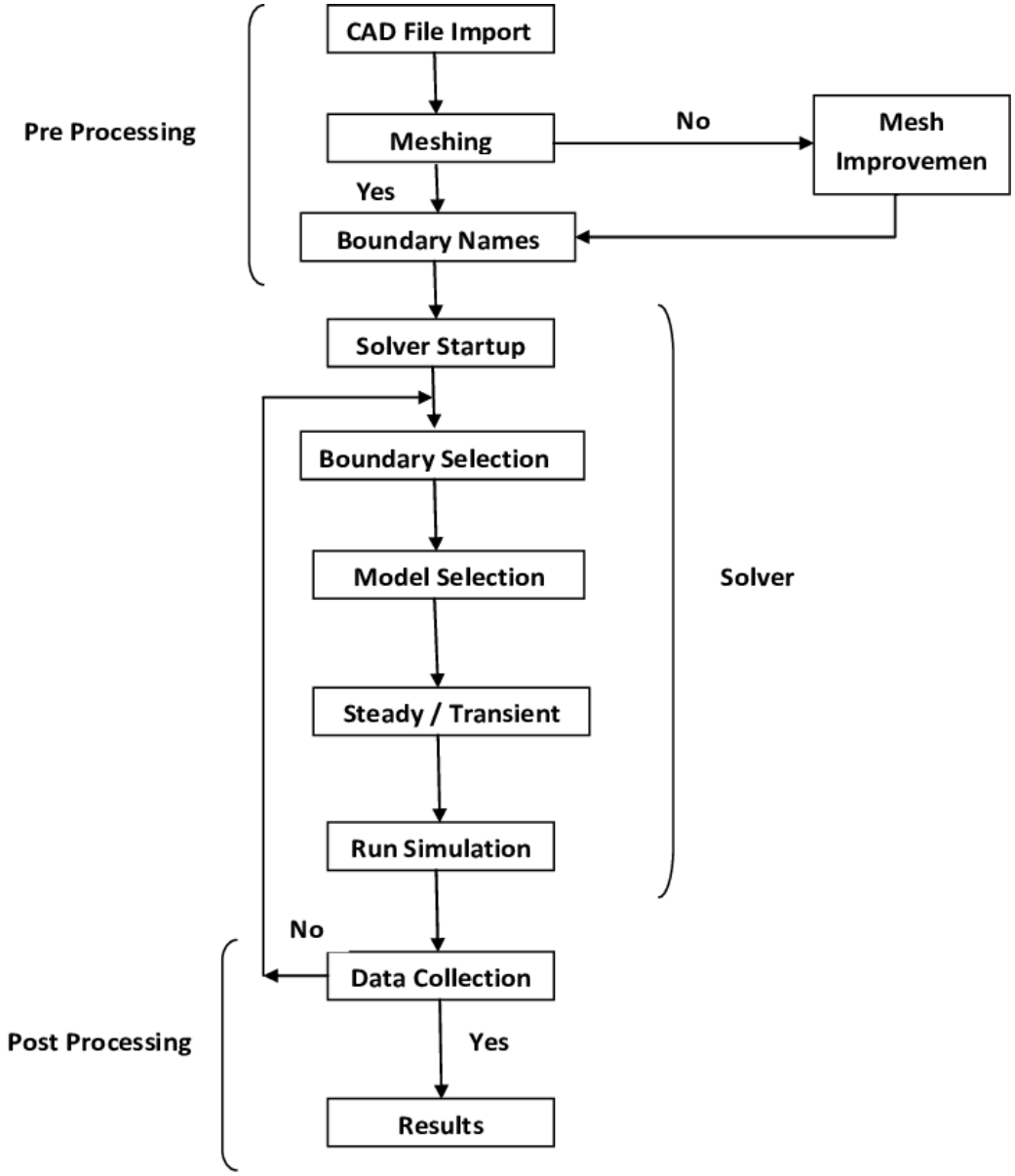

Figure 3.7. Flow chart of simulation in Ansys program.

3.1.8.3. Convergence Criteria

The CFD method requires emphasizing the arrangement of the liquid stream conditions until they are met. The emphases are halted when the arrangement continues as before within the exactness of the chosen intermingling models. The most commonly utilized strategy to check arrangement combinations is the mistake residuals, which is the contrast between the upsides of a variable in two continuous emphases standardized by the biggest outright leftover for the initial five cycles. The

arrangement is supposed to be united when the residuals are under a resilience breaking point of 10^{-6} for all the liquid stream conditions introduced previously.

3.2. MATLAB SIMULINK EQUATIONS

Many factors affect the photovoltaic panel's ability to convert sunlight into power. In this simulation analysis, focus on the two most critical parameters: solar irradiance and panel temperature. Panel voltage and power were found to vary in response to variations in radiation and temperature. During the simulation, the maximum power of the PV module was determined using experimental and formulation relations between the properties of the PV module (Voc, Isc, Temperature. And Power). Parameters for a photovoltaic panel may be calculated using its electrical equivalent diagram. Which includes equations for the panel's output current (I), its dark saturation current (Ios), and its generating current (Ilg) [48].

$$I = I_{LG} - I_{OS}\exp\left(\frac{q}{nkT_P}\left(V + IR_f\right)\right) - 1\Big] - \frac{V+IR_S}{R_{SH}} \qquad (3.27)$$

$$I_{OS} = I_{OS}\left(\frac{T_P}{T_R}\right)^3 \exp\left[\frac{qE_{GO}}{Ak}\left(\frac{1}{T_R} - \frac{1}{T}\right)\right] \qquad (3.28)$$

$$I_{LG} = [I_{SCR} + K(T_P - 25)]G/100 \qquad (3.29)$$

where; ILG is light current, Ios is reverse saturation current in a pin diode, R_s is series resistance to the cell, RSH is shunt resistance, measured by Ω, and N is the number of cells. K is Boltzmann's constant = $1.381\cdot10^{-23}$ J/K, q is electron charge = $1.602\cdot10^{-19}$ coulomb, and n is the factor of an ideal diode = 1 and 1~2 for a real diode. Finally, qE is the band gap energy of silicon. The figure (3.8) below shows the equivalent circuit of a photovoltaic cell [48].

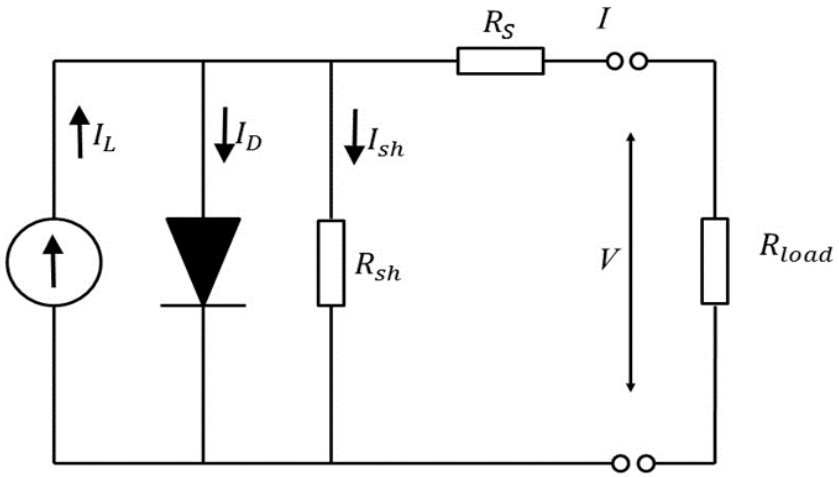

Figure 3.8. Equivalent electrical-circuit for a PV module.

The I-V characteristic curve of a solar cell with a constant cell temperature, T-P, is seen in Fig. 3.9. PV cell current is proportional to the external voltage supplied and the quantity of sunlight falling on the cell. There is no voltage across a cell when it is short-circuited, but the current is at its highest possible value (short-circuit current, I_{SC}). Voltage is highest (open circuit voltage, V_{OC}.), and current is zero when the PV cell circuit is open, with the leads not constituting a circuit [48].

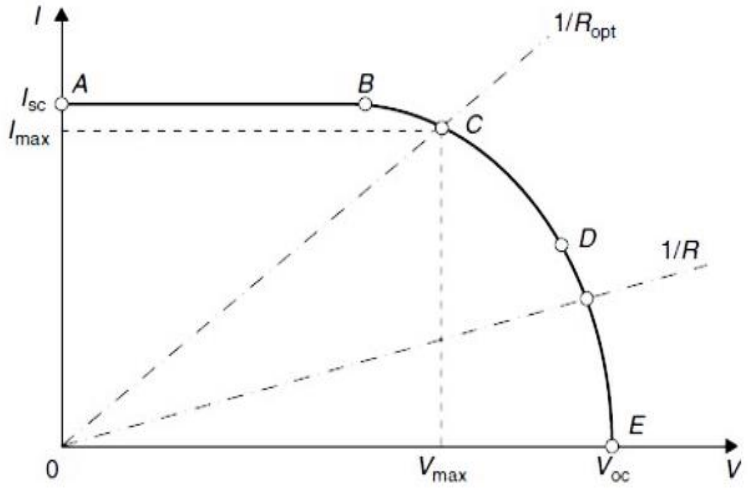

Figure 3.9. Representative current-voltage curve for photovoltaic cells.

The operational point of a solar cell is found at the point where its IV characteristic intersects with the load IV characteristic, which is a function of the variable resistance, R, linked to the cell's terminals. The load characteristic for a resistive load is a straight line with a slope 1/V = 1/R. Cells act as a continuous current source, almost equivalent to the short-circuit current, in the area AB of the curve when the load resistance is low. However, if the load resistance is high, the cell runs in the DE area of the curve, where it more closely resembles a constant voltage source with an output voltage that is practically identical to the open circuit voltage. The maximum power point, or P-max, is the operational point when the output power is at its highest, and it corresponds to point C [48].

$$P_{\max} = I_{\max} V_{\max} \tag{3.30}$$

$$P_{\max} = I_{sc} V_{oc} FF \tag{3.31}$$

$$FF = \frac{P_{\max}}{I_{sc} V_{oc}} \tag{3.32}$$

When the produced current is zero, the open circuit voltage is equal to the voltage drop across the diode caused by the photocurrent, I_{LG}. In other words, V_{OC}. Can be determined by solving this problem [48].

$$V_{oc} = \frac{kT_R}{e} \ln\left(\frac{I_{sc}}{I_o} - 1\right) = V_t \ln\left(\frac{I_{sc}}{I_o} + 1\right) \tag{3.33}$$

where V_t – thermal voltage (V) given by

$$V_t = \frac{kT_R}{e} \tag{3.34}$$

The manufacturer's specifications for the PV array, as well as the array's published or measured I-V curves, may be used to calculate all of the constants in the aforementioned equations. To get the results of this experiment, MATLAB and

Simulink are utilized with these formulas. The photovoltaic effect of semiconductor material is the basis of the photovoltaic cell hypothesis. Solar energy is converted into electrical energy by a process known as the photovoltaic effect, in which an electron and a hole are dug from a semiconductor material by a photon. The $\mathrm{I}-\mathrm{V}$ characteristic of the photovoltaic cell changes with the sunshine intensity $G(\mathrm{W/m^2})$ and cell temperature $t(^{\circ}\mathrm{C})$, that is $I = f(V.G.t)$.

Testing data for PV modules' temperatures and open-circuit voltages are linearly related, as shown by [48]:

$$V_{OC} = 22.384 - 0.0627T_P \tag{3.35}$$

Where $\mathrm{T_P}$ is in $^{\circ}\mathrm{C}$.

In addition, the linearity between solar radiation (G) and short circuit current $(\mathrm{I_{SC}})$ data is represented by [48]:

$$I_{SC} = 0.0967 + 0.0032G \tag{3.36}$$

Where G is in $\mathrm{W/m^2}$.

These are empirical equations of previous works [43]

The electrical efficiency (η) of a photovoltaic (PV) panel can be calculated using the following equation [48]:

$$\eta = \frac{P_{\text{out}}}{P_{\text{in}}} \times 100\% \tag{3.37}$$

where:

- P_{out} is the electrical power output of the PV panel (measured in watts, W).
- P_{in} is the solar power input to the PV panel (measured in watts, W).

The solar power input P_{in} is determined by the solar irradiance (E) and the area (A) of the PV panel [48]:

$$P_{in} = E \times A \quad (3.38)$$

where:

- E is the solar irradiance, usually measured in watts per square meter $(\mathrm{W/m^2})$. Standard test conditions (STC) often use $1000\ \mathrm{W/m^2}$.
- A is the area of the PV panel in square meters $(\mathrm{m^2})$.

Figure 3.10 represents the icons used in MATLAB Simulink to realize the electrical and thermal circuit of the system.

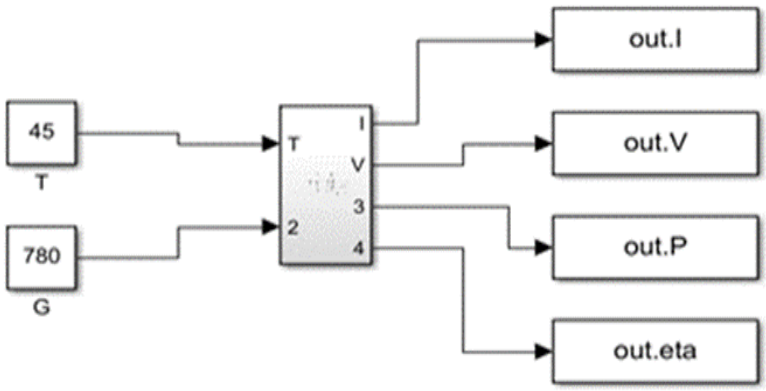

(a)

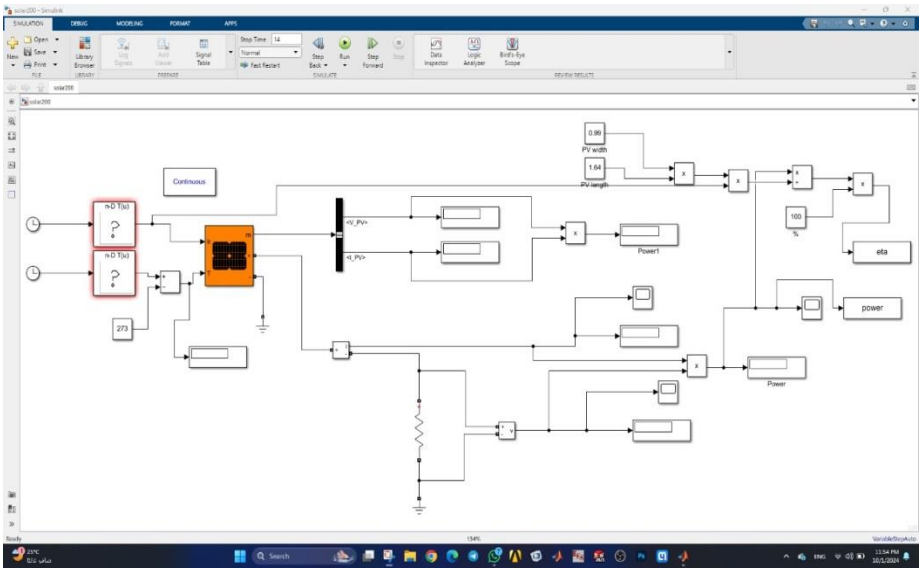

(b)

Figure 3.10. Simulink programing of (a) PV block and (b) full system.

Table 3.2. Jinko solar PV module.

Nominal efficiency	14.5%
PV module rating	450W
Maximum power voltage	36.8V
Maximum power current	7.61A
Open circuit voltage	43.8V
Short circuit current	8.52A
Weight	26 kg

PART 4

RESULTS AND DISCUSSION

In this chapter, the results obtained through the simulation program of temperature, pressure, and fluid velocity diagrams will be reviewed. The results obtained through the Simulink program will also be reviewed with regard to the electrical aspect of the system, and the obtained energy and electrical efficiency will be reviewed.

4.1. VALIDATION

The influence of cell temperature on the performance and efficiency of a three-layer solar cell is explored in this study using a three-dimensional CFD model. A serpentine circular pipe has been installed beneath the aluminum plate and utilized as a heat exchanger to transport heat from the solar cell to the pipe fluid, lowering the temperature of the photovoltaic cell. When adopting the water-cooling approach, the solar electricity efficiency improved by around 10%. It was compared with it, and similar results were obtained with a 1% error.

The figure illustrate the temperature variation on the surface of the PV cells where the right side is hotter while the left side is cooler. The effect of Reynolds number is also considered where low Reynolds numbers and correspondingly low rates of heat transfer and pronounced temperature gradients along the plate length.

The results presented herein reveal that the convective heat transfer rate enhances with the Reynolds number so that cooling is enhanced. As the process progresses the color gradient appears to be more evenly spread showing that the heat distribution is smoother over the surface. At Reynolds numbers of 8000 and 10000, there is an enhancement in cooling performance with surface temperature becoming more bluish in appearance, thus implying efficient cooling especially at Re = 10000.

A comparison of the current work and Salim et al.'s [49] numbers reveals that both sets of results indicate that the higher the Reynolds number the better the cooling. Nevertheless, Salim et al.'s simulations show that the temperature difference across the PV surface is slightly smaller and it can be inferred that their setup achieves slightly better cooling performance. Nevertheless, in the highest Reynolds number cases (Re=10000 and 12000), both sets of results yielded good cooling performance with almost negligible thermal gradients, which seems to indicate the fact that at high enough flow rates, the differences between the two no longer play a significant role.

The results imply that keeping the Reynolds number high in realistic PV systems will result in the operation at much lower temperatures. It has been widely documented that lower operating temperatures in PV cells increase efficiency and longevity of the cells, which makes water cooling an effective way of increasing the performance of a PV system, particularly in regions with high heat indexes.

Further research might consider the intricacies of improving the layouts of such cooling systems for other climate or searching for other coolants with better thermal characteristics. Moreover, understanding how the PV material and geometry affects the cooling performance could assist in creating better systems.

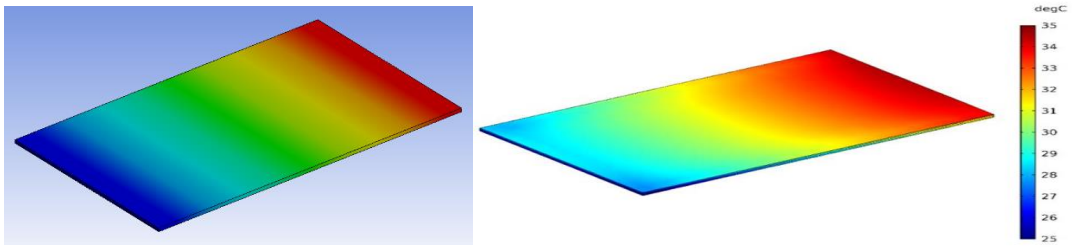

(a) (b)

Figure 4.1. Temperature distribution in the photovoltaic cell structure with water cooling for Re = 2242 (a) present work, (b) Salim et. al. [49].

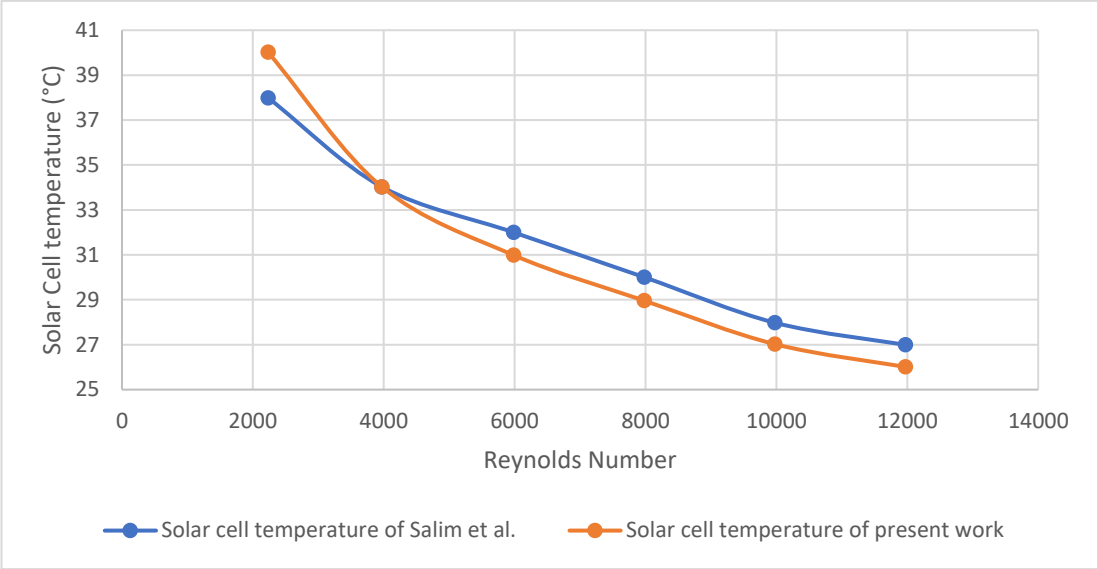

Figure 4.2. Photovoltaic average cell temperature as a function of Reynolds numbers.

4.2. THE EFFECT OF INLET TEMPERATURES ON THE RESULTS

The temperature of a photovoltaic (PV) board can essentially affect its exhibition and effectiveness. At the point when a PV board works at high temperatures, its electrical result diminishes, which can bring about a decrease in generally speaking framework effectiveness. At the point when a PV board is presented to daylight, it ingests energy and converts it into electrical energy. In any case, a piece of the retained energy is lost as intensity, which makes the temperature of the board increase. This intensity can accumulate after some time, and in the event that the board isn't cooled adequately, it can prompt a decreased electrical result and an abbreviated board life expectancy. One method for moderating the impacts of temperature on a PV board is through cooling. By decreasing the temperature of the board, the electrical result can be expanded, and the general proficiency of the framework can be moved along. The viability of cooling strategies, notwithstanding, can be impacted by the section temperature of the cooling medium. Studies have shown that cooling a PV board with colder water or air can prompt expanded proficiency, yet the viability of cooling diminishes as the passage temperature of the cooling medium increases. This is on the grounds that the temperature contrast between the cooling medium and the board diminishes, which lessens the intensity of the movement. The temperatures taken from the ocean help greatly in cooling the solar energy system.

Figure 4.3 shows the temperature distribution and the cooling process on the solar panel through the simulation program. Where it is noted that the value of the maximum temperatures decreases with decreasing the inlet temperature of the cooling tube. Where the temperature during entering the water at a temperature of 6°C reached 34.86°C, which is the best condition that has been reached compared to the remaining cases.

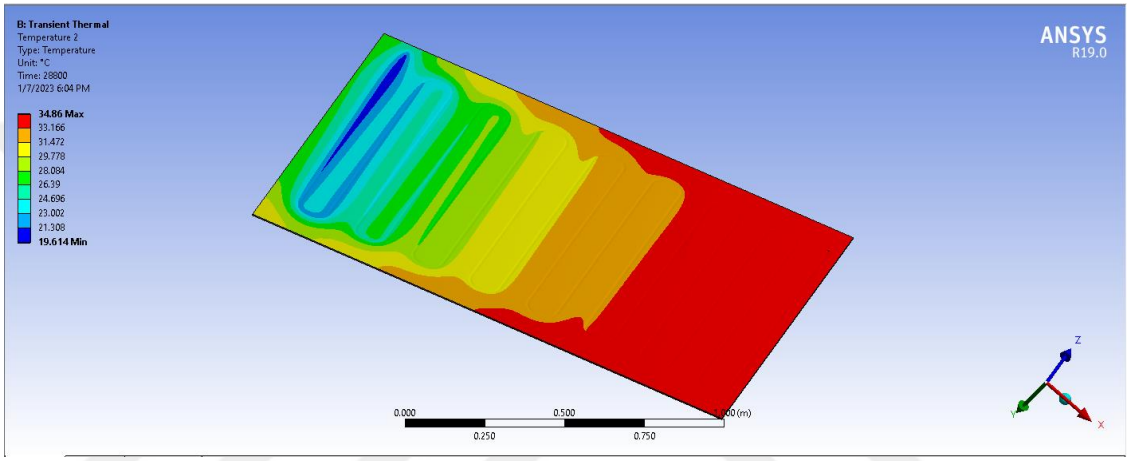

(a)

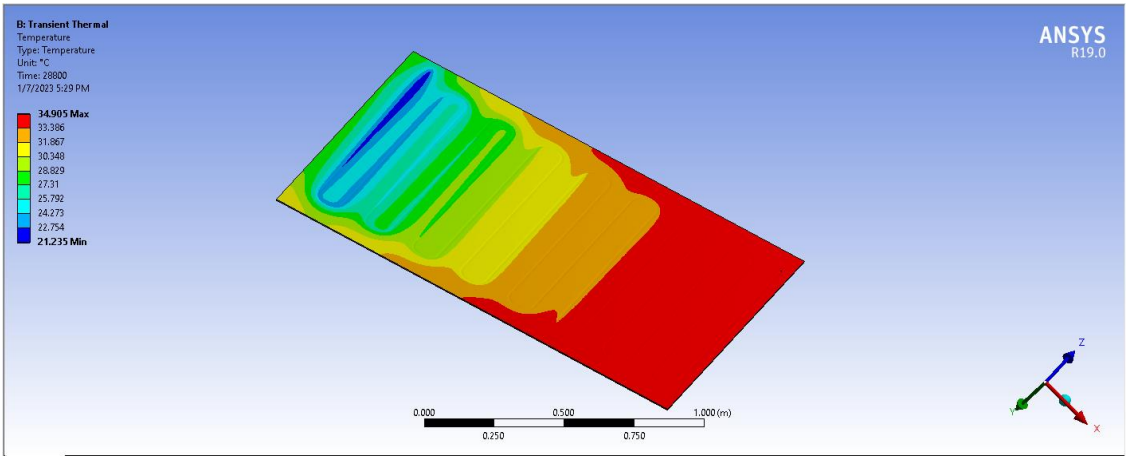

(b)

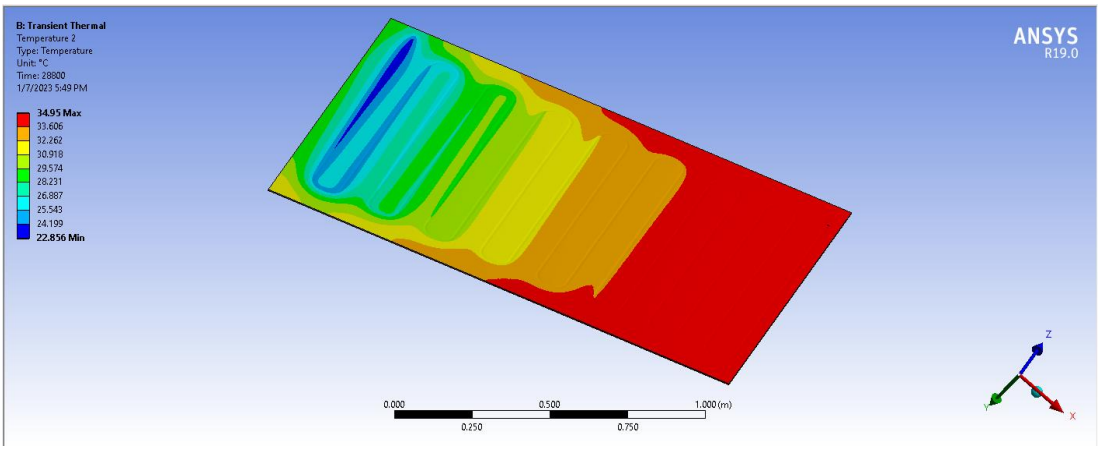

(c)

Figure 4.3. Temperature contour of PV panel at velocity inlet 0.1 m/s in winter with different inlet temperature. (a) 6°C, (b) 9°C, (c) 12°C.

As for the cooling tube of the solar panel, it can be seen from the apparent results in Figure 4.4 that the value of the maximum temperature for the simulation process decreases at the outlet of the tube as the inlet temperature decreases. When the exit temperature reached 6°C, the exit temperature was 25.2°C.

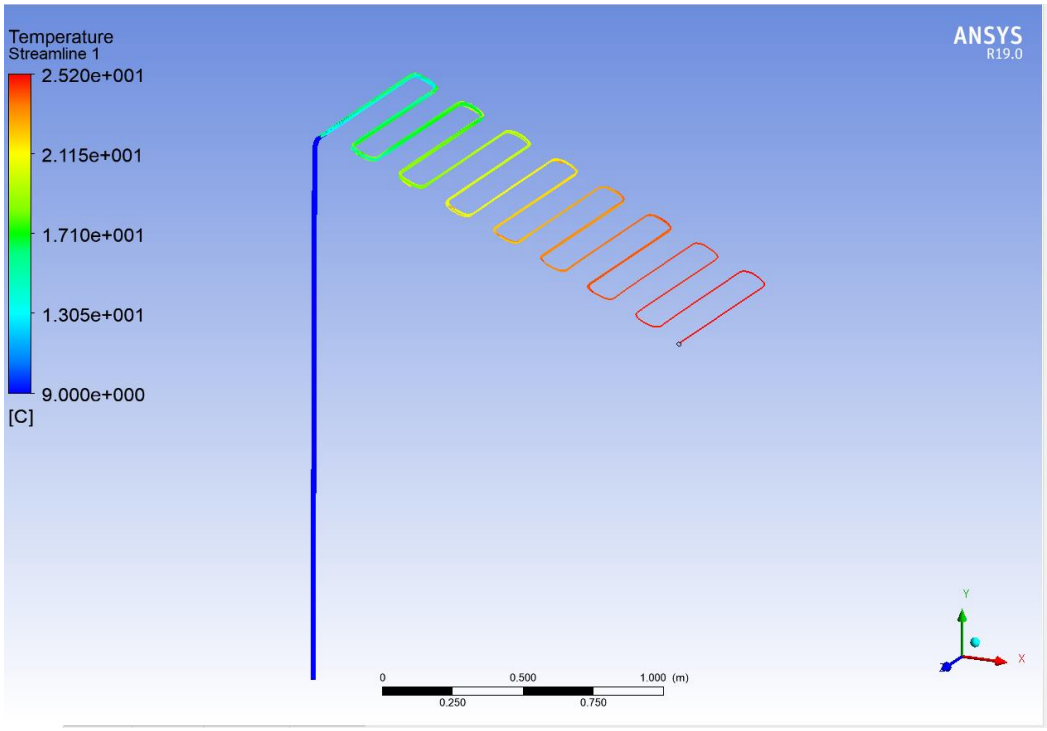

(a)

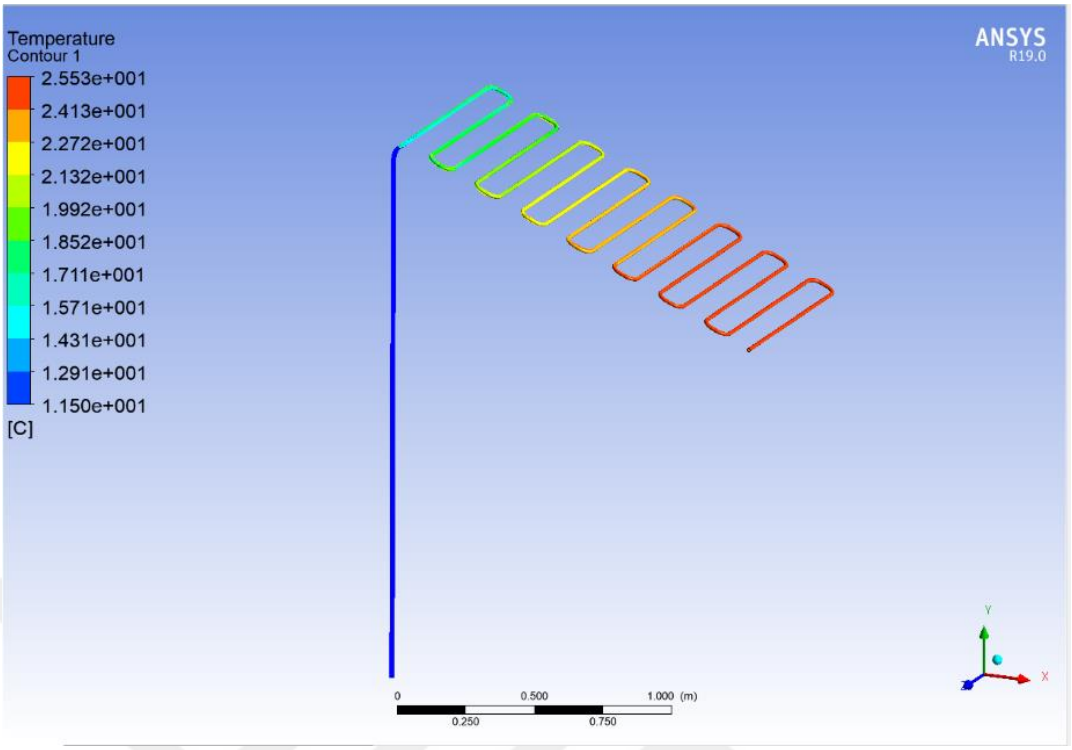

(b)

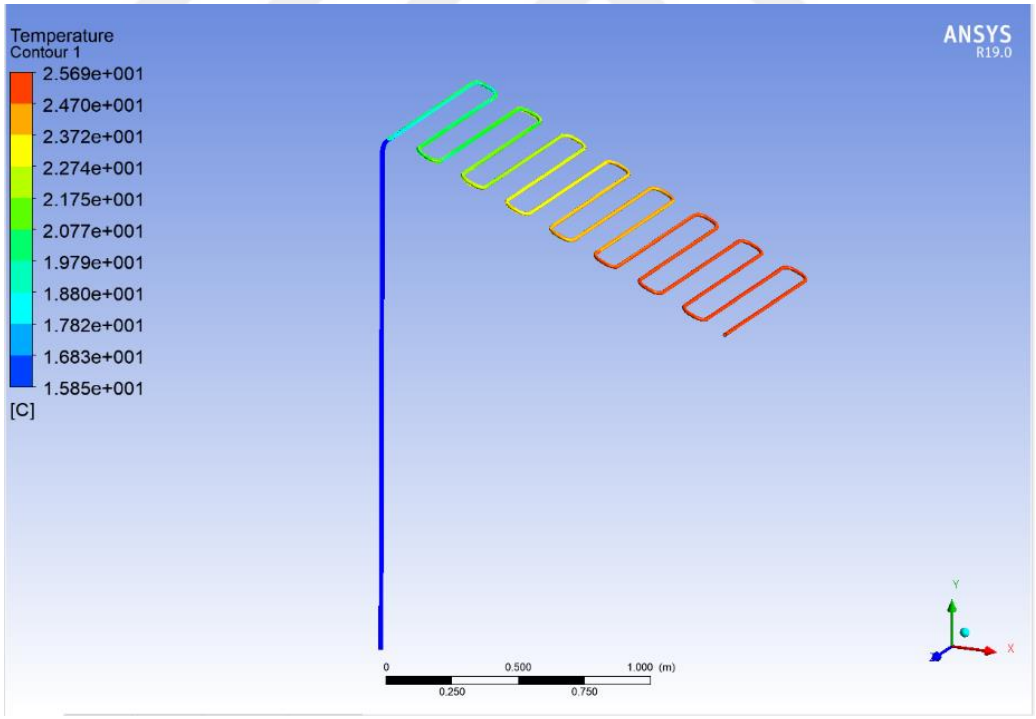

(c)

Figure 4.4. Temperature contour of cooling pipe at velocity inlet 0.1 m/s in winter with different inlet temperature. (a) 6°C, (b) 9°C, (c) 12°C.

Figure 4.5 shows the distribution of temperatures over time at different inlet temperatures. Where it is noted that the temperature value decreases on the surface of the solar panel with a decrease in the temperature of the water entering the cooling system. In addition, the highest temperature value was at 12:00 in the afternoon, with a temperature of 32.42°C, at the water inlet temperature of 12°C.

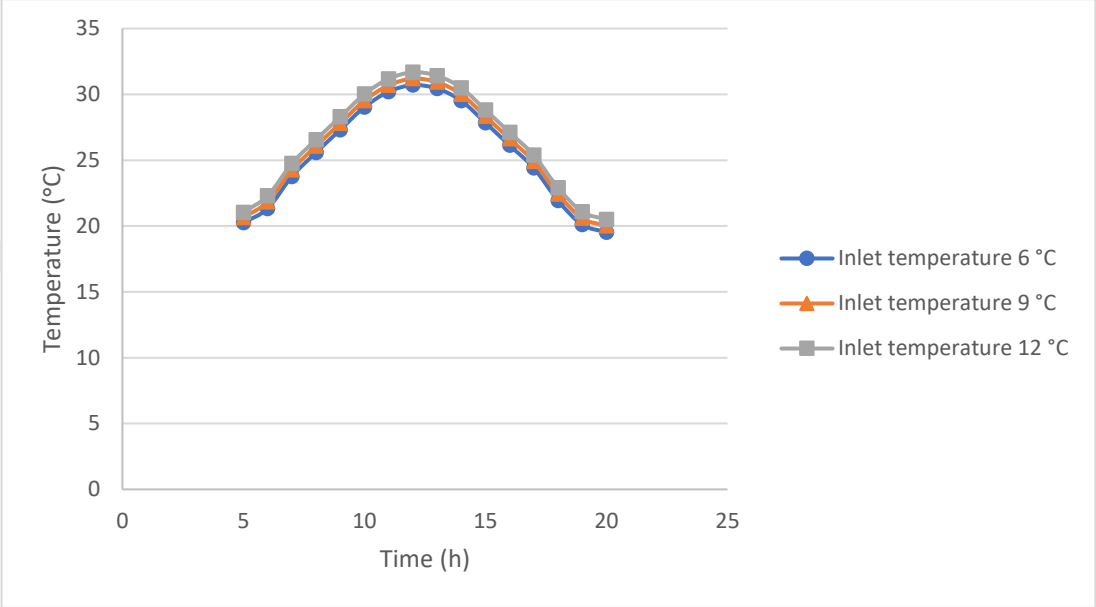

Figure 4.5. Temperature distribution of PV panel with time at velocity inlet 0.1 m/s in winter with different inlet temperature.

Water cooling of solar chargers can emphatically affect the power result of the boards, particularly in hot and bright conditions. At the point when solar chargers get too hot, their power yield diminishes because of the impact of temperature on the presentation of solar cells. This lessening in power yield is known as the temperature coefficient. By cooling the solar chargers with water, the temperature of the boards can be decreased, which diminishes the temperature coefficient and builds the power result of the boards. Contingent upon the surrounding temperature and different variables. Water cooling frameworks work by coursing water through cylinders or directs that are in touch with the rear of the sunlight-powered chargers. As the water courses through the channels, it ingests the intensity produced by the sunlight powered chargers and diverts it, diminishing the temperature of the boards. This

assists with keeping up with the solar charger at a lower temperature, which can expand its power yield.

Water-cooling of sunlight-powered chargers can work on their electrical productivity by lessening their working temperature. Sun-powered chargers are less effective at changing over daylight into power at high temperatures, and water cooling can assist with keeping the boards at the boards at a lower temperature, working on their electrical productivity. At the point when sunlight-powered chargers get too hot, their electrical proficiency diminishes because of the temperature coefficient of the solar cells. By cooling the sunlight-powered chargers with water, the temperature of the boards can be diminished, which lessens the temperature coefficient and builds the electrical proficiency of the boards. The water-cooling framework works by circling water through cylinders or directs that are in touch with the rear of the solar charger. As the water moves through the channels, it ingests the intensity produced by the sunlight-powered charger and diverts it, diminishing the temperature of the board. This assists with keeping up with the sunlight-powered charger at a lower temperature, which can expand its electrical productivity. The level of progress in electrical productivity relies upon a few variables, for example, the plan of the water-cooling framework, the stream pace of the cooling water, the temperature of the cooling water, and the encompassing temperature and dampness.

The main objective of the cooling process is to obtain the largest possible efficiency that can be obtained through the process of calculations and simulations that were carried out through the program. From Figure 4.6, the electrical efficiency was reached when the inlet temperature was 6°C, and the value of the electrical efficiency reached 7.59%. It is the best case reached compared to the rest of the cases at 12:00.

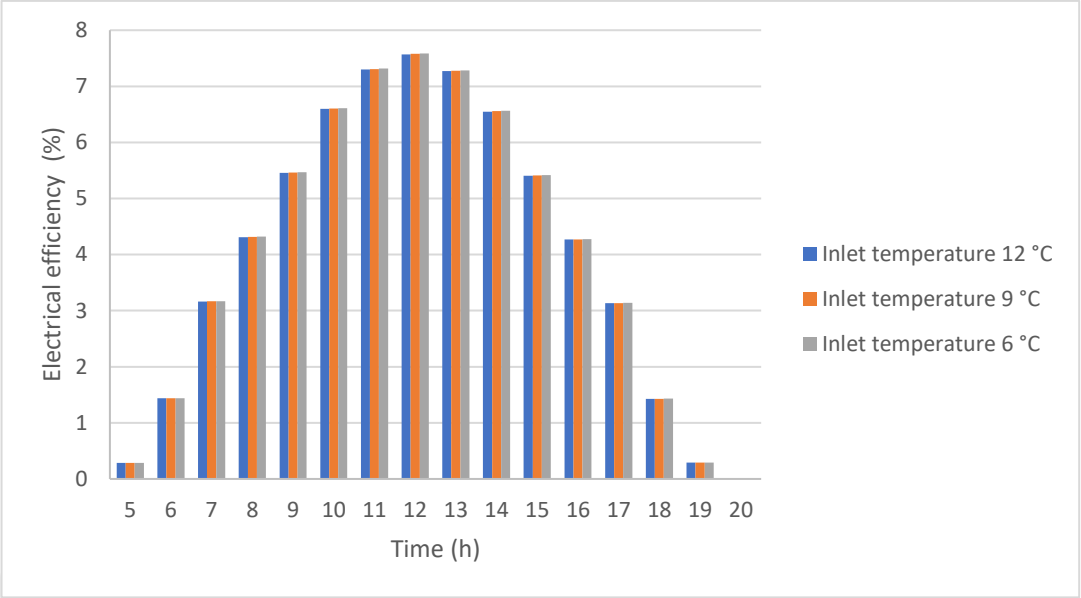

Figure 4.6. Electrical efficiency distribution of PV panel with time at velocity inlet 0.1 m/s in winter with different inlet temperature.

4.3. THE EFFECT OF INLET VELOCITY ON THE RESULTS

The impact of channel velocity on the water cooling of PV boards depends on different variables, for example, the plan of the cooling framework, the size and direction of the PV boards, and the surrounding temperature and humidity. Largely, expanding the gulf velocity of the cooling water can increase the viability of water cooling by lessening the working temperature of the PV boards. This is because higher velocity can build the pace of intensity between the PV board and the cooling water, bringing about more viable cooling. Nevertheless, expanding the bay velocity past a specific point may not bring about additional upgrades in cooling productivity. This is because higher velocities can cause choppiness in the stream, which can lessen the contact time between the water and the PV board, bringing about diminished heat movement. Accordingly, the ideal bay velocity for water-cooling PV boards will depend on the particular plan of the cooling framework and the working circumstances. The gulf velocity ought to be sufficiently high to provide powerful cooling, but not so high that it causes choppiness and decreases the contact time between the water and the PV board. The temperatures taken from the lake help enormously in cooling the sun-powered energy framework.

Figure 4.7 shows the temperature appropriation and cooling process on the sun, powered chargers are powered through the reenactment program. It is noticed that the value of the greatest temperature diminishes with the expansion in the section velocity of the cooling tube. The temperature when entering the water at a velocity of 1 m/s came to 28.1°C, which is the best case compared with the excess cases.

For the cooling line of the sun-powered charger, it tends to be seen from the outcomes displayed in Figure 4.8 that the greatest temperature worth of the reproduction cycle diminishes at the power source of the line with the expansion in the section velocity. At the point when the water passage velocity was 1 m/s, the leave temperature was 16.6°C.

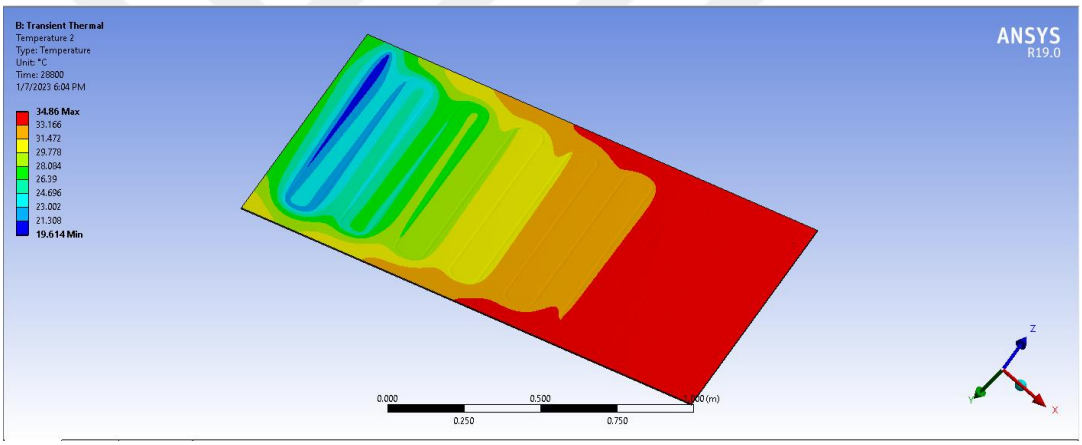

(a)

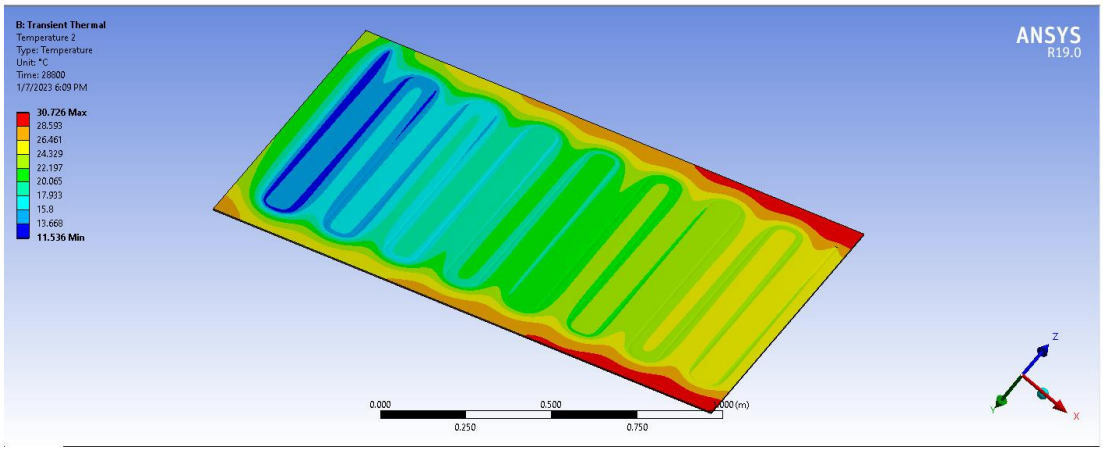

(b)

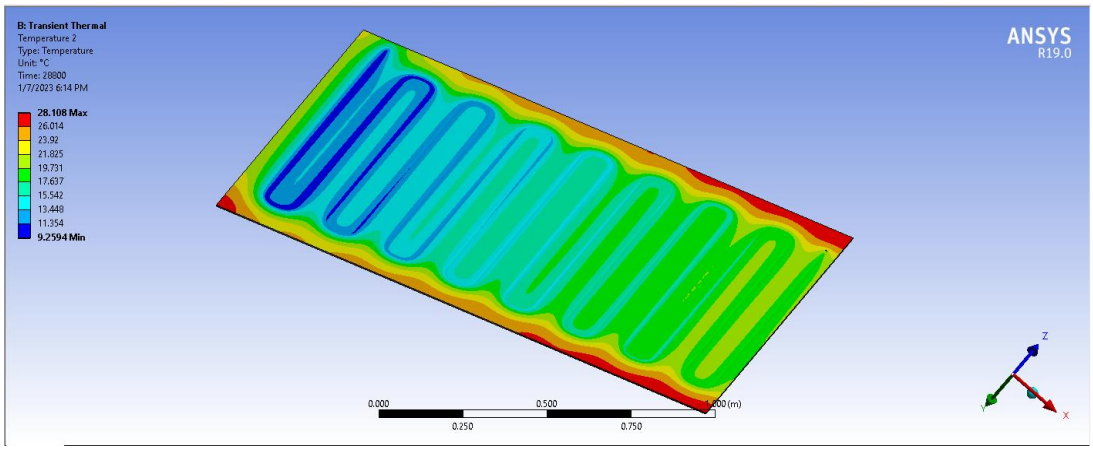

(c)

Figure 4.7. Temperature contour of PV panel at inlet temperature 6°C in winter with different velocity inlet. (a) 0.1 m/s, (b) 0.5 m/s, (c) 1 m/s.

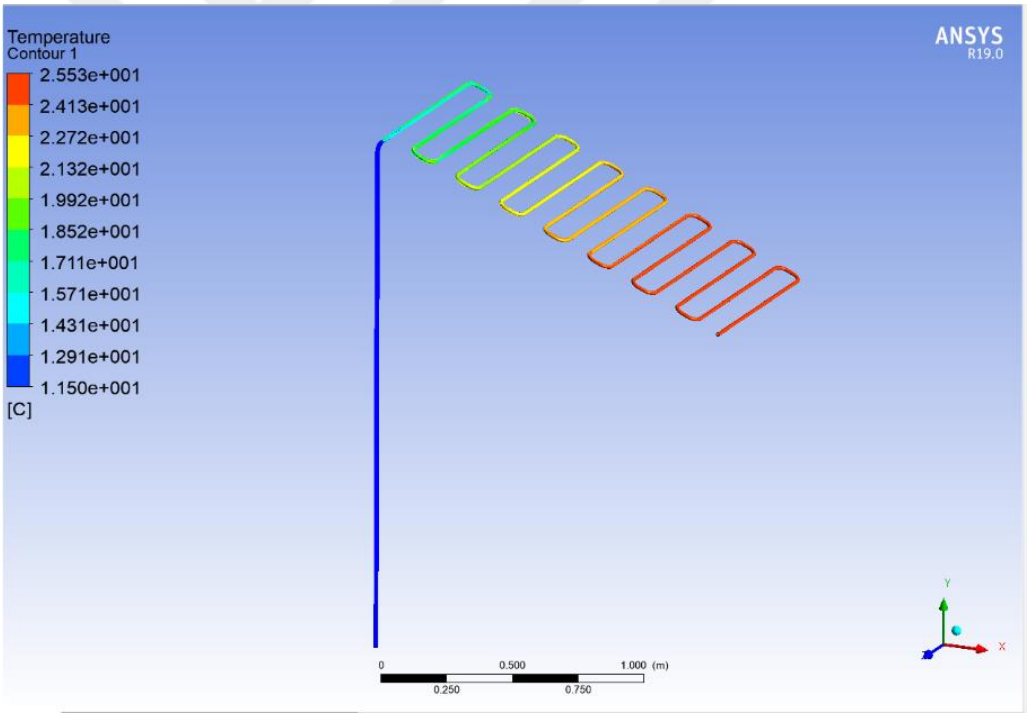

(a)

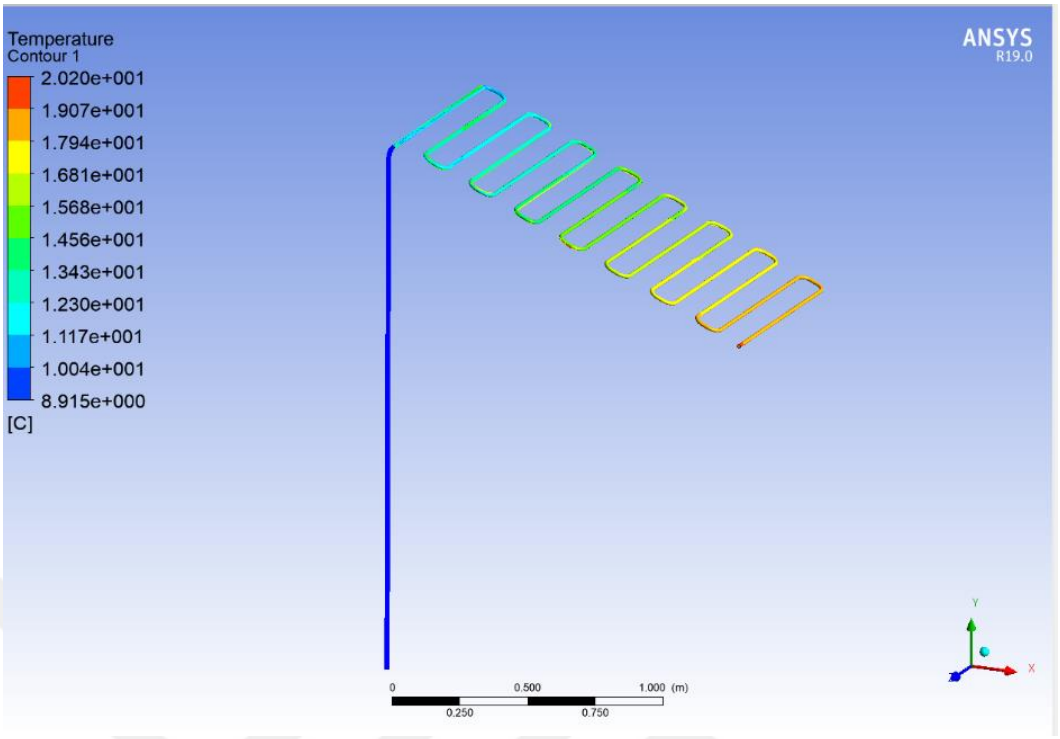

(b)

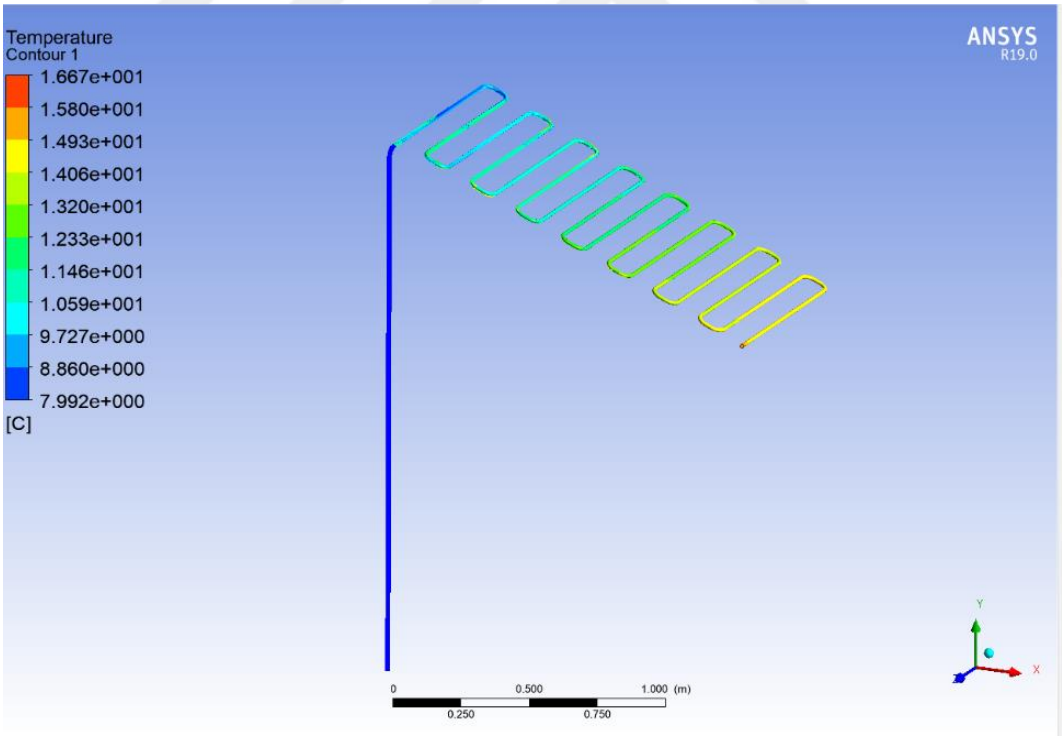

(c)

Figure 4.8. Temperature contour of cooling pipe at inlet temperature 6°C in winter with different velocity inlet. (a) 0.1 m/s, (b) 0.5 m/s, (c) 1 m/s.

Figure 4.9 shows the temperature conveyance over the long haul at various delta velocities. It is noticed that the temperature esteem diminishes on the outer layer of the sunlight-powered chargers with the velocity-up water entering the cooling framework. Furthermore, the least worth was at 12 early afternoons. In the early evening, with a temperature of 18.34°C and a water passage velocity of 1 m/s,.

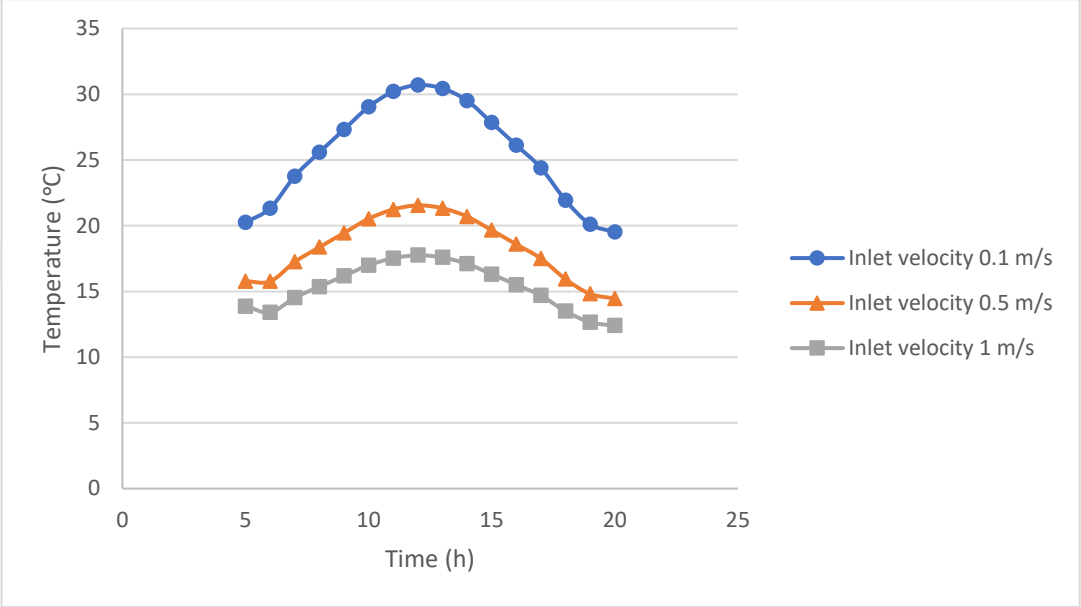

Figure 4.9. Temperature distribution of PV panel with time at inlet temperature 6°C in winter with different velocity inlet.

The bay velocity of the cooling water utilized in a water-cooled PV board can meaningfully affect the power result of the board. This is because the temperature of the board influences the productivity of the cells, and higher bay velocities can assist with dispersing heat from the board all the more successfully, which can prompt an expansion in power yield. At the point when water moves through the cooling framework at a higher channel velocity, it expands the intensity of the movement from the board to the water. This decreases the temperature of the board, which can work on the effectiveness of the PV cells and increase the power yield. In any case, there is a furthest cutoff to the adequacy of expanding the bay velocity of the cooling water. Assuming the velocity is excessively high, it can cause disturbance and lessen the productivity of the intensity move. Moreover, on the off chance that the water stream rate is excessively high, it can prompt higher strain drops, which can expand the energy utilization of the cooling framework. The ideal channel velocity of the

cooling water will depend on the particular plan of the cooling framework and the attributes of the PV board. An equilibrium should be struck between the cooling viability and energy utilization of the framework. Thus, it is fundamental to painstakingly improve the plan and activity of the cooling framework to expand the power result of the PV board.

The principal work through the review is to get the biggest measure of energy, and the outcomes got because of the great cooling of the sunlight-powered charger, through Figure 4.10, which shows the distinction in energy esteem as per time and hour. Velocity up the section of water into the different cooling framework. The energy esteem was 65.15 W while entering the water at a velocity of 1 m/s at 12:00, and this demonstrates that the cooling esteem helps in expanding the electrical energy.

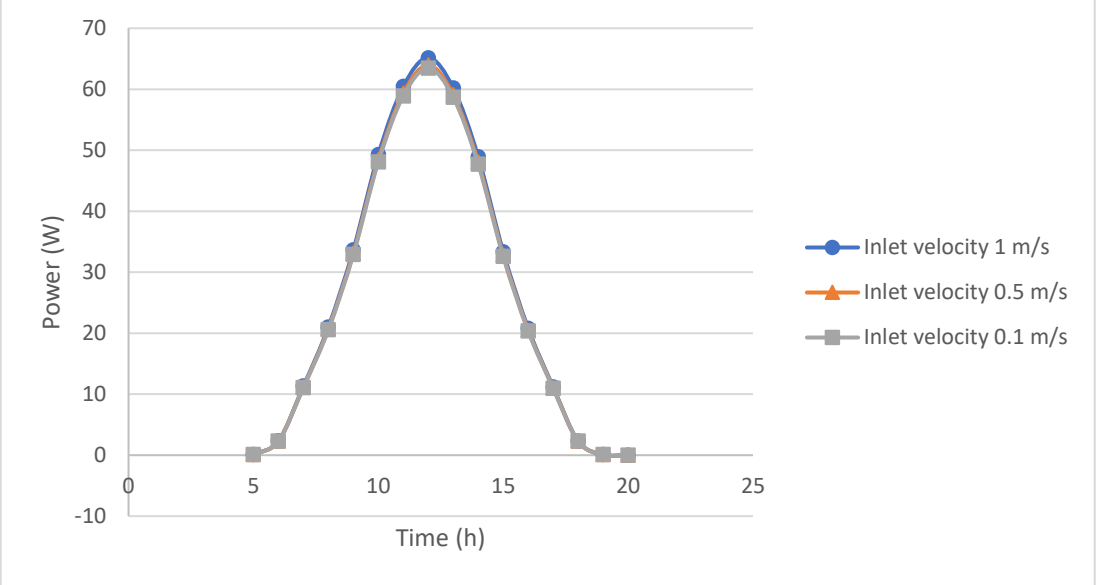

Figure 4.10. Power distribution of PV panel with time at inlet temperature 6°C in winter with different velocity inlet.

The gulf velocity of the cooling water utilized in a water-cooled PV board can meaningfully affect the electrical productivity of the board. This is because the electrical proficiency of the board is straightforwardly connected with the temperature of the cells, and the bay velocity of the cooling water influences the cooling pace of the board. At the point when water moves through the cooling

framework at a higher bay velocity, it expands the pace of intensity move from the board to the water. This decreases the temperature of the board, which can work on the electrical productivity of the PV cells. In any case, the adequacy of expanding the gulf velocity of the cooling water has limits. Assuming the velocity is excessively high; it can cause choppiness and diminish the proficiency of intensity move. In addition, assuming the water stream rate is excessively high; it can prompt higher tension drops, which can build the energy utilization of the cooling framework. The ideal channel velocity of the cooling water will rely upon the particular plan of the cooling framework and the attributes of the PV board. An equilibrium should be struck between the cooling viability and energy utilization of the framework. Hence, it is fundamental to painstakingly enhance the plan and activity of the cooling framework to amplify the electrical proficiency of the PV board.

The primary objective of the cooling system is to get the best conceivable proficiency that can be acquired through the computations and reproductions made through the product. From Figure 4.11, the electrical effectiveness was reached when the water passage velocity was 1 m/s, and the electrical proficiency esteem was 7.66%, which is the best-case came to contrasted with the other cases at 12:00.

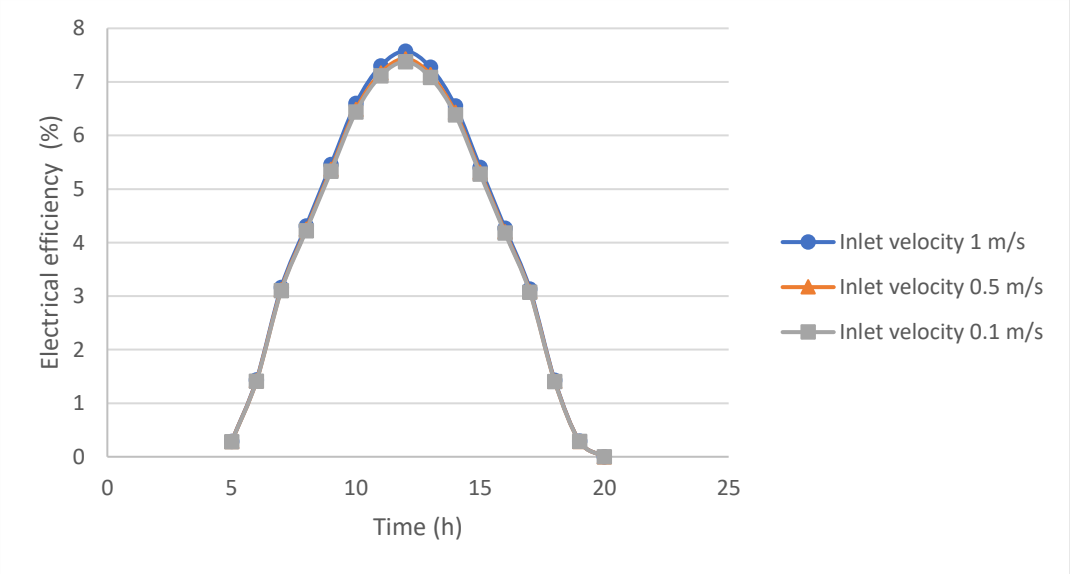

Figure 4.11. Electrical efficiency distribution of PV panel with time at inlet temperature 6°C in winter with different velocity inlet.

4.4. THE EFFECT OF SEASON ON THE RESULTS

The impact of season on the water cooling of PV boards depends on the surrounding temperature and moisture, which can influence the cooling productivity of the framework. As a rule, water cooling can be more powerful during hot and bright seasons when the temperature of the PV boards is higher. This is because higher temperatures can decrease the electrical effectiveness of the PV boards, and water cooling can assist with keeping a lower temperature, bringing about superior electrical productivity and power yield. During cooler seasons, for example, fall and winter, the surrounding temperature might be lower, and the cooling proficiency of the framework might be less basic. In any case, water cooling can be advantageous during cooler seasons by decreasing the temperature of the PV boards and working on their electrical productivity. The adequacy of water cooling may likewise depend on the moisture levels during various seasons. Higher mugginess can influence the vanishing pace of the cooling water, and on the off chance that the water is not dissipating productively, the cooling effectiveness of the framework might be decreased. At times, it very well might be important to utilize extra cooling techniques, for example, air-cooling or a blend of air and water-cooling, to keep up with ideal execution during damp seasons.

Figure 4.12 demonstrates the cooling process and temperature distribution on the solar panels as calculated by the simulation software. Where it is observed that December's maximum temperature values are lower than those of other months. In the worst scenario, the temperature hit 28.1°C in July, and in the best situation, it reached 21.2°C in December.

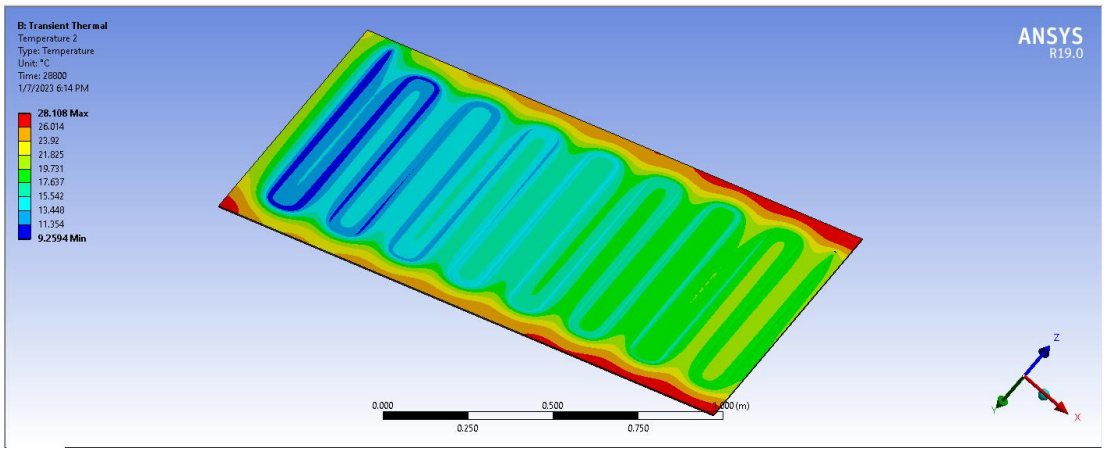

(a)

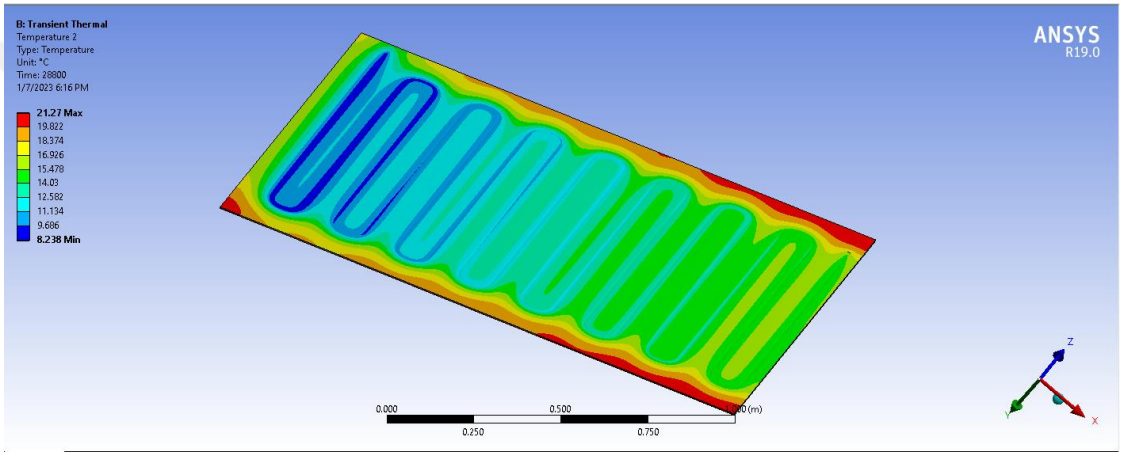

(b)

Figure 4.12. Temperature contour of PV panel using inlet velocity of 1 m/s with different season. (a) July, (b) December.

As can be observed in Fig. 4.13, the maximum temperature value of the simulation drops in December for the cooling pipe of the solar panel. The exit temperature in the month of July was 20.2°C.

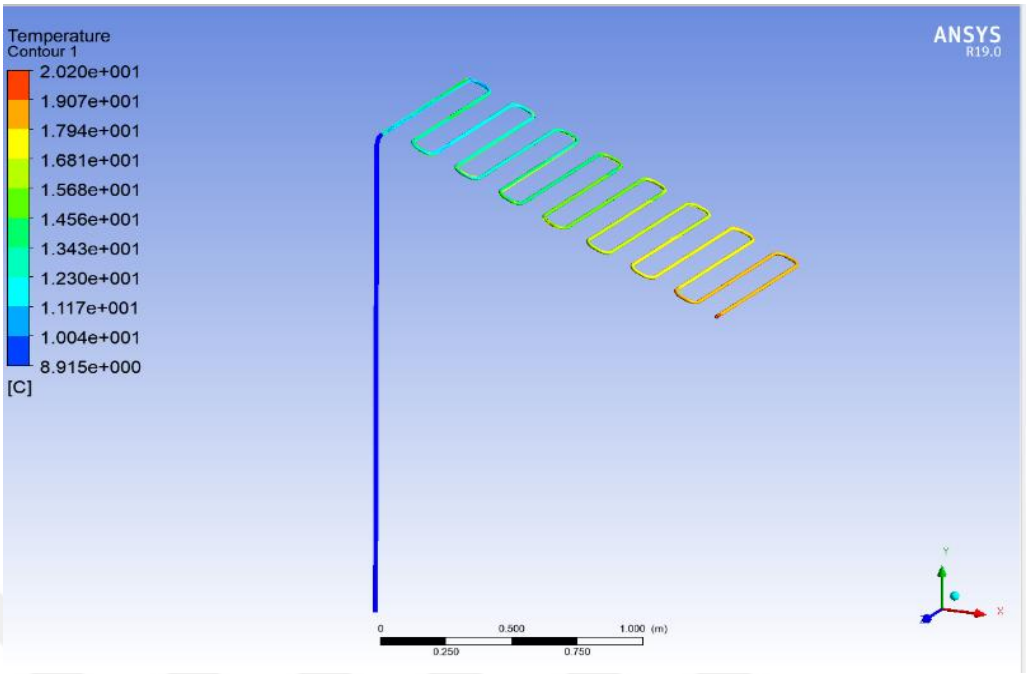

(a)

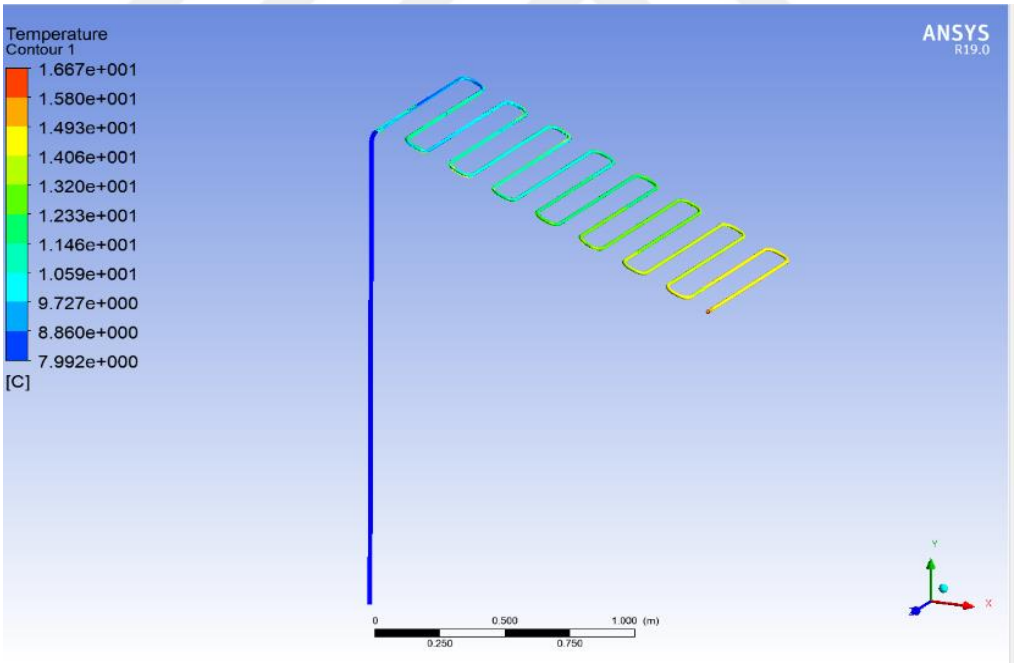

(b)

Figure 4.13. Temperature contour of cooling pipe using inlet velocity of 1 m/s at different season. (a) July, (b) December.

Figure 4.14 shows the seasonal variation in temperature. It has been observed that the surface temperature of solar panels drops in December. In addition, the lowest point occurred at midday. It was 23.42°C in the afternoon.

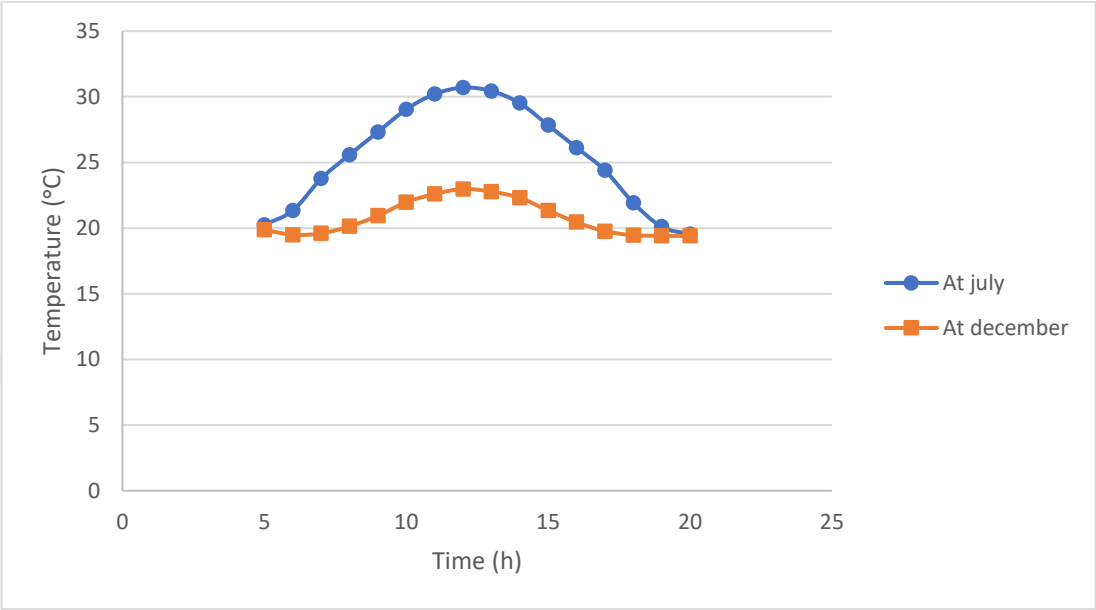

Figure 4.14. Temperature distribution of PV panel with time using inlet velocity of 1 m/s at different seasons.

The season can fundamentally affect the power result of a PV board. This is on the grounds that the power result of a PV board is straightforwardly related to how much daylight it gets and how much daylight fluctuates with the season. As a general rule, the power result of a PV board will be most elevated throughout the late spring months, when the days are longest and the sun is most elevated overhead. During this time, the board will get the most daylight, which will prompt a more powerful result. Alternately, throughout the cold weather months, the power result of the board will regularly be lower. This is because the days are more limited and the sun is lower overhead, and that implies that the board will get less daylight. Moreover, in locales where there is snow cover throughout the cold weather months, the power result of the board might be additionally diminished because of the impression of daylight created by the snow. The spring and fall seasons can be temporary periods where the power result of the board might shift depending on the atmospheric conditions and the length of the day. It is vital to take note that while the season can essentially affect the power result of a PV board, different factors like overshadowing, residue,

and soil collection on the board, as well as the board's age and condition, can likewise influence its power yield. Ordinary support and cleaning can assist with guaranteeing that the board is working at ideal proficiency, no matter what the season.

Figure 4.15 displays the variation in energy value throughout time and hour, and its major purpose throughout the research has been to get the maximum amount of energy possible because of the high cooling of the solar panel. Quicken the pace at which water enters each of the various cooling systems. The cooling value aids in boosting the electrical energy, as measured at 65.15 W while the energy was entering the water at a velocity of 1 m/s at 12:00.

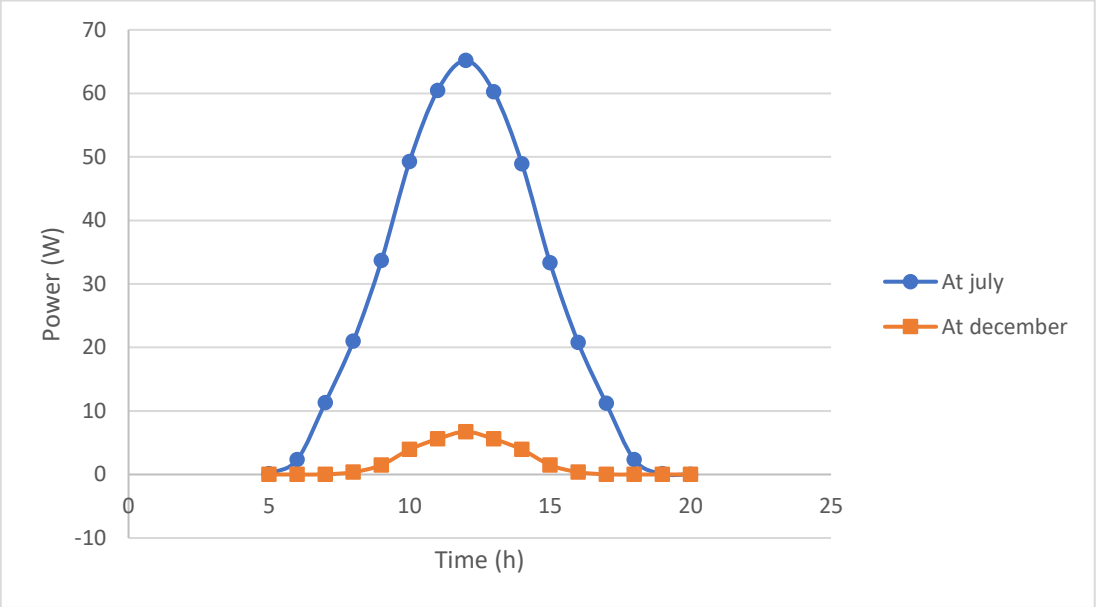

Figure 4.15. Power distribution of PV panel with time using inlet velocity of 1 m/s at different seasons.

The effectiveness of a photovoltaic (PV) board is impacted by a few elements, including the temperature of the board. Water cooling is one method for decreasing the temperature of the board, which can prompt an expansion in productivity. Notwithstanding, the impact of time on the water cooling effectiveness of PV boards can fluctuate contingent upon a few elements. By and large, water cooling is more compelling in sweltering seasons when the surrounding temperature is higher. This is

on the grounds that the distinction between the temperature of the board and the water is more noteworthy, and that implies that more intensity can be transferred from the board to the water. In colder seasons, water cooling may not be as powerful, as the temperature distinction between the board and the water is more modest. Notwithstanding, it's vital to take note that the viability of water cooling in expanding the productivity of a PV board likewise relies upon the plan and development of the cooling framework. The pace of the water stream, the size and material of the lines, and the kind of coolant utilized can all influence the cooling effectiveness.

The primary goal of the refrigeration process is to achieve maximum efficiency, which may be achieved via the use of software calculations and simulations. As can be seen in Figure 4.16, the highest possible electricity efficiency was achieved at 12:00 in the month of July, with a value of 7.66%.

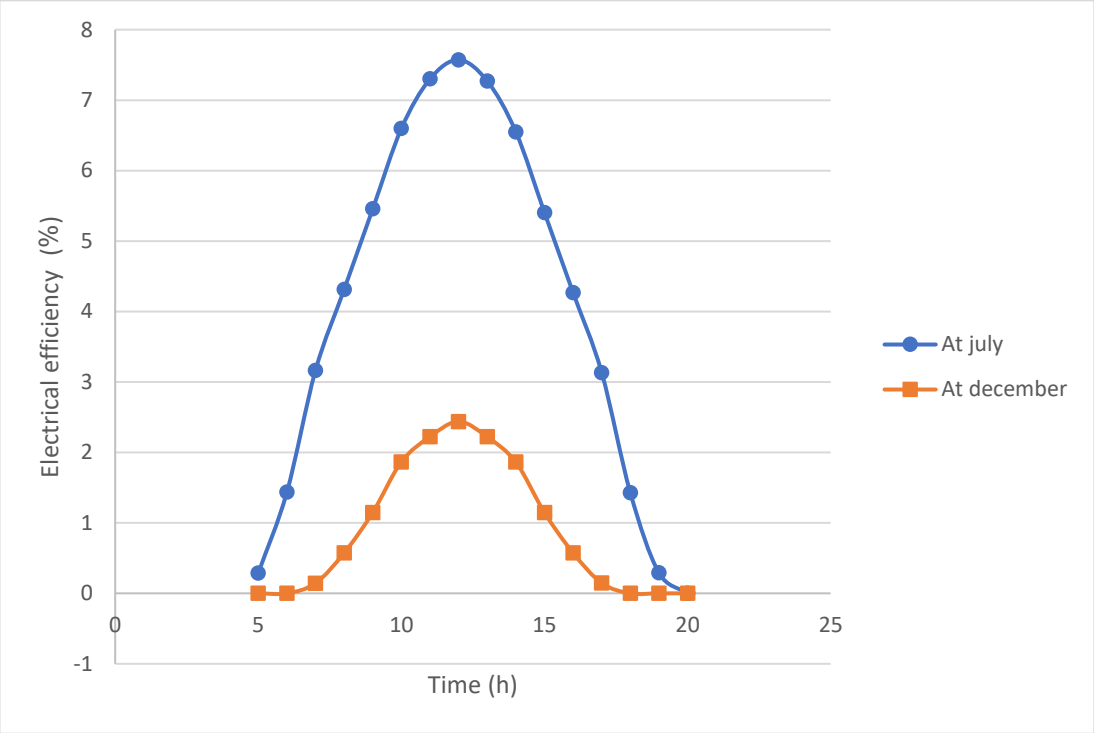

Figure 4.16. Electrical efficiency distribution of PV panel with time using inlet velocity of 1 m/s at different seasons.

4.5. THE EFFECT OF SUMMER SEASON

The summer season was studied as a variable for lake temperature, where an inlet temperature of 26°C was used, representing the lake temperature and a variable inlet velocity. It can be seen in Figure 4.17 that the velocity changes in relation to the change in conditions with different inlet velocity.

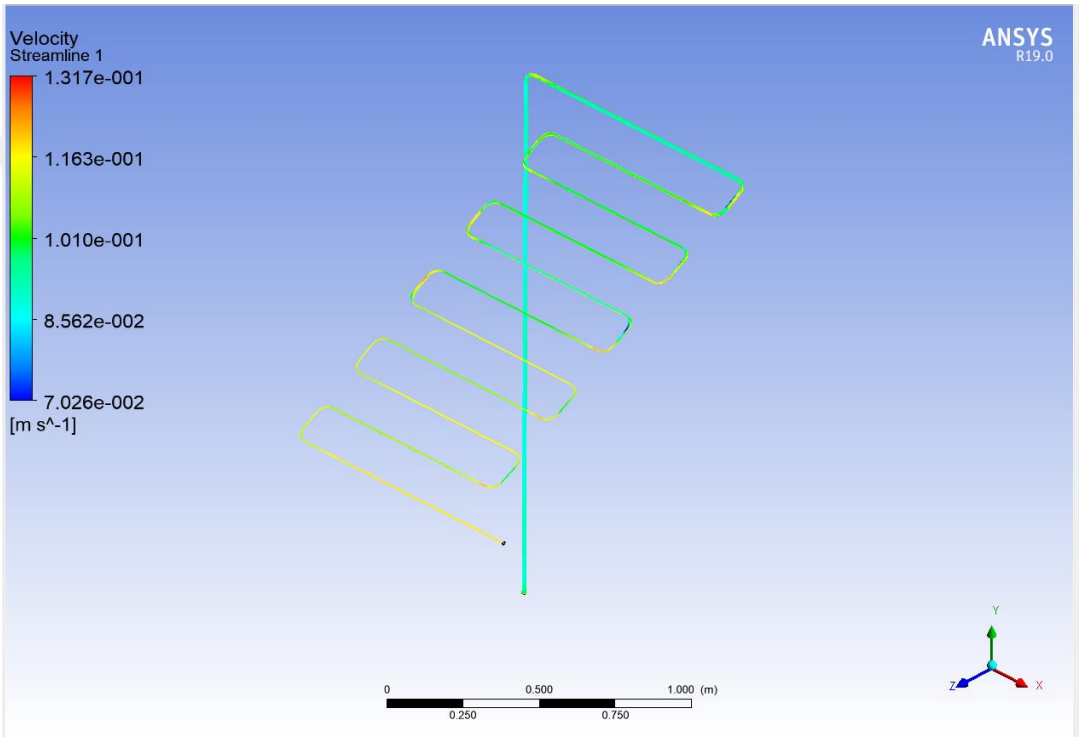

(a)

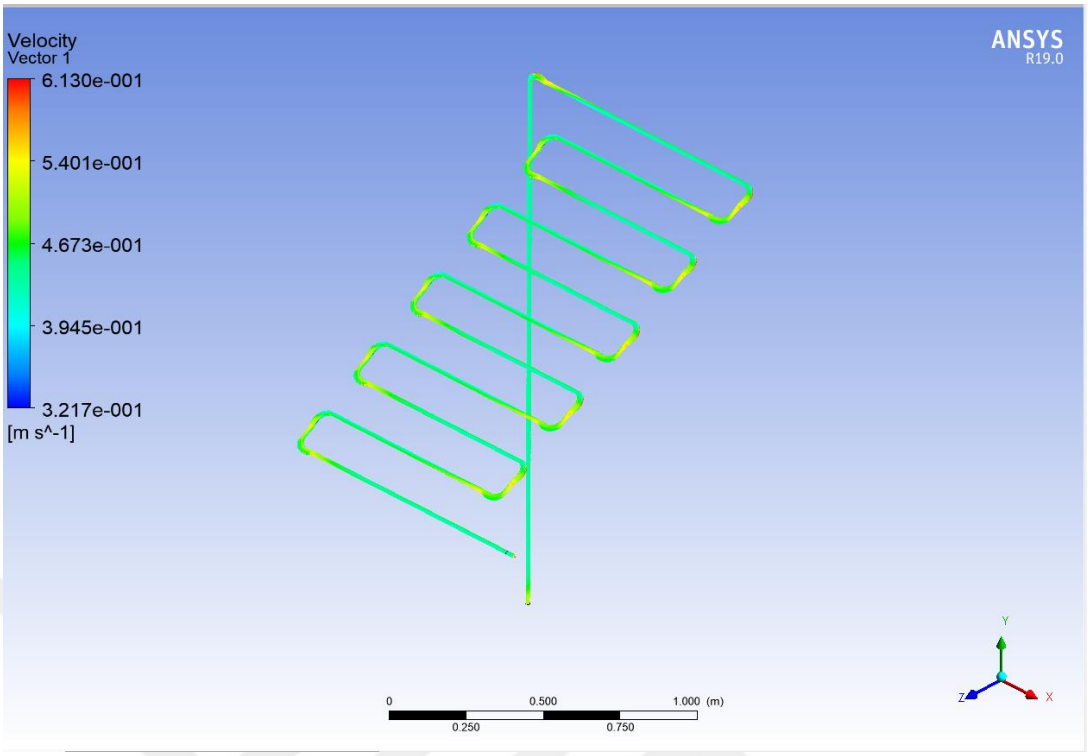

(b)

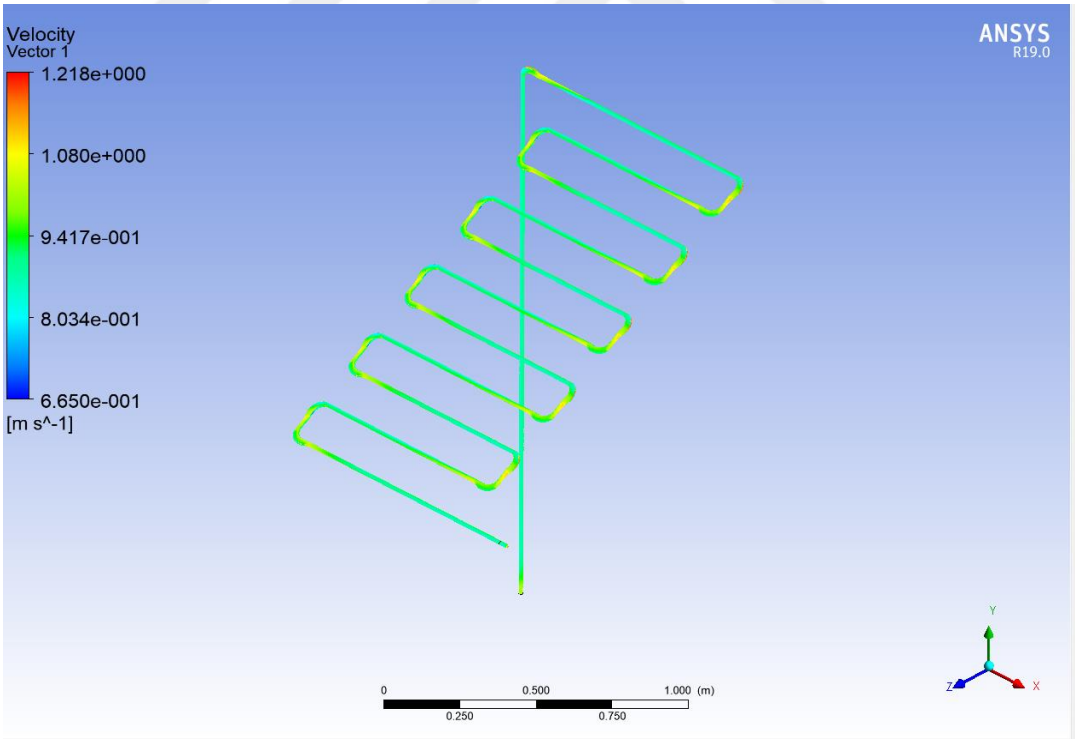

(c)

Figure 4.17. The velocity contour of cooling pipe at inlet temperature of 26°C with inlet velocity of (a) 0.1 m/s, (b) 0.5 m/s, (c) 1 m/s.

As for Figure 4.18, which shows the temperature gradient of the pipe, the maximum temperature reached 58°C at the inlet velocity of 0.1 m/s, while at 1 m/s the maximum temperature reached 48°C, which gives clear evidence of weak heat transfer in a short time.

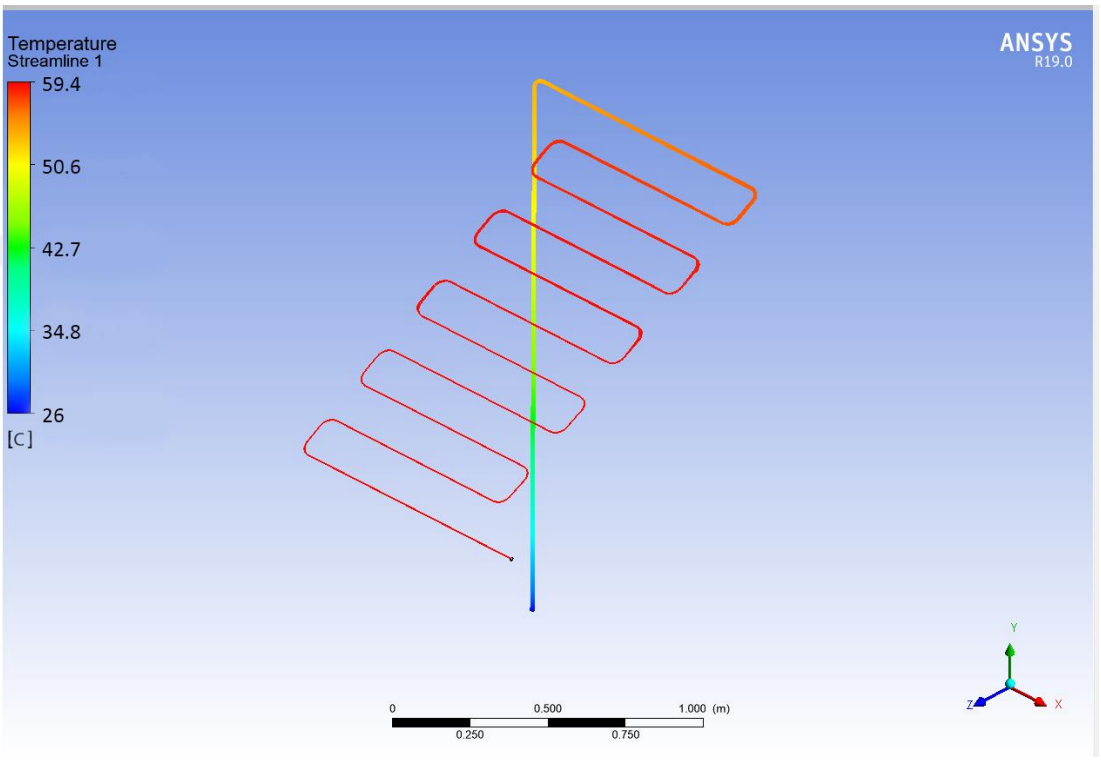

(a)

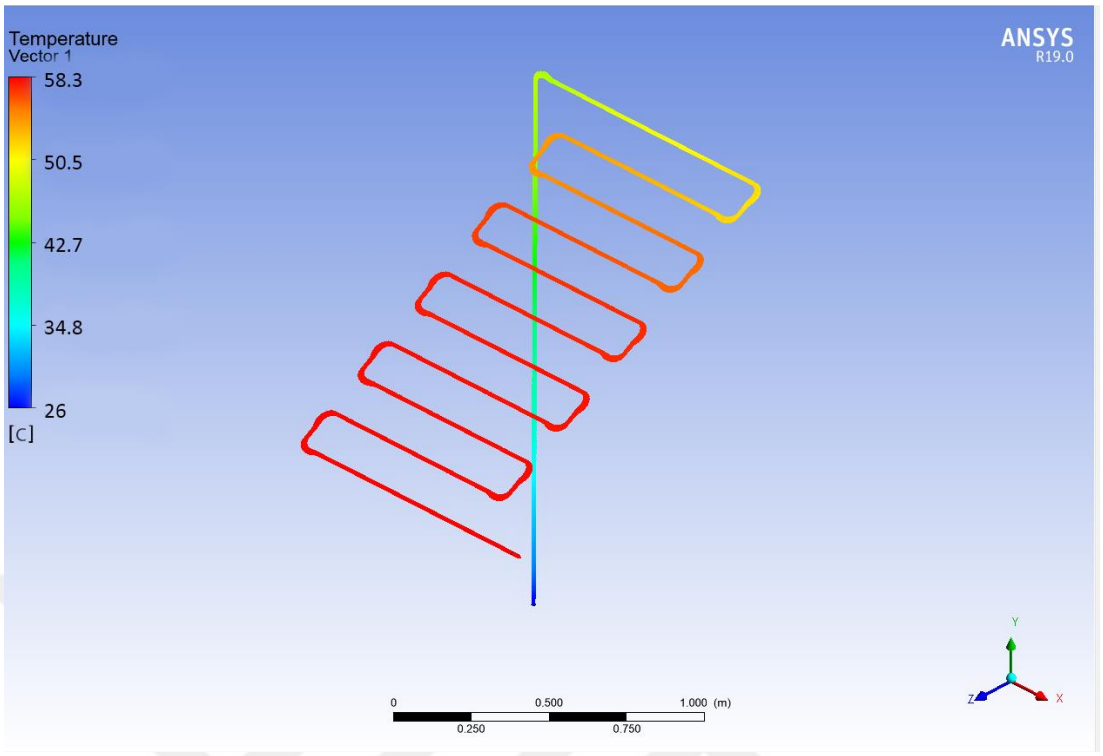

(b)

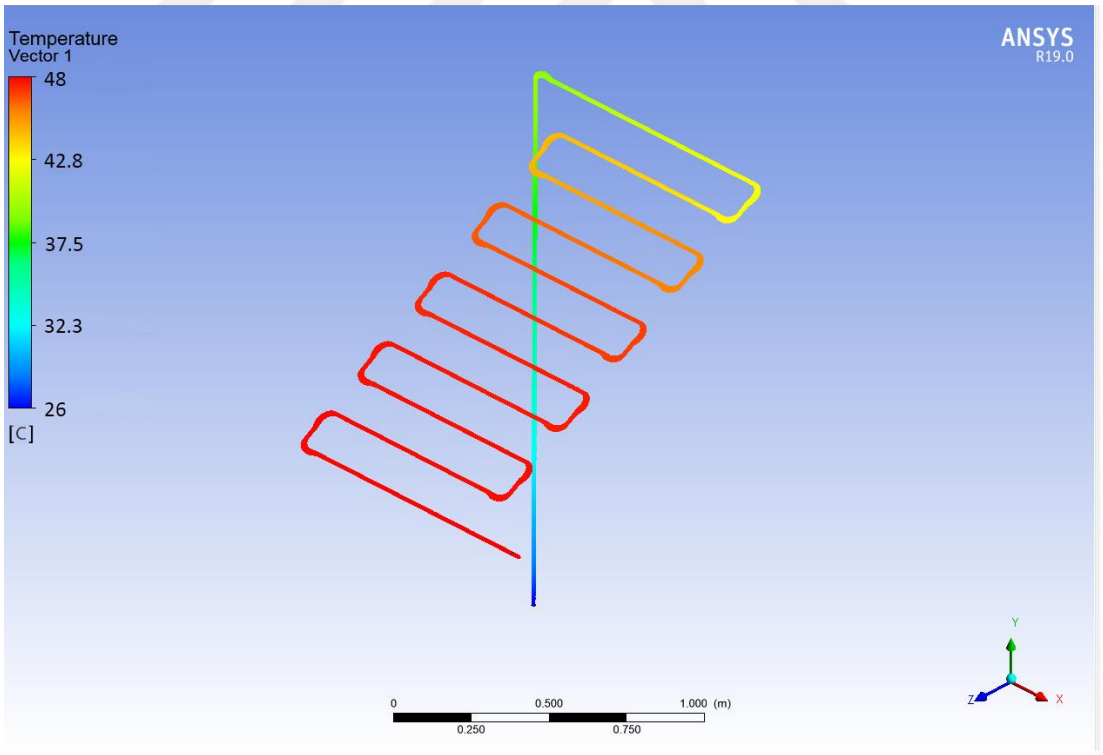

(c)

Figure 4.18. Temperature contour of cooling pipe at inlet temperature of 26°C with inlet velocity of (a) 0.1 m/s, (b) 0.5 m/s, (c) 1 m/s.

Figure 4.19 shows the temperature gradient of the solar panel. It is noted that the temperature decreases as the inlet velocity increases. The reason is not having enough time for the heat transfer between the water and the solar panel. The temperature reached 58°C at the velocity of 0.1 m/s and 55°C at the velocity of 0.5 m/s and 49°C at a velocity of 1 m/s.

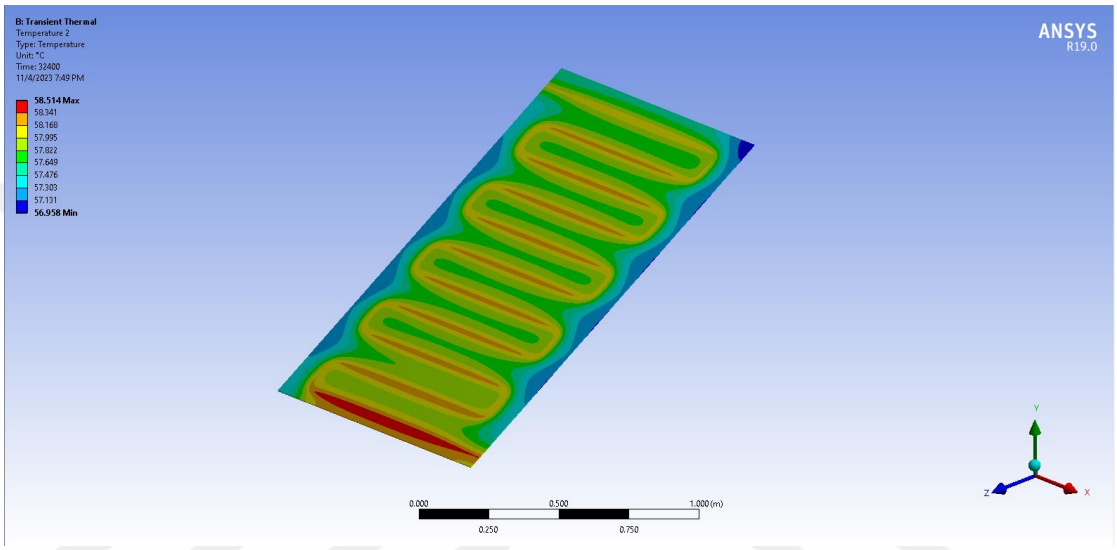

(a)

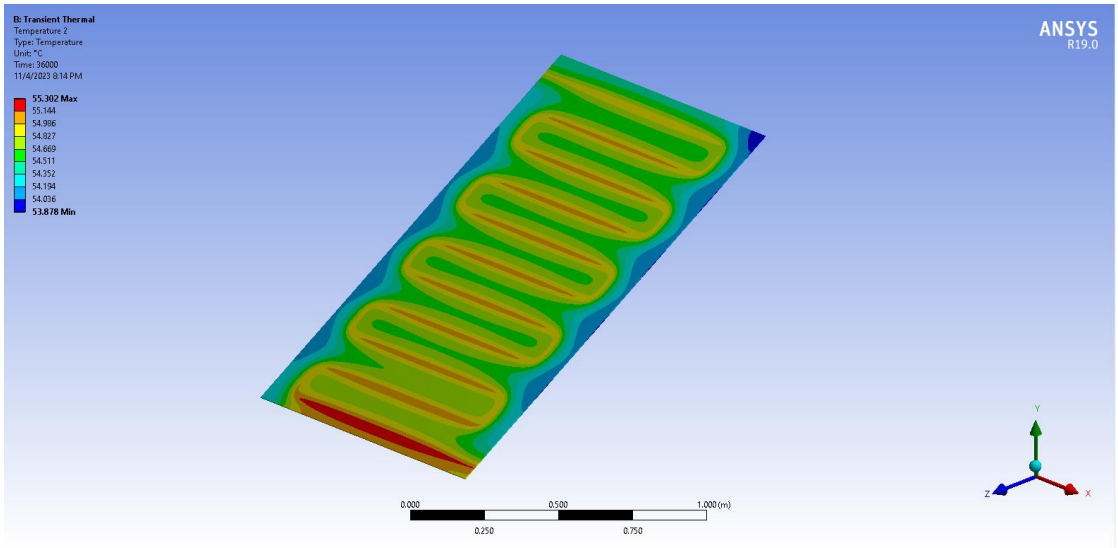

(b)

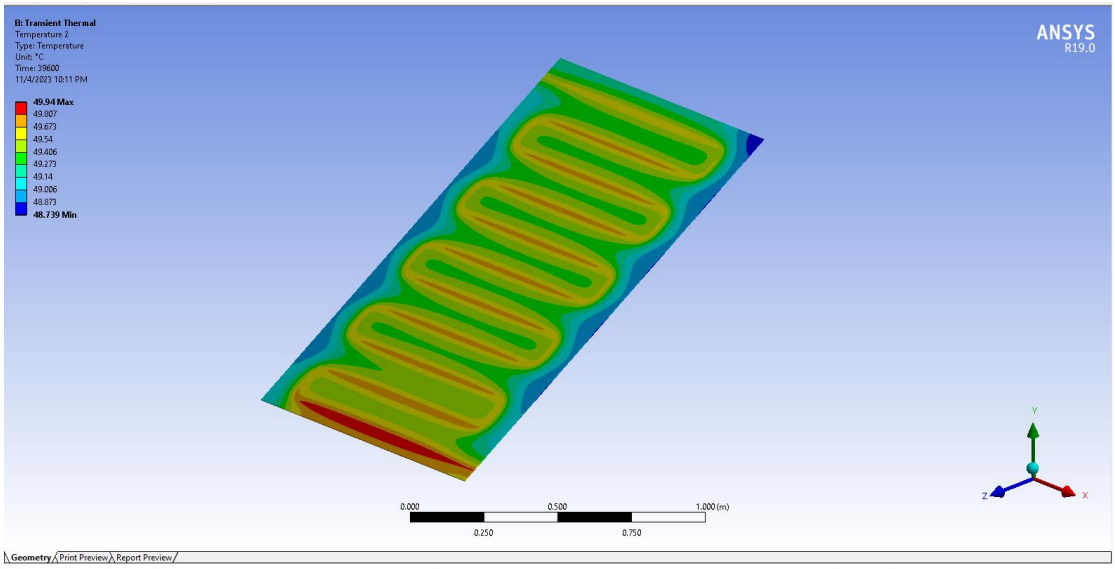

(c)

Figure 4.19. Temperature contour of PV at inlet temperature of 26°C with inlet velocity of (a) 0.1 m/s, (b) 0.5 m/s, (c) 1 m/s.

4.6. THE EFFECT OF RADIATION MODEL

The type flux membrane scheme is surely the most effective simulation tool in CFD calculations for radiative heat transfer in various engineering applications, from PV cooling systems to others. This is done by ensuring that the percentage of the area that is not shaded closely resembles the heat transfer process between PV modules and their surroundings, which can have a negative impact on their power and lifespan. Taking into account static variables such as the distribution of temperature and emissivity, the model allows for prudent simulations of the systems of PV cooling and ensures the most effective discharge of heat and consequently the highest performance. Like this, the dyadic non-selective radiation model is critical for the design and optimization of cooling systems in photovoltaic systems in different environmental positions and conditions.

It can be seen from Figure 4.20 that the temperatures in the exit platform for the case in which the radiation model is a coupling system, and the flow chart is because the radiation value is added directly and not by calculating it through the simulation program. This also indicates its height compared to other models. Where the temperature reached 31°C, while in surface-to-surface it reached 30.3°C, followed by

the Roseland model, in which the temperature reached 29.7°C, and then discrete ordinates, in which the maximum temperature reached 29°C, and in the worst condition it was in the model. P1, in which the temperature reached 28°C.

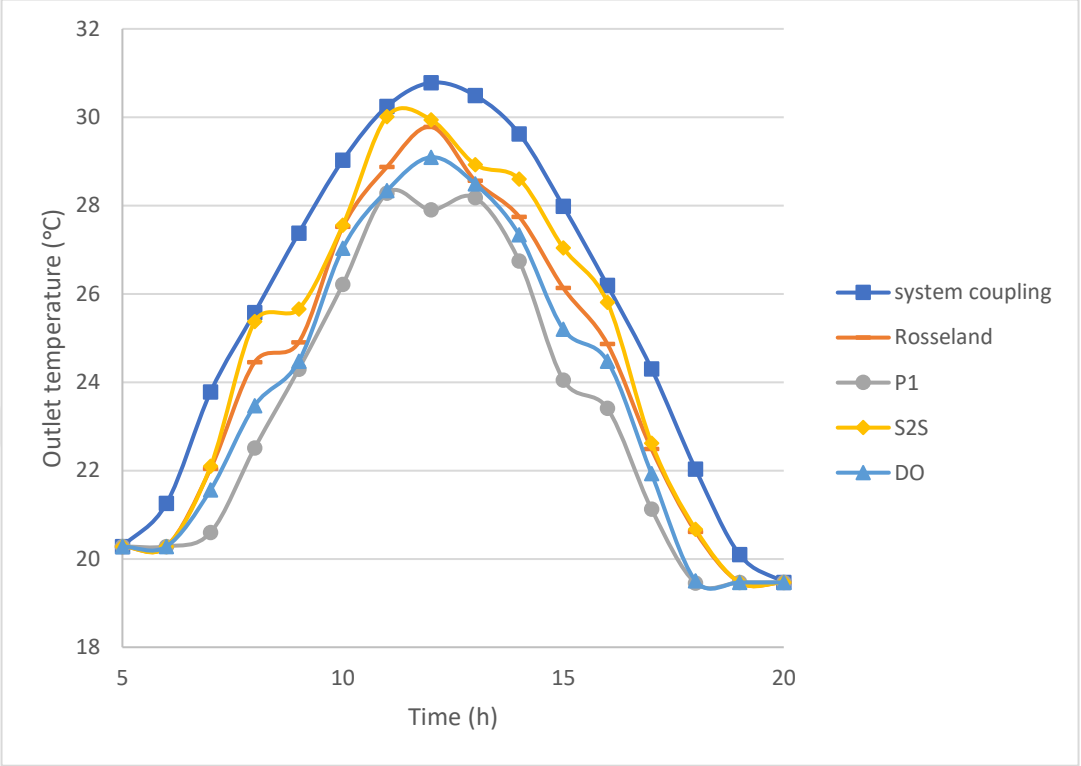

Figure 4.20. Outlet temperature with time for different radiation model.

It is known that an increase in the exit temperature means greater cooling of the solar panel and thus a greater output of power, as can be seen in Figure 4.21, which shows the amount of power over time. The power reached 67 W, while in the surface to surface it reached 65 W, followed by the Roseland model, in which the power reached to 64 W, then discrete ordinates, in which the maximum power reached 62 W. In the worst case, it was in the P1 model, in which the power reached 59 W.

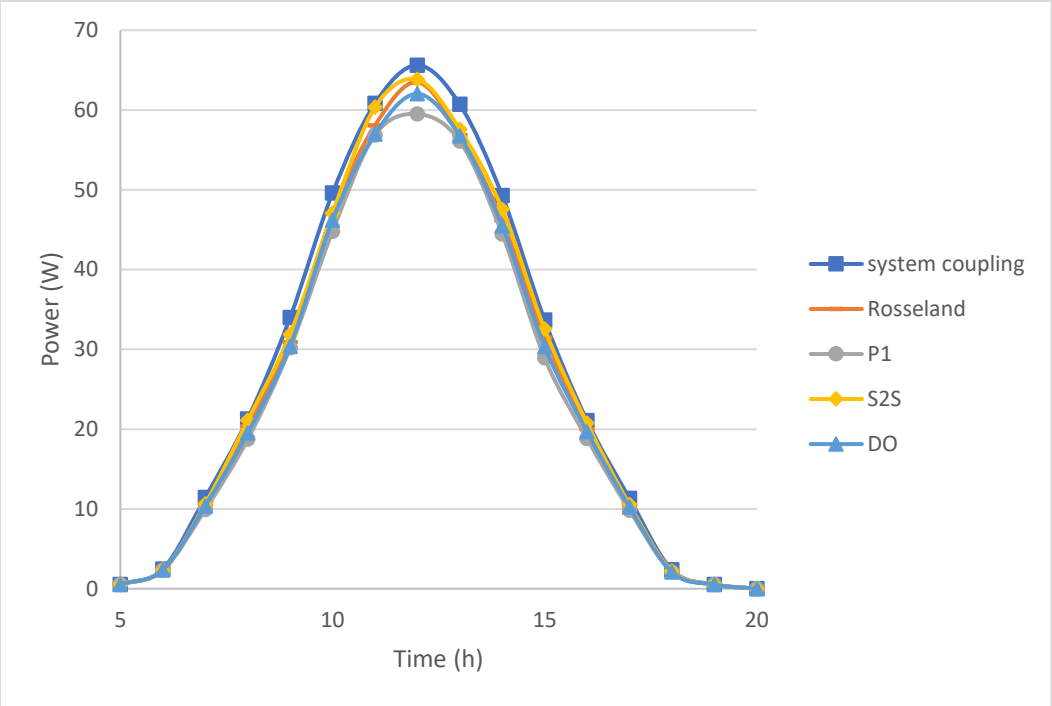

Figure 4.21. Power with time for different radiation model.

It is known that an increase in power means greater efficiency, as can be seen in Figure 4.22, which shows the amount of efficiency over time. The efficiency reached 7.6%, while on the surface, it reached 7.4%, followed by the Roseland model, in which the efficiency reached 7.2%, and then discrete coordinates, in which the maximum efficiency reached 7.1%. In the worst case, it was in the P1 model, in which the efficiency reached 6.8%.

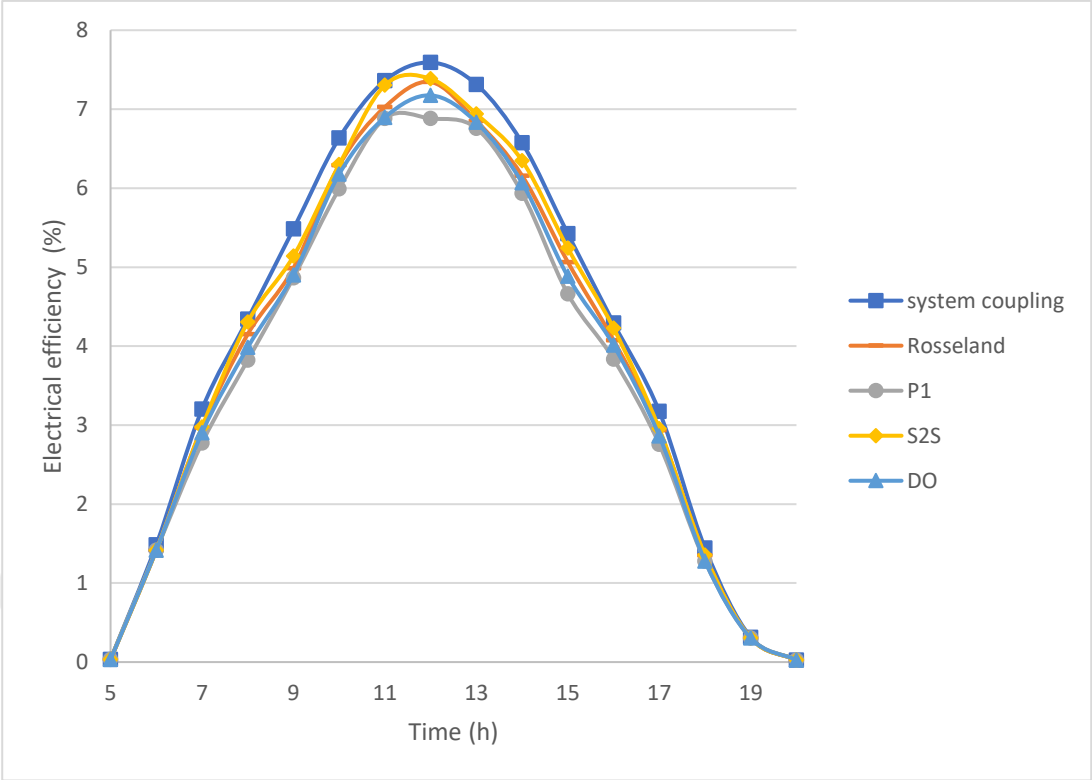

Figure 4.22. Electrical efficiency with time for different radiation model.

4.7. THE EFFECT OF DIMPLED TUBE ON PV COOLING

Dimpled tubes are probably a kind of passive cooling system that drives the improvement of the cooling efficiency of PV cells. Such systems pump fluids, which, in most cases, are water, flowing through a tube network on or along the PV panel surface in order to capture heat from the panels and reduce their temperature. Therefore, this greatly increases heat transfer, results in uniform cooling, cools down the operating temperature, and makes the system more efficient. Furthermore, dimpled tubes aid in keeping the panels in a lower temperature range, which increases their lifetime and can protect them against potential efficiency losses due to overheating. They also contribute to the cooler plates higher efficiency, longer duration, and greater energy yield, which eventually leads to improved system performance. The dimpled tubes are beneficial for the environment due to their use of water as a work fluid, which makes them a cleaner and greener way to cool solar photovoltaic systems. Ultimately, dimpled tube cooling systems should improve PV

panel performance and long-term operation in ways that favor the application of solar panels as an environmentally friendly and reliable source of power.

Through Figure 4.23, which shows the effect of the dimpled tube and the effect of its diameter, it shows that the value of the exit temperature increases by reducing the diameter of the dimpled due to its ability to create turbulence in the cooling stream. The exit temperature value was 34°C when the diameter of the dimpled was 2 mm, while it reached 33°C when the diameter of the dimpled was 4 mm. At 6 mm, the temperature reached 30°C.

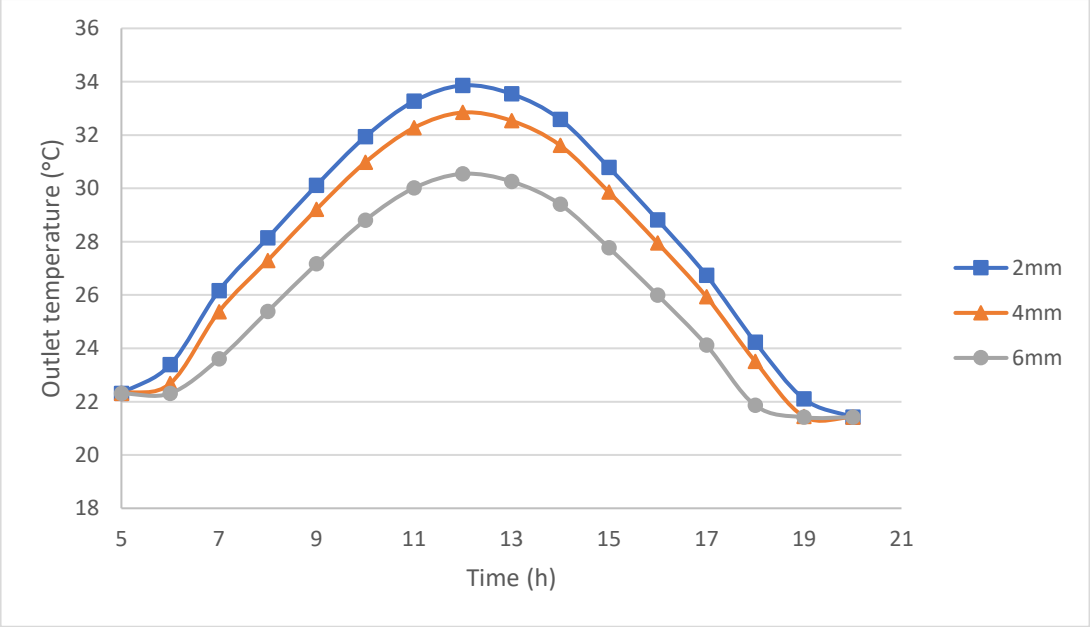

Figure 4.23. Outlet temperature with time for different dimpled tube dimeter.

It is known that an increase in the exit temperature means an increase in the cooling of the solar panel and thus an increase in the resulting power. This is shown in Figure 4.24, which shows the effect of the dimpled tube and the effect of its diameter. The power value was 88 W when the dimple diameter was 2 mm, while it reached 86 W when the dimple diameter was 4 mm. At 6 mm, the power reached 80 W.

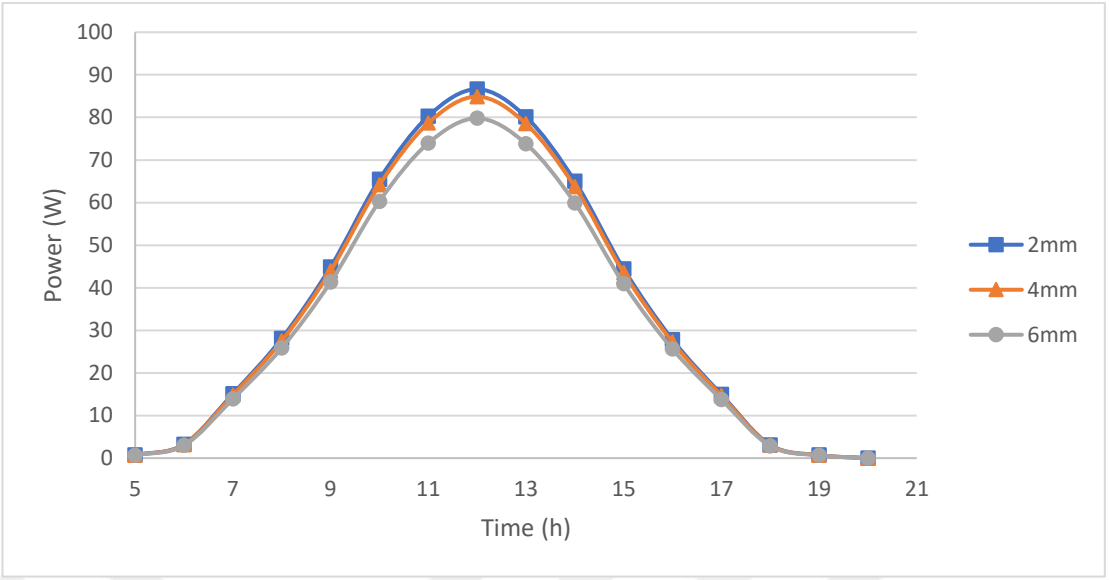

Figure 4.24. Power with time for different dimpled tube dimeter.

It is known that an increase in the power means an increase the resulting efficiency. This is shown in Figure 4.25, which shows the effect of the dimpled tube and the effect of its diameter. The efficiency value was 12.5% W when the dimple diameter was 2 mm, while it reached 12.4% when the dimple diameter was 4 mm. At 6 mm, the efficiency reached 11.6%.

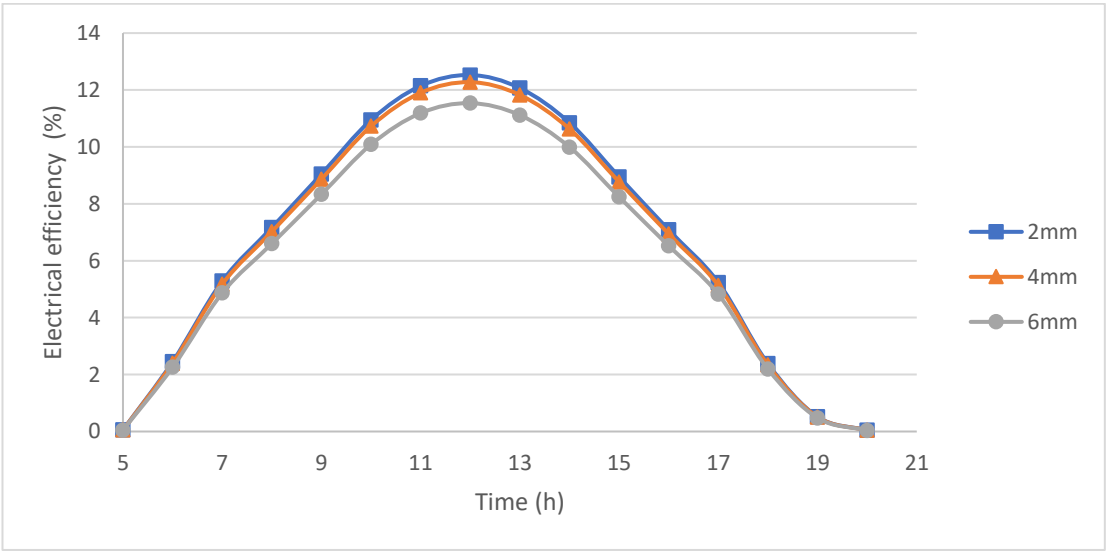

Figure 4.25. Electrical efficiency with time for different dimpled tube dimeter.

PART 5

CONCLUSIONS AND RECOMMENDATIONS

5.1. CONCLUSIONS

- The most important details in this text are the temperature distribution and cooling process on the solar panel through the simulation program. It is noted that the value of the maximum temperatures decreases with decreasing the inlet temperature of the cooling tube, and that the highest temperature value was at 12:00 in the afternoon, with a temperature of 32.42°C. The main objective of the cooling process is to obtain the largest possible efficiency that can be obtained through the process of calculations and simulations. The difference in the energy value according to the time and at the water inlet temperatures of the different cooling system was 65.28W, which indicates that the cooling value helps in increasing the electric power.
- The temperature appropriation and cooling process on the sun-powered chargers through the reenactment program showed that the greatest temperature worth of the reproduction cycle diminishes with the expansion in the section velocity of the cooling tube. The temperature when entering the water at a velocity of 1 m/s came to 28.1°C, which is the best case compared with the excess cases. The temperature conveyance over the long haul at various delta velocities also showed that the temperature esteem diminishes on the outer layer of the sunlight-powered chargers with the velocity-up water entering the cooling framework. The principal objective of the cooling system is to get the best conceivable proficiency that can be acquired through the computations and reproductions made through the product. The electrical effectiveness was reached when the water passage velocity was 1 m/s and the electrical proficiency esteem was 7.66%. This demonstrates that the cooling effect helps expand the electrical energy.

- The cooling process and temperature distribution on solar panels as calculated by the simulation software shows that December's maximum temperature values are lower than those of other months. The maximum temperature value of the simulation drops in December for the cooling pipe of the solar panel, and the exit temperature in the month of Jola was 20.2°C. The seasonal variation in temperature has been observed that the surface temperature of solar panels drops in December, and the lowest point occurred at midday. The cooling value aids in boosting the electrical energy, as measured at 65.15 W while the energy was entering the water at a velocity of 1 m/s at 12:00 in July. The primary goal of the refrigeration process is to achieve maximum efficiency, which may be achieved via the use of software calculations and simulations.
- The impact of lake temperature and inlet velocity on the summer season. The inlet temperature was 26°C and the velocity varied with the change in conditions. The pipe temperature gradient showed a maximum temperature of 58°C at 0.1 m/s inlet velocity, while at 1 m/s it reached 48°C. The temperature gradient of the solar panel showed a decrease as inlet velocity increased due to insufficient heat transfer time between the water and the panel. The temperature reached 58°C at 0.1 m/s, 55°C at 0.5 m/s, and 49°C at 1 m/s.
- The exit platform temperature (to be a coupling system between) the radiation model (with temperatures) reached 31°C, 30.3°C, 29.7°C, and 29.7°C in surface-to-surface, Roseland, and discrete ordinates models. The case study was P1, and the temperature was scorching hot at 28°C. Power during the last buildups of the P1 model grew from 67 W to 65 W, 64 W, 62 W, and 59 W, respectively. Efficiency was 7.6%, 7.4%, 7.2%, 7.1%, and 6.8% in the first stage after adjustment. In fact, the P1 model was the hardest, with only a 6.8% efficiency rate. Computer simulations and temperature measures provided the data used for this study.
- The coolant temperature exiting the solar panel is higher as tube thickness increases due to the creation of turbulence. As the size of the star is larger, temperatures are higher proportionally, which produces a higher cooling rate and hence power output. The capability of the solar cell grows with size,

resulting in 88 W of power for a 2 mm diameter, 86 W of power for a 4 mm diameter, and 80 W of power for a 6 mm diameter. The efficiency of the solar system also increases with the transfer of 12.5% of W if the diameter is 2 mm, 12.4% if the diameter is 4 mm, and 11.6% if the diameter is 6 mm.

5.2. RECOMMENDATIONS

- Manufacture of the solar panel system connected to the cold lake water experimentally, taking the results and comparing them with the numerical results.
- Using a large range of solar panels to find out the full capacity of a large network of solar panels.
- Changing the shapes of the cooling tube will increase the heat transfer value and the electrical efficiency.
- Using the MPPT combination to solve the problem the problem and find the maximum energy extracted from the solar panel to increase the electrical efficiency.
- Sustainable practices promote renewable energy sources for hot water consumption. A system uses a collection system, an insulated pipe network, and storage tanks to harvest and distribute water throughout residential spaces. The collected lake is directed into insulated tanks connected to residential spaces, and solar water heaters are integrated. The pump system ensures consistent hot water flow, aligning with sustainability goals and local regulations.

REFERENCES

1. S. J. Hayter, A. Kandt, and F.-A. Kandt, “Renewable Energy Applications for Existing Buildings Preprint Renewable Energy Applications for Existing Buildings Applicazioni dell’energia rinnovabile su edifici esistenti,” 2011. [Online]. Available: http://www.osti.gov/bridge

2. A. G. Lupu, V. M. Homutescu, D. T. Balanescu, and A. Popescu, “A review of solar photovoltaic systems cooling technologies,” *IOP Conf Ser Mater Sci Eng*, vol. 444, p. 082016, Nov. 2018, doi: 10.1088/1757-899X/444/8/082016.

3. “Energy from the Sun Student Guide INTERMEDIATE 2 0 1 9-2 0 2 0.” [Online]. Available: www.NEED.org

4. A. El Hammoumi, S. Chtita, S. Motahhir, and A. El Ghzizal, “Solar PV energy: From material to use, and the most commonly used techniques to maximize the power output of PV systems: A focus on solar trackers and floating solar panels,” *Energy Reports*, vol. 8, pp. 11992–12010, Nov. 2022, doi: 10.1016/j.egyr.2022.09.054.

5. energypedia, “Solar Energy.”

6. “solar-components.” Accessed: May 11, 2024. [Online]. Available: https://www.solaris-shop.com/solar-components

7. “what are the main components of a solar energy system.” Accessed: May 11, 2024. [Online]. Available: https://gemenergy.com.au/what-are-the-main-components-of-a-solar-energy-system

8. L. Liu, Q. Wang, H. Lin, H. Li, Q. Sun, and R. wennersten, “Power Generation Efficiency and Prospects of Floating Photovoltaic Systems,” *Energy Procedia*, vol. 105, pp. 1136–1142, May 2017, doi: 10.1016/j.egypro.2017.03.483.

9. R. Parthiban and P. Ponnambalam, “An Enhancement of the Solar Panel Efficiency: A Comprehensive Review,” *Front Energy Res*, vol. 10, Jul. 2022, doi: 10.3389/fenrg.2022.937155.

10. M. Herrando and A. Ramos, “Photovoltaic-Thermal (PV-T) Systems for Combined Cooling, Heating and Power in Buildings: A Review,” *Energies (Basel)*, vol. 15, no. 9, p. 3021, Apr. 2022, doi: 10.3390/en15093021.

11. V. Ramasamy and R. Margolis, “Floating Photovoltaic System Cost Benchmark: Q1 2021 Installations on Artificial Water Bodies,” Golden, CO (United States), Oct. 2021. doi: 10.2172/1828287.

12. M. Ebrahim, “Performance Evaluation of a Photovoltaic/Thermal (PVT) Collector with Numerical Modelling.”

13. S. H. Bandaru, V. Becerra, S. Khanna, J. Radulovic, D. Hutchinson, and R. Khusainov, “A Review of Photovoltaic Thermal (PVT) Technology for Residential Applications: Performance Indicators, Progress, and Opportunities,” *Energies (Basel)*, vol. 14, no. 13, p. 3853, Jun. 2021, doi: 10.3390/en14133853.

14. J. H. Lee, S. G. Hwang, and G. H. Lee, “Efficiency Improvement of a Photovoltaic Thermal (PVT) System Using Nanofluids,” *Energies (Basel)*, vol. 12, no. 16, p. 3063, Aug. 2019, doi: 10.3390/en12163063.

15. M. C. Alonso García and J. L. Balenzategui, “Estimation of photovoltaic module yearly temperature and performance based on Nominal Operation Cell Temperature calculations,” *Renew Energy*, vol. 29, no. 12, pp. 1997–2010, Oct. 2004, doi: 10.1016/j.renene.2004.03.010.

16. P. Sawicka-Chudy, M. Sibiński, M. Cholewa, M. Klein, K. Znajdek, and A. Cenian, “Tests and theoretical analysis of a pvt hybrid collector operating under various insolation conditions,” *Acta Innovations*, no. 26, pp. 62–74, Jan. 2018, doi: 10.32933/ActaInnovations.26.7.

17. A. Sanz, “Numerical simulation tools for PVT collectors and systems,” Sep. 2020. doi: 10.18777/ieashc-task60-2020-0006.

18. D. Boureima, M. K. Thierry Sikoudouin, O. Emmanuel, H. Koami Soulemane, and B. Dieudonn Joseph, “Theoretical Study of a Thermal Photovoltaic Hybrid Solar Collector,” *Indian J Sci Technol*, vol. 11, no. 43, pp. 1–9, Nov. 2018, doi: 10.17485/ijst/2018/v11i43/132133.

19. M. Abakam, S. A. Alkaff, Y. I. Go, and V. K. Venkiteswaran, “Modelling and Performance Analysis of a New PVT System, with Two Semi-Transparent PV Panels,” *Process Integration and Optimization for Sustainability*, vol. 3, no. 3, pp. 359–373, Sep. 2019, doi: 10.1007/s41660-019-00084-9.

20. A. Fudholi, I. Taslim, M. A. Indrianti, M. Fazleena Musthafa, I. N. Manyoe, and M. Y. Othman, “Efficiency and energy modelling for PVT air collector with extended heat transfer area: a review Mariyam Fazleena Ministry of Environment, Republic of Maldives Efficiency and energy modelling for PVT air collector with extended heat transfer area: a review,” *Article in International Journal of Power Electronics and Drive Systems*, vol. 10, no. 4, pp. 2029–2036, 2019, doi: 10.11591/ijpeds.v10.i4.2029-2036.

21. F. T. Zohora and R. Nasrin, “A Numerical Analogy of Improving Efficiency for the PVT System in Bangladesh,” *International Journal of Photoenergy*, vol. 2022, pp. 1–21, Aug. 2022, doi: 10.1155/2022/1901925.

22. L. Liu, Q. Wang, H. Lin, H. Li, Q. Sun, and R. wennersten, “Power Generation Efficiency and Prospects of Floating Photovoltaic Systems,” *Energy Procedia*, vol. 105, pp. 1136–1142, May 2017, doi: 10.1016/j.egypro.2017.03.483.

23. S.-M. Kim, J.-H. Kim, and J.-T. Kim, “Experimental Study on the Thermal and Electrical Characteristics of an Air-Based Photovoltaic Thermal Collector,” *Energies (Basel)*, vol. 12, no. 14, p. 2661, Jul. 2019, doi: 10.3390/en12142661.

24. J.-H. Kim, S.-H. Park, and J.-T. Kim, “Experimental Performance of a Photovoltaic-thermal Air Collector,” *Energy Procedia*, vol. 48, pp. 888–894, 2014, doi: 10.1016/j.egypro.2014.02.102.

25. M. Ghadiri, M. Sardarabadi, M. Pasandideh-fard, and A. J. Moghadam, “Experimental investigation of a PVT system performance using nano ferrofluids,” *Energy Convers Manag*, vol. 103, pp. 468–476, Oct. 2015, doi: 10.1016/j.enconman.2015.06.077.

26. A. Numan Özakın, M. Kaan Yeşilyurt, K. Yakut, A. Numan ÖZAKIN, and M. Kaan YEŞİLYURT, “Experimental Investigation of Thermal Performance of Photovoltaic Thermal (PVT) Systems,” vol. 3, 2017, [Online]. Available: https://www.researchgate.net/publication/322525513

27. Z. Fu *et al.*, “Experimental investigation on the enhanced performance of a solar PVT system using micro-encapsulated PCMs,” *Energy*, vol. 228, p. 120509, Aug. 2021, doi: 10.1016/j.energy.2021.120509.

28. M. Saadoon, I. Hasan, and M. Mohammed, “Preparing Nanofluids (Al2O3) for Enhancement Performance of Photovoltaic,” *Engineering and Technology Journal*, vol. 39, no. 9, pp. 1445–1453, Sep. 2021, doi: 10.30684/etj.v39i9.2110.

29. S. Gundala, M. M. Basha, V. Madhurima, N. Praveena, and S. V. Kumar, “An Experimental Performance on Solar Photovoltaic Thermal Collector with Nanofluids for Sustainable Development,” *J Nanomater*, vol. 2021, pp. 1–6, Oct. 2021, doi: 10.1155/2021/6946540.

30. M. F. Jaffar, A. Th. Mohammad, and A. Q. Ahmed, “An Experimental Study for Enhancing the Performance of the Photovoltaic Module Using Forced Air,” *Journal of Techniques*, vol. 4, no. 2, pp. 1–9, Jun. 2022, doi: 10.51173/jt. v4i2.462

31. H. A. Hasan *et al.*, “Experimental Evaluation of the Thermoelectrical Performance of Photovoltaic-Thermal Systems with a Water-Cooled Heat Sink,” *Sustainability*, vol. 14, no. 16, p. 10231, Aug. 2022, doi: 10.3390/su141610231.

32. Y. A. Sheikh, A. D. Butt, K. N. Paracha, A. B. Awan, A. R. Bhatti, and M. Zubair, “An improved cooling system design to enhance energy efficiency of floating photovoltaic systems,” *Journal of Renewable and Sustainable Energy*, vol. 12, no. 5, Sep. 2020, doi: 10.1063/5.0014181.

33. I. Hasan, “Enhancement the Performance of PV Panel by Using Fins as Heat Sink,” *Engineering and Technology Journal*, vol. 36, no. 7A, pp. 798–805, Jul. 2018, doi: 10.30684/etj.36.7A.13.

34. A. L. Abdullah, S. Misha, N. Tamaldin, M. Afzanizam, M. Rosli, and F. A. Sachit, “A Review: Parameters Affecting the PVT Collector Performance on the Thermal, Electrical, and Overall Efficiency of PVT System,” *Journal of Advanced Research in Fluid Mechanics and Thermal Sciences Journal homepage*, vol. 60, pp. 191–232, 2019, [Online]. Available: www.akademiabaru.com/arfmts.html

35. C. A. F. Ramos, A. N. Alcaso, and A. J. M. Cardoso, “Photovoltaic-thermal (PVT) technology: Review and case study,” *IOP Conf Ser Earth Environ Sci*, vol. 354, no. 1, p. 012048, Oct. 2019, doi: 10.1088/1755-1315/354/1/012048.

36. M. R. Gomaa, W. Hammad, M. Al-Dhaifallah, and H. Rezk, “Performance enhancement of grid-tied PV system through proposed design cooling techniques: An experimental study and comparative analysis,” *Solar Energy*, vol. 211, pp. 1110–1127, Nov. 2020, doi: 10.1016/j.solener.2020.10.062.

37. A. Majumder, R. Innamorati, A. Frattolillo, A. Kumar, and G. Gatto, “Performance Analysis of a Floating Photovoltaic System and Estimation of the Evaporation Losses Reduction,” *Energies (Basel)*, vol. 14, no. 24, p. 8336, Dec. 2021, doi: 10.3390/en14248336.

38. J. Yazdanpanahi, F. Sarhaddi, and M. Mahdavi Adeli, “Experimental investigation of exergy efficiency of a solar photovoltaic thermal (PVT) water collector based on exergy losses,” *Solar Energy*, vol. 118, pp. 197–208, Aug. 2015, doi: 10.1016/j.solener.2015.04.038.

39. J. Yao, E. Chen, Y. Dai, and M. Huang, “Theoretical analysis on efficiency factor of direct expansion PVT module for heat pump application,” *Solar Energy*, vol. 206, pp. 677–694, Aug. 2020, doi: 10.1016/j.solener.2020.04.053.

40. Ansys, “Engineering Simulation Software,” Www.ansys.com, ansys.com.

41. M. F. Modest, Radiative Heat Transfer, 3rd ed., Academic Press, USA, 2013.

42. R. Siegel and J. R. Howell, Thermal Radiation Heat Transfer, 4th ed., Taylor & Francis, USA, 2002.

43. H. K. Versteeg and W. Malalasekera, An Introduction to Computational Fluid Dynamics: The Finite Volume Method, 2nd ed., Pearson Education, UK, 2007.

44. F. P. Incropera and D. P. DeWitt, Introduction to Heat Transfer, 5th ed., Wiley, USA, 2002.

45. J. R. Howell, M. P. Mengüç, and R. Siegel, Thermal Radiation Heat Transfer, 6th ed., CRC Press, USA, 2016.

46. Flipkart, "/amaze-sport-submersible-water-pump-0-1-hp," www.flipkart.com/amaze-sport-submersible-water-pump-0-1-hp/p/itmfg7trknpmrpfb. Accessed 26 Nov. 2023.

47. B. A. Denfeld, M. Klaus, H. Laudon, R. A. Sponseller, and J. Karlsson, "Carbon Dioxide and Methane Dynamics in a Small Boreal Lake During Winter and Spring Melt Events," *J Geophys Res Biogeosci*, vol. 123, no. 8, pp. 2527–2540, Aug. 2018, doi: 10.1029/2018JG004622.

48. MathWorks, "MATLAB," www.mathworks.com/products/matlab.html.

49. Salim, T., Aswad, N., Al-Baghdadi, M., Al-Waily, M., Azahari, M., & Razali, B. (2021). Performance Enhancement of a Photovoltaic Cell Working in Hot Environment Conditions using Al2O3 Nanofluids: A CFD Study. International Journal of Nanoelectronics and Materials, 14(4).

APPENDIX A

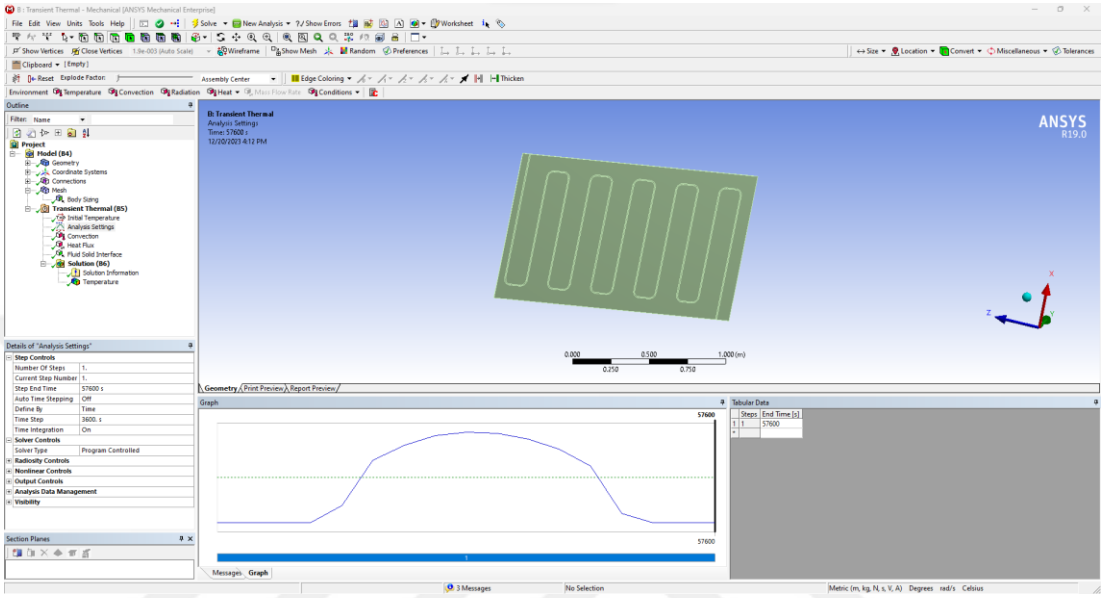
ANSYS
R19.0
Transient Thermal
Geometry
Graph
Tabular Data

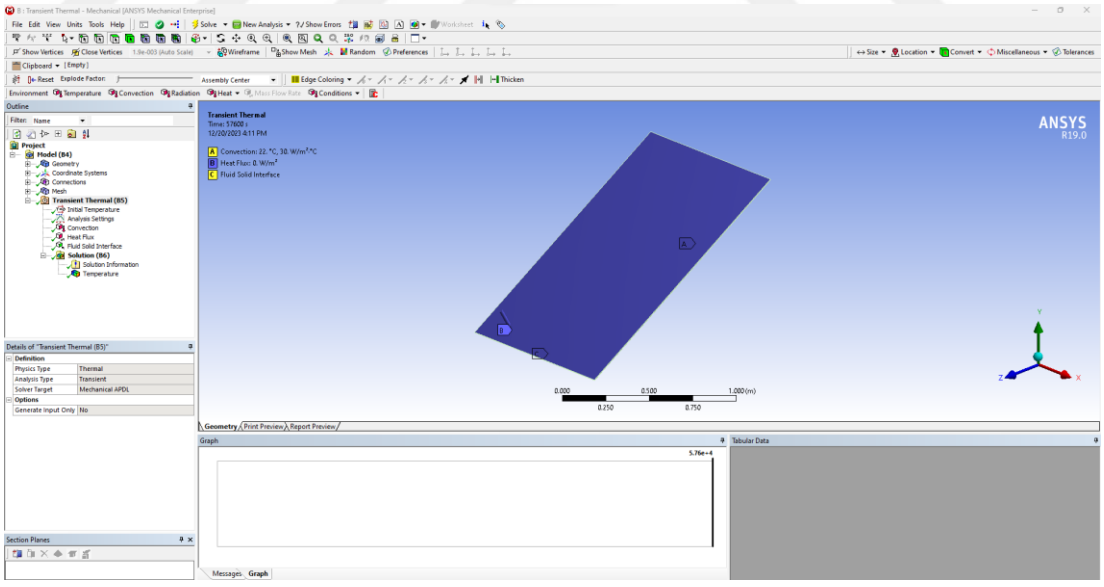
ANSYS
R19.0
Transient Thermal
Geometry
Graph
Tabular Data

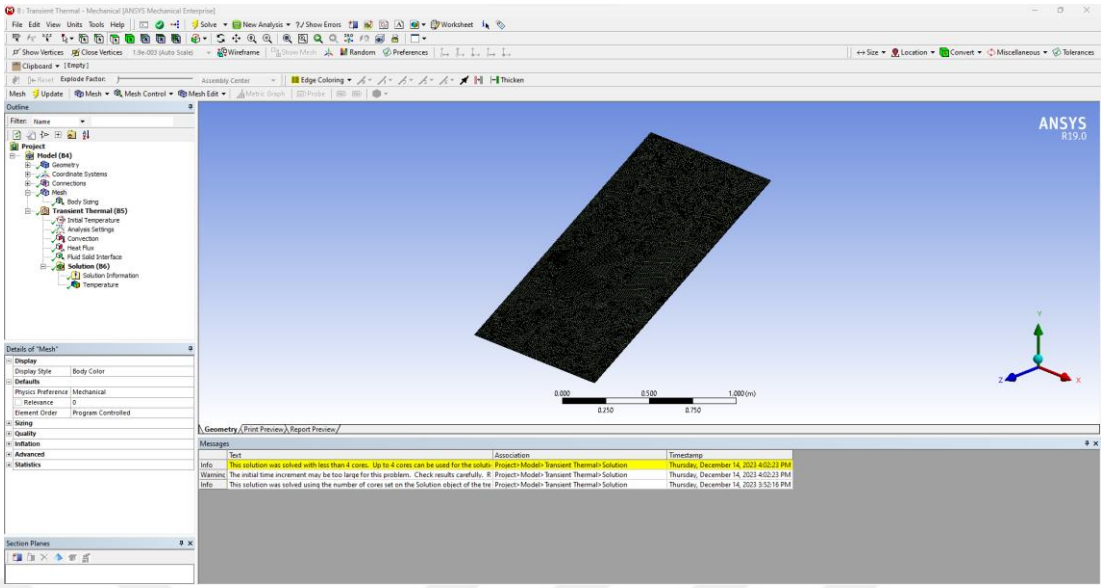
ANSYS
R19.0

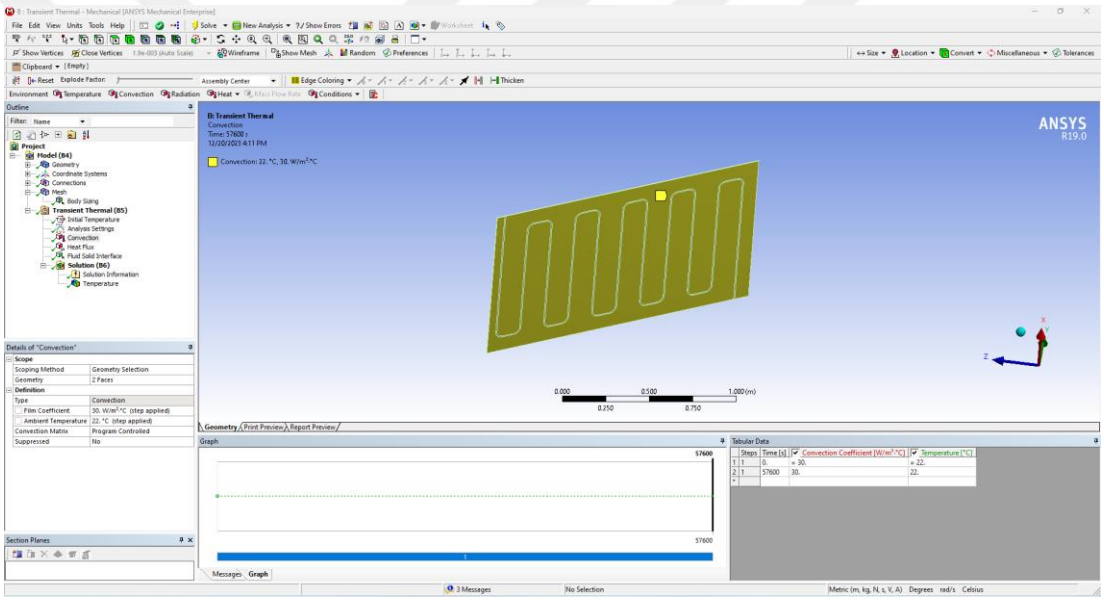
ANSYS
R19.0

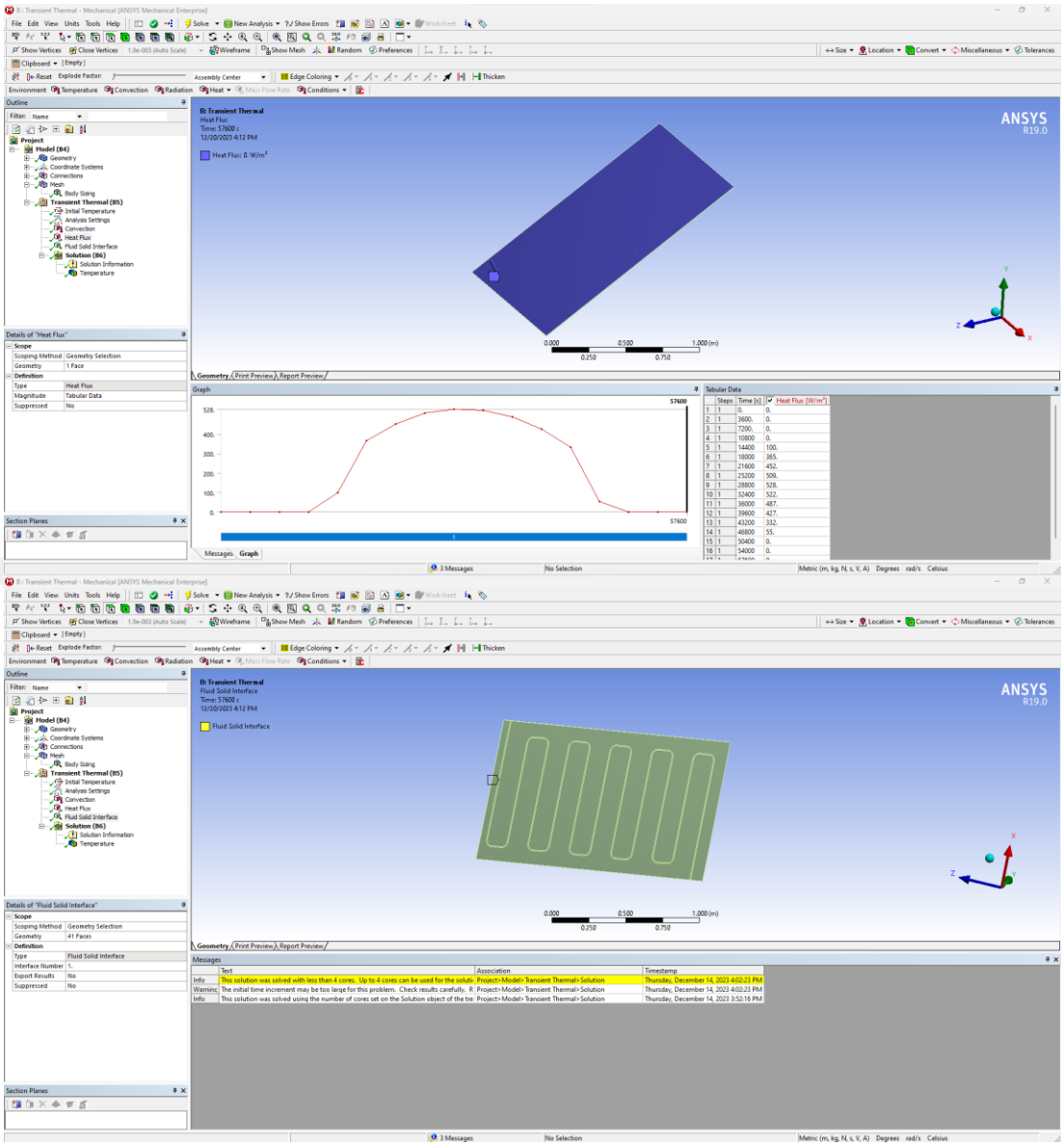
B: Transient Thermal
Heat Flux
Time: 57600 s
12/20/2023 4:12 PM
Heat Flux: 0. W/m²
ANSYS
R19.0
Graph
Tabular Data
Steps Time [s] Heat Flux [W/m²]
1 1 0. 0.
2 1 3600. 0.
3 1 7200. 0.
4 1 10800 0.
5 1 14400 100.
6 1 18000 365.
7 1 21600 452.
8 1 25200 509.
9 1 28800 528.
10 1 32400 522.
11 1 36000 487.
12 1 39600 427.
13 1 43200 332.
14 1 46800 55.
15 1 50400 0.
16 1 54000 0.
Messages
3 Messages
No Selection
Metric (m, kg, N, s, V, A) Degrees rad/s Celsius
B: Transient Thermal
Fluid Solid Interface
Time: 57600 s
12/20/2023 4:12 PM
Fluid Solid Interface
ANSYS
R19.0
Messages
Info This solution was solved with less than 4 cores. Up to 4 cores can be used for the soluti Project>Model>Transient Thermal>Solution Thursday, December 14, 2023 4:02:23 PM
Warning The initial time increment may be too large for this problem. Check results carefully. R Project>Model>Transient Thermal>Solution Thursday, December 14, 2023 4:02:23 PM
Info This solution was solved using the number of cores set on the Solution object of the tre Project>Model>Transient Thermal>Solution Thursday, December 14, 2023 3:52:16 PM
3 Messages
No Selection
Metric (m, kg, N, s, V, A) Degrees rad/s Celsius

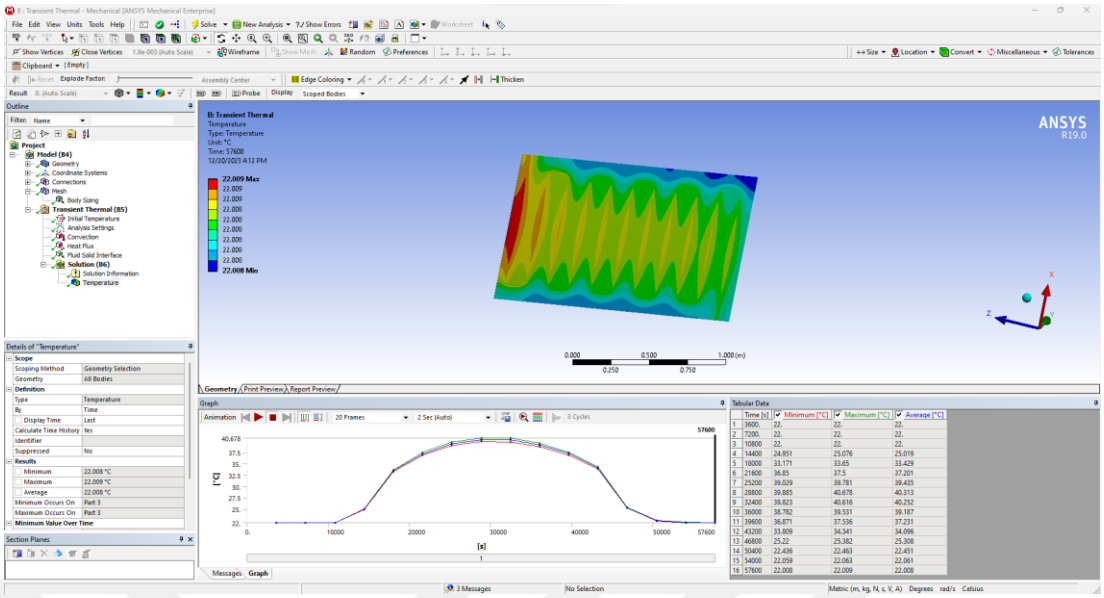
B: Transient Thermal
Temperature
Type: Temperature
Unit: °C
Time: 57600
12/20/2023 4:12 PM
22.009 Max
22.009
22.009
22.009
22.009
22.009
22.009
22.009
22.008 Min
ANSYS
R19.0
Geometry
Print Preview
Report Preview
Graph
Tabular Data
Messages
Graph
3 Messages
No Selection
Metric (m, kg, N, s, V, A)
Degrees
rad/s
Celsius

CURRICULUM VITAE

Baseem Hasan Hammadi, graduated from the Mechanical Engineering Department, University of Technology-Baghdad 2001, and is currently a master's student at Karabuk University.